

DISSERTATION

3D FINITE ELEMENT MODELING OF TIME-DEPENDENT BEHAVIOR OF
WOOD-CONCRETE COMPOSITE BEAMS

Submitted by

Lam Giang To

Department of Civil and Environmental Engineering

In partly fulfillment of the requirements

For the Degree of Doctor of Philosophy

Colorado State University

Fort Collins, Colorado

Spring 2009

UMI Number: 3374628

INFORMATION TO USERS

The quality of this reproduction is dependent upon the quality of the copy submitted. Broken or indistinct print, colored or poor quality illustrations and photographs, print bleed-through, substandard margins, and improper alignment can adversely affect reproduction.

In the unlikely event that the author did not send a complete manuscript and there are missing pages, these will be noted. Also, if unauthorized copyright material had to be removed, a note will indicate the deletion.

UMI[®]

UMI Microform 3374628
Copyright 2009 by ProQuest LLC
All rights reserved. This microform edition is protected against
unauthorized copying under Title 17, United States Code.

ProQuest LLC
789 East Eisenhower Parkway
P.O. Box 1346
Ann Arbor, MI 48106-1346

COLORADO STATE UNIVERSITY

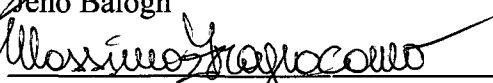
December 31, 2008

WE HEREBY RECOMMEND THAT THE DISSERTATION PREPARED UNDER OUR SUPERVISION BY LAM GIANG TO ENTITLED 3D FINITE ELEMENT MODELING OF TIME-DEPENDENT BEHAVIOR OF WOOD-CONCRETE COMPOSITE BEAMS BE ACCEPTED AS FULFILLING IN PART REQUIREMENTS FOR THE DEGREE OF DOCTOR OF PHILOSOPHY.

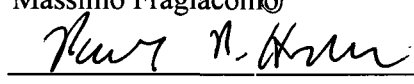
Committee on Graduate Work



Jeno Balogh



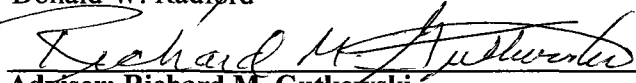
Massimo Fragiaco



Paul R. Heyliger



Donald W. Radford



Adviser: Richard M. Gutkowski



Department Head: Luis Garcia

ABSTRACT OF DISSERTATION

3D FINITE ELEMENT MODELING OF TIME-DEPENDENT BEHAVIOR OF WOOD-CONCRETE COMPOSITE BEAMS

The wood-concrete composite beam structure with notched shear keys has some advantages such as high composite efficiency and ease of construction with low labor cost compared to other wood-concrete composite beam structures. Made up from two rheological materials, wood and concrete, the time-dependent behavior of the wood-concrete composite beam is not only affected by the long-term load but also driven by the variation of the environmental conditions such as temperature and relative humidity. To consider the effects of the environmental conditions, the modeling process must include the moisture diffusion analysis for the wood layer, the heat transfer analysis and the stress/displacement analysis where the first two analyses provide input parameters for the third analysis. This research focused on modeling the time-dependent behavior of the layered wood-concrete composite with notched shear keys by using 3D finite element method. The main goals of the research are to expand available constitutive models of wood and concrete so that they can be used in the 3D FEM. The 3D constitutive models of wood and concrete were then implemented in the commercial software ABAQUS by using the subroutine UMAT for the stress/displacement analysis. To provide data to validate the theoretical model, a long-term creep test on two specimens has been performed. The results of the verification analysis on one test specimen captured closely the time-dependent behavior of the test specimen for the first 123 days of the test. The verification analysis revealed that the heat transfer analysis is not necessary in long-term analysis. The application of the 3D model with solid elements not only predicts the long-term behavior of the wood-concrete composite beam structures better than 1D models do, but it can be also applied for wood-concrete composite structures with complex geometry where the 1D model cannot be applied. In addition, the application of the 3D model with solid element can be used to perform parametric studies to address remaining questions about time-dependent of the wood-concrete composites structures.

Lam Giang To
Civil and Environmental Engineering Department
Colorado State University
Fort Collins, CO 80523
Spring 2009

ACKNOWLEDGMENTS

I would like to thank the Vietnamese government, represented by Vietnam International Education Development Bureau - Ministry of Education and Training, for providing me a scholarship so that I had a chance to work on my Ph.D. degree in the United States. I would like to express my appreciation to my adviser, Professor Richard M. Gutkowski, for his academic guidance and financial support since I took my first class of him until I complete this work. I would like to thank Dr. Massimo Fragiaco for his enthusiastic guidance relating to this research. Beside my advisers, I would like to thank the rest of my dissertation committee: Dr. Paul R. Heyliger, Dr. Donald W. Radford and Dr. Jeno Balogh for their suggestions on the research. I also thank graduate students who work in the Structural Engineering Laboratory at Colorado State University for their helps in building the test specimens.

DEDICATION

This dissertation is dedicated to my parent as a fulfillment to my dad's will before he passed away.

This dissertation is dedicated to my beloved wife for her tireless sacrifices when I worked toward my Ph.D. degree.

This dissertation is dedicated to my son and daughter as an inspiration for the road of exploring knowledge in their life.

Table of Contents

Abstract	iii
Acknowledgements	iv
Dedication	v
Table of Contents	vi
Chapter 1 – Introductions	1
1.1. Overviews	1
1.2. Problem Statement	5
1.3. Hypothesis	5
1.4. Research and Contributions	7
Chapter 2 – Literature reviews	9
2.1. Structural types and applications	9
2.2. Computational models	19
2.2.1. Development of structural computational models	19
2.2.2. Computational models for long-term analysis of wood and applications for layered wood-concrete composite systems	24
2.2.3. Creep and shrinkage prediction models for concrete	32
2.2.4. Reasons for a new computational model for the layered wood-concrete composite beams with notched shear keys	35
Chapter 3 – Related physical phenomena in the research	38
3.1. Introduction	38
3.2. Moisture diffusion and heat transfer	40
3.2.1. Mathematic expression of heat transfer and diffusion problem	41
3.2.2. Finite element method to solve heat transfer and diffusion	44
3.3. Basic of rheological characteristics	47
3.3.1. Introduction	47
3.3.2. Constitutive models of visco-elastic materials	49
3.4. Rate type of constitutive equations	56
Chapter 4 – Mathematical model for long-term structural behavior of wood	68
4.1. Introduction	68
4.2. Hypothesis	72
4.3. Toratti model formulations	73
4.4. Incremental form of the constitutive equation for wood	77

4.5. Expansion of the constitutive equation of wood for three-dimensional analysis	81
Chapter 5 – Mathematical model for long-term structural behavior of concrete	87
5.1. Introduction	87
5.2. Shrinkage formulation based on ACI-209R-92	89
5.3. Creep formulation based on CEB-FIP 1990	90
5.4. Determination of parameters of generalized Maxwell model for concrete of concrete based on CEB-FIP 1990	93
5.5. Incremental form of creep for concrete	96
5.6. Expansion of the constitutive equation of concrete for three-dimensional analysis	97
Chapter 6 – Finite element implementations in ABAQUS	100
6.1. Basic equations of finite element method of solid mechanics	100
6.2. Modeling time dependent of wood-concrete composite beam with ABAQUS	105
6.2.1. Implementation of the diffusion and heat transfer analysis	108
6.2.2. Implementation of the stress/displacement analysis	112
6.2.3. Element types, mesh sizes and time steps	113
Chapter 7 – Creep test and model verifications	115
7.1. Creep test	115
7.1.1. Beam parameters and material properties	116
7.1.2. Long-term static loads	119
7.1.3. Monitoring and measurements	121
7.2. Model verifications and prediction analysis	124
7.2.1. Diffusion and heat transfer analysis results	126
7.2.2. Test results and model verifications	133
7.2.3. Time-dependent behavior prediction based on the proposed model	141
7.2.4. Comparison between the proposed 3D model and available 1D model	142
Chapter 8 – Discussions and recommendations	149
8.1. Discussions	149
8.1.1. Discussion of the environmental conditions	149
8.1.2. Discussion of the creep test results	150
8.1.3. Discussion of the numerical model and results of the model	151

8.1.4. Discussion of the results of the proposed 3D model and the available 1D mode	152
8.2. Conclusions	153
8.3. Recommendations	155
References	158
Appendix A	169
Appendix B	174
Appendix C	176
Appendix D	179
Appendix E	180

Chapter 1

Introduction

1.1 Overview

Wood-concrete composite systems can be used effectively in bending resistant components in some types of civil engineering structures such as floors for buildings and decks for short-span bridges. In general, the composite system includes a concrete layer, a wood layer and the inter-layer connections to gain composite action between two layers. The concrete layer is placed on top of the wood layer, so that under service loading, most of the concrete layer will be in the compression or low tension stress zone and the wood layer will be in the tension stress zone. This set up not only permits the use of the strongest abilities of both materials, but also eliminates their weaknesses when using them in bending structural components. Beside, the wood-concrete composite system shows some advantages in dead load and seismic performance if compared with a solid reinforced concrete slab, in acoustic insulation and fire resistance if compared with light-frame systems or wood decks.

Most of research of wood-concrete composite systems has been done in Europe, and nowadays with awareness of energy problems, this kind of structure has been encouraged for use in other countries. The wood-concrete composite structure is still new in the United States where, however, with a large market for multi-building floors and the great need for replacement and rehabilitation of short-span bridges in low volume routes, this type of structure could gain a reasonable portion of the future market if its behavior is well understood.

In a wood-concrete composite system, the interlayer connection plays an important role in gaining and keeping composite action. Many types of connections have been proposed and studied. The connections of wood-concrete composite structures can be categorized as: mechanical connection, glued connection, notched connection, or a combination of them. Under the support of the U.S. Department of Agriculture (USDA) and the U.S. Department of Transportation (USDOT), a series of wood-concrete composite systems have been tested at Colorado State University (CSU). These studies focused on the wood-concrete composite system with a notched shear key connection.

There are several variations of notched shear key connection applied in layered wood-concrete composite systems. The studied system at CSU originated and evolved for multi-story buildings in Europe (Natterer et al. 1996 [1]). The wood-concrete composite floor/deck systems studied at CSU consist of a wood layer, a concrete layer and notched shear keys (Figure 1.1). The wood layer is made by laterally nailing dimension lumber boards together. After all the boards are tightly joined to make the wood layer plate-like, the notches are cut, and the sleeved Hilti dowels are inserted and glued into the wood layer at center line of the notches. Then the side formwork is set up and concrete is placed on top of the wood layer. The plastic sleeve covers only the portion of dowel in concrete layer, so that when the concrete develops enough strength the dowel can be tightened to restore the tight fit around the notch.

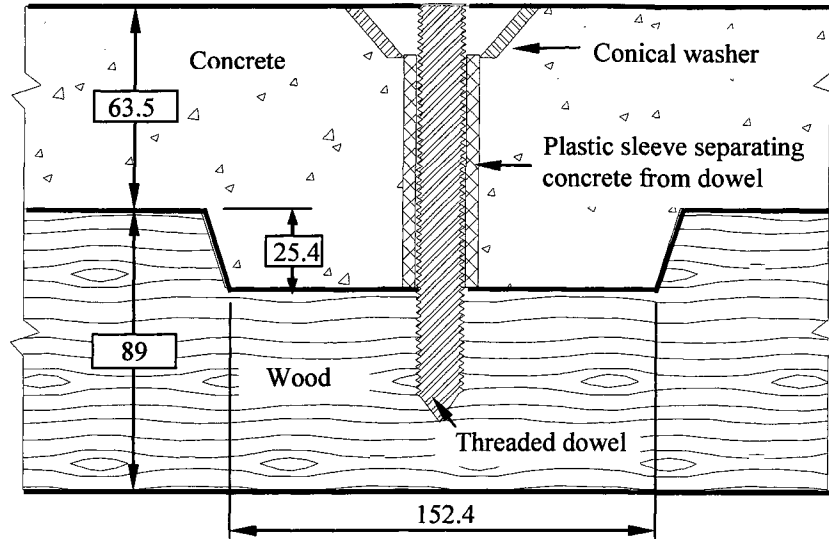


Figure 1.1 Notched shear key with Hilti dowel connector. Length unit is in mm

In this type of connection, shear force acting between two layers is transferred mostly by shear keys. Tightening the dowels (after the concrete cures) increases composite efficiency of the composite structure. The composite efficiency gained in the previous static tests at CSU ranged from 54.9 to 96.4% [2, 3, 111, 113]. At this composite action level, the notched shear key layered wood-concrete composite structures would be competitive with other layered wood-concrete composite structures. Before this type of composite structure can be introduced and applied as a commercial structure, the behavior must be studied and fully understood. This behavior includes the short-term behavior due to static load (normal service load and ultimate failure load), behavior due to service dynamic load, fatigue behavior due to repeated load, and long-term behavior due to long-term static load and the change of environmental conditions such as temperature and humidity.

Past research done at CSU focused on optimizing structural configurations, and on understanding structural behavior of selected configurations under static load and

repeated load. The most important shortcoming in understanding structural behavior of layered wood-concrete composite structure is the time-dependent behavior under the long-term static load because both wood and concrete are rheological materials. In addition, in service life conditions, the time-dependent behavior of wood is not only dependent on temperature, time, and applied stress level but also on the level of moisture content and its variation. For structures exposed to the environment such as a bridge, the variations of temperature and relative humidity play important roles in time-dependent behavior of wood-concrete composite structures in general and in layered wood-concrete composite with notched shear key in particular. To close the gap in understanding structural behavior of layered wood-concrete composite structures with notched shear keys, this research studies the time-dependent behavior of layered wood-concrete composite beams interconnected by notched shear keys under long-term static load and the variation of ambient environmental conditions.

The time-dependent behavior of this specific type of structure can be understood by performing long-term load tests. However, long-term tests take time and cost to keep track if one monitor all data for a whole life time of service. For that reason, both theoretical and experimental studies are employed herein. As described subsequently, a creep test is being performed to provide data about behavior of the wood-concrete composite beams (for the first 4-5 months duration of the service life). The data will be used to verify the numerical model so that the numerical model can then be used to predict the time-dependent behavior over the whole service life for the test beams. The numerical model can also be used to investigate time-dependent behavior of similar beams in different load conditions (both normal load and environmental conditions).

1.2 Problem Statement

This research focuses on modeling the time-dependent behavior of a layered wood-concrete composite beam with notch shear keys under long-term static load as well as the variations of ambient environmental conditions such as temperature and relative humidity. The research starts with the studies of available long-term constitutive models for wood and concrete, then extends and develops selected models so that they can be applied in 3D finite element modeling. Finite element models for a wood-concrete composite beam with notched shear key are developed to model the diffusion of moisture content and heat transfer within the materials. By solving the moisture content diffusion and the heat transfer problems, the moisture content profile in the wood layer and temperature profile in the wood layer, concrete layer and the dowels over the time are determined. The moisture content and temperature profiles are used together with long-term static load as input parameters for the time-dependent analysis problem. The results of the developed FEM numerical model are verified by comparison with measured experimental results as well as with numerical prediction obtained by using a 1D beam model (Fragiacomo 2000 [4]). Although there are experimental creep test data available, those data are not sufficient for verifying the model due to the lack of detailed relative humidity and temperature records. Data and results from ongoing creep tests being conducted at CSU will be used to verify the model.

1.3 Hypothesis

Time-dependent behavior of a wood-concrete composite beam is affected by long-term behavior of the materials and the type of inter-layer connection. Both concrete and wood are rheological materials. With concrete, under normal service condition, the time-

dependent behavior depends mostly on the level and duration of applied stress. But with wood, the variations of temperature and moisture content inside the wood also affect its time-dependent behavior. Temperature and moisture content inside the wood layer are functions of space and time and are driven by the variations of ambient temperature and relative humidity. The changes of temperature in the wood, concrete and interlayer connection also create a thermal expansion phenomenon which is the results of a thermal stress field that varies over time. Similarly, the change in moisture content in the wood layer causes moisture expansion in the wood layer thereby causing another time-dependent stress field in the whole structure.

All the above physical phenomena happen simultaneously and interactively during the service life of the structure and affect the time-dependent behavior of wood-concrete composite beam. Those physical phenomena are complex to model for heterogeneous materials like wood and concrete, thus to confirm the variables the following assumptions are adopted:

- The classical diffusion theory is applied to find the moisture content field in wood layer; wood is modeled as an orthotropic material in the diffusion problem.
- The classical heat transfer theory is applied to find the temperature field in wood layer, concrete layer, and dowels. All materials are assumed as isotropic materials in the heat transfer problem.
- The diffusion process in wood is assumed to be independent of the temperature field. Ambient temperature is one input parameter for the diffusion problem.
- The stress analysis is solved independently from the diffusion analysis and the heat transfer analysis. Moisture content and temperature fields are input

parameters for the stress analysis, somehow they play a role as the static load does. In the stress analysis, concrete and steel are isotropic materials, wood is an orthotropic material.

- The interaction between wood and concrete layers is solved as a contact problem in stress analysis.

1.3 Research and contributions

The research described in this dissertation was conducted to develop an advanced numerical model to analyze the time-dependent behavior of wood-concrete composite beam with notched shear key. The modeling process includes the diffusion analysis, heat transfer analysis and the stress/displacement analysis. The main focus of the research was to expand available constitutive models of wood and concrete materials so that they can be used in the 3D finite element method. The 3D constitutive models of wood and concrete were then implemented in the commercial software ABAQUS by using the user-subroutine UMAT. A creep test with two wood-concrete composite beams with notched shear keys has been conducted to provide data to validate the model.

The results of verification model for one test specimen captured closely the observed time-dependent behavior of the test specimen. It indicates that the assumptions used in the research are acceptable and the proposed model is reliable. The results of the proposed 3D model also showed some improvement if compared with the obtained results from using an available 1D model (Fragiacomo [4, 5]). The application of a 3D finite element model with solid elements allows one to model the time-dependent behavior of wood-concrete composite structures with any level of geometric and boundary complexities. The application of the proposed model can be used in various

parametric studies to address remaining questions about time-dependent behavior of any type of the wood-concrete composite beams and decks.

Chapter 2

Literature Review

In civil engineering, the first composite structure was likely a wood-wood composite structure. The appearance of this type of structure was necessary because of two main reasons: the limit of natural dimension of tree-trunk cross-sections, and low efficiency in load-carrying purpose of wood in its natural form. The composite cross-section is often made by super-imposing element cross-sections together with mechanical joints or adhesives. Wood-wood composite structures with various types of cross-sections are widely used for beam and floor structures.

The attempts to configure wood-concrete structures began in the period of 1934-1954. A total of 198 timber-concrete composite deck bridges were built in the state of Oregon [6]. However, there were not many subsequent reports about wood-concrete composite structures until 1970s; and the wood-concrete composite structures with various type of connection technologies accompanied by analytical models only has focused the interests of other researchers since 1980s.

In general, wood-concrete composite used in bending resistant applications consist of the lower layer – solid sawn wood or glulam, the upper layer – plain or reinforced concrete, and the connection between two layers. The primary difference between the various systems proposed is the interlayer connection concept.

2.1 Structural types and applications

For the timber-concrete bridges in the state of Oregon, the bridge deck consisted of a reinforced concrete roadway slab, acting compositely with creosote-treated timber

stringers via a shear connection between the concrete and timber layer. McCullough et al. [6] investigated timber-concrete composite decks including steel dowels, steel rings and notched shear type connectors. The authors showed that the timber - concrete composite bridge construction was technically and economically feasible. As noted by Eby [7], many of the bridges built using this technology were still in service in 1989.

In early 1980's wood-concrete composite structures were used in the building either for new residential floors and renovation and strengthening historic building floors. Godycki et al. [8] studied the composite efficiency of nail and notched connection in wood-concrete composite floors such as illustrated in figure 2.1. As a result, in 1981 more than 1000 m² of existing timber slabs in public buildings in Lodz, Poland were strengthened by using this technique.

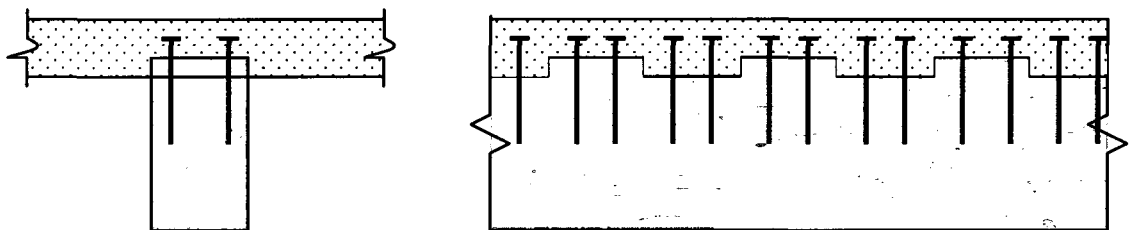


Figure 2.1 – Nail and notch connection.

To strengthen existing timber slabs in Vienna in 1984, Zajicek [9, 10] used screwing bolts ($\Phi 16$ mm) as shear connectors between old timber floors and an added reinforced concrete layer on top (figure 2.2). The static load bearing ability of composite system was reported to be 250% higher than that of the old timber slab.

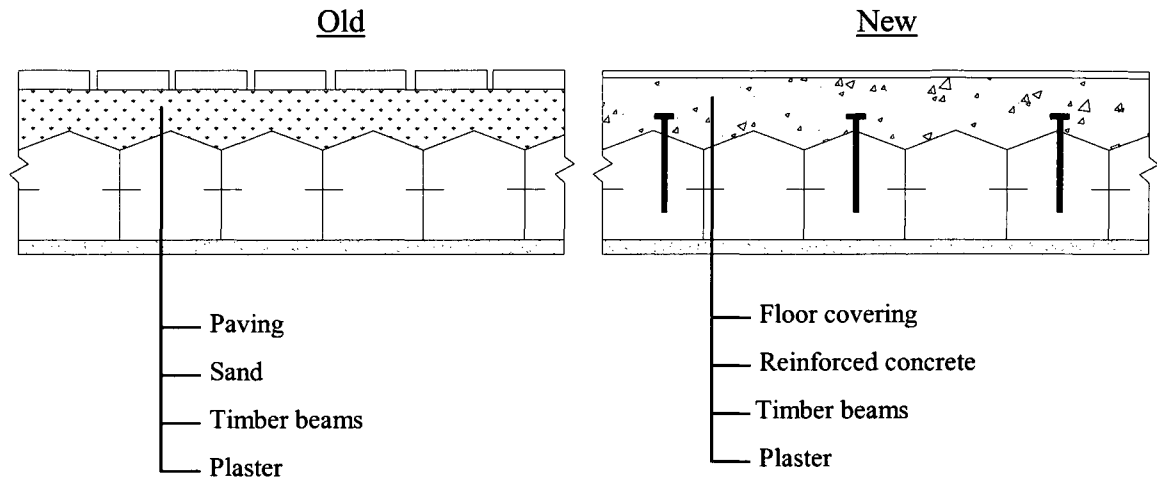


Figure 2.2 – Restrengthening of existing timber slabs, Vienna 1984.

In the early 1980's, Murthy [11] reported his use of a timber-concrete floor system in buildings. In that system, he used horizontal mild steel dowels that pass through the timber beams and are embedded in concrete as shear connectors (Figure 2.3). It was mentioned that the connection prevented almost all inter-layer slip with high composite efficiency; the composite actions being not only contributed by horizontal shear connectors but also by frictional resistance between the wood and concrete surfaces. He also states that the up-lift resistance of the horizontal shear connectors increased considerably.

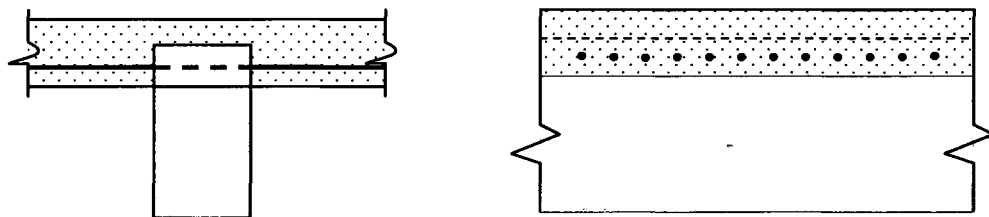


Figure 2.3 – Horizontal dowel connection.

To improve mechanical behavior of the connection system, in some cases, epoxy resin was used. In one variation of dowel connector type, holes were drilled slightly larger than nominal diameter of the dowels; the holes were then filled with epoxy resin; and after

which the dowels were inserted as depicted in Figure 2.4. The advantage of this type of connections is the stiffness provided in both vertical and horizontal directions [12].

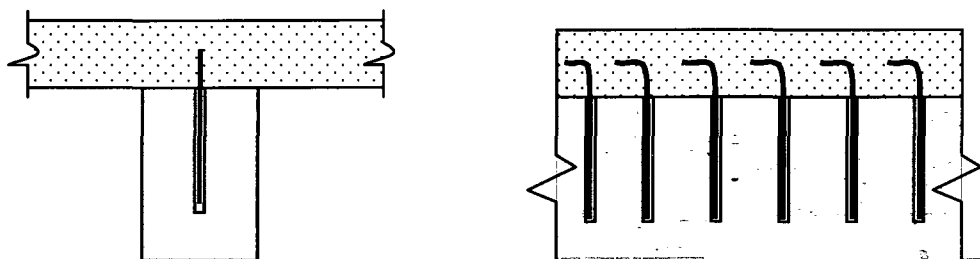


Figure 2.4 – Glued steel bar connection.

In a similar way, Messina [12] attempted a connection system where steel C and V sections were positioned on the top surface of a timber beam by screws, and then epoxy would be applied to develop the strength between wood layer and screws.

In 1984, Nauta [13] described two different wood-concrete composite systems applied in bridges in New Zealand since 1970. One of those systems consisted of a glue, laminated beam connected with a concrete slab by glued shear timber blocks combined with mechanical fasteners (Figure 2.5). This system has been used in some bridges with spans ranging from 10.8 m to 24.5 m. The other system consists of a nailed timber slab connected to the concrete slab by using notches and triangular steel plates. The second system has been used in a bridge of 4.8 m span.

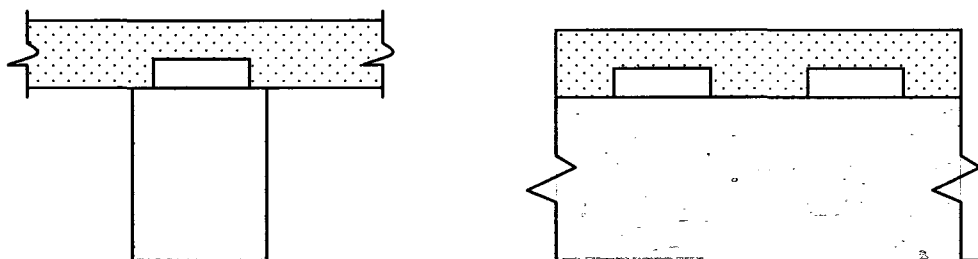


Figure 2.5 – Glued timber block connection.

In 1987, Küng [14] tested a system using screws in various arrangements. The results show that if screws are driven in an angle of 60° to the inter-layer surface the load capacity as well as the slip modulus doubles in magnitude compared to use of a vertical screw arrangement. The enhancement of this arrangement is due to the fasteners being oriented so not only could they carry shear but also compression and tension forces.

In 1990, Ceccotti and Covan [15] presented one of the strongest and stiffest joints. A “T” steel profile used as shear connectors with the web inserted and glued into the timber beam by epoxy resin (Figure 2.6). The flange of the “T” has an iron lattice welded to it, to be embedded within the concrete. The continuity of the connections along the beam with wide steel flange provides high composite action and resists uplift.

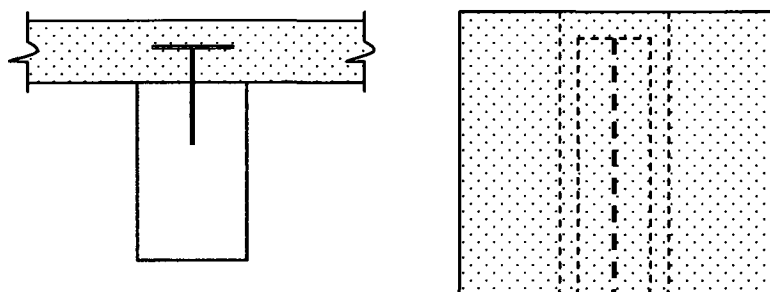


Figure 2.6 - “T” steel profile connection

Another continuous connector system was introduced by Bathon and Graf [16] in 2000. The shear connector used was a steel mesh, with the lower half inserted and glued into the wood layer and the upper half embedded in concrete layer. This shear connector can be applied for either a T-beam system or a plate system. In a report by Clouston et al. in 2005 [17] about testing the system based on this shear connector, the authors stated that this system achieved a very high composite action (97%) if compared with other wood-concrete composite systems. That solution is suitable for both new and upgraded floor

systems; however, to apply it for bridge structures under repeated loading, further investigation must be done.

In 1993, Ahmadi and Saka [18] tested timber-concrete T-beams using high-strength nails as shear connectors. This research showed that the proposed system satisfies the limits set by standard building codes such as AITC Timber Construction Manual [19] and ACI 318-89 [20], improves stiffness, reduces number of timber joists, and attains the same receptivity to a hot and aggressive environment if compared with non-composite timber-concrete floors widely used in the Persian Gulf regions.

To reduce the labor cost in construction of wood-concrete composite structures, some standard commercial shear connectors were presented. SFS Provis AG developed a high strength steel fastener specialized for timber-concrete structures [21]. This screw-type fastener has two heads; the upper head is used to screw the fastener into the timber and afterward anchors it to the concrete layer; the lower head is used to calibrate the depth of the fastener when it is positioned at the surface of the wood layer. Another wood-concrete fastener was introduced by Sonda [22] in 2001. It has a stud welded into a toothed plate; attached to the wood layer by two screws.

In 1999, Mungwa et al. [23] reported an experimental study of a wood-concrete beam with the flexible shear connectors developed by INSA-Hilti (Figure 2.7a, 2.7b). These connectors are driven to the wood-layer by using the multi-purpose Hilti cartridge-operated gun. The results from the tests showed that this connector possesses high rigidity, ductility and ultimate strength. Another type of Hilti fastener (Figure 2.7c) that can be applied in wood-concrete composite was reported by Said [24] in 2002. The upper

part of this fastener has conical shape which increases the plastic deformation capacity before failure, and the lower part is glued into a hole in the wood.

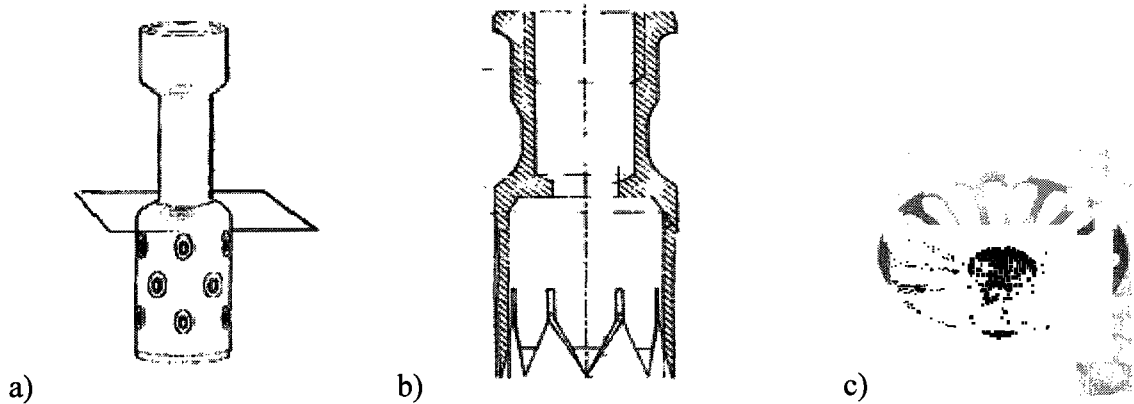


Figure 2.7 - Hilti's fasteners.

In wood-concrete composite structures, the composite efficiency depends on ability to transfer the interlayer shear force. One of the most efficient ways to transfer the shear force is to create contact compression surfaces between wood and concrete layers; as a consequence of that, many notched type connections have been developed in wood-concrete composite structures. The simplest version of notched type connections was used in bridges built in New Zealand as cited above. In 1996, Yttrup and Nolan [25] presented another system combining notches on the horizontal surface and the vertical surface of the timber beam to provide both shear and uplift resistant abilities (Figure 2.8). The solution proved that this connection is strong and stiff, but it time consuming to make the notches and difficult to fill them completely with concrete. In 1999, van der Linden [26] tested a notched joint which consisted of drilled circular notches in a laminated veneer lumber (LVL). With a diameter of each notch of 125 mm, this type of connection is only suitable for floors or wide beam structures with a minimum width of 160 mm (Fig 2.8).

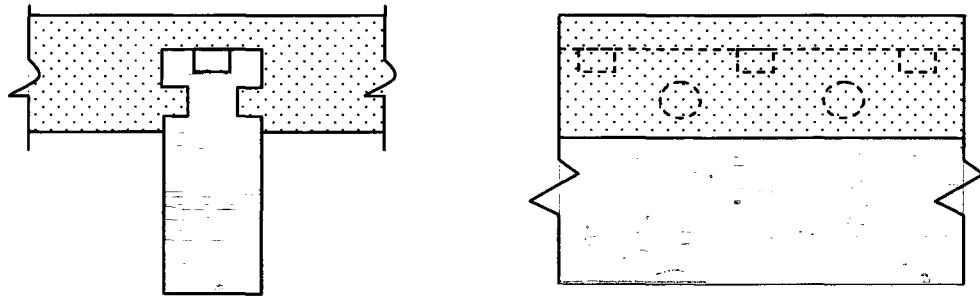


Figure 2.8 – Combined notches.

In spite of its efficiency to transmit the shear forces, the notched type connection itself cannot prevent the uplift when a structure is loaded (except for the combined notch type in Figure 2.8), so to do that it must be used in combination with other types of fasteners. The aforementioned application of Godycki [8] in Poland is an example. In 1992, Wenner [27] combined circular notch with steel bar in his approach to increase shear strength and stiffness.

One of most efficient notched joints was proposed by Natterer [28] in 1990, see earlier in Fig 1.1. He combined the notch with threaded dowel that will be post-tensioned after the concrete cures. The post-tensioned dowels prevent uplifting of concrete, transfer a small portion of shear force, and increase the frictional resistance between two layers. They also allow the partial recovery of bearing lost during curing of the concrete due to shrinkage. When the floor/decks are loaded, most of interlayer shear force is transferred through the contact compression surfaces (the inclined or vertical surface in the support side of the notch), and a small portion of the interlayer shear force is transfer through the dowels and through the friction at the contact regions. This type of joint was applied successfully in some pilot projects in Europe. For example, early applications included a 5-story apartment building and a 4-story school building, among others.

This notched joint has been the subject of further study at CSU with a goal of applying it to commercial building and bridge structures in the USA. Various facets of Natterer's connection detail and the optimum values of its variables have been examined extensively at Colorado State University. Details are available in several theses (Brown 1998 [29]; Koike 1998 [30]; Etournaud 1998 [31]; Fast 2003 [2]), proceedings papers (Gutkowski et al. 1999 2000, 2001 [3, 32, 33]), and journal papers (Gutkowski et al. 2004 [34, 35]).

Brown [29] and Etournaud [31] performed various withdrawal tests to ascertain which adhesive, of three considered, would provide the best bond of the bolt to the wood. As a result of these withdrawal tests the Hilti HIT HY 150 adhesive was selected as the adhesive system for this application. Brown [29] and Thompson [36] performed various slip tests to ascertain the slip modulus of the notch. Thompson examined various types of dowels and washers; on the other hand, Brown varied the notch depth and width of the wood component to see how these variables affected the resulting slip modulus. In these test, the angle of the notches was 15° from vertical plane. This work led to the adoption of the detail shown earlier in Figure 1.1 for further research on floor systems. Etournaud also tested two wood-concrete decks: 1) a one-way span rectangular deck with clear span of 136 inches (345cm), and 2) a skewed one-way span deck with clear span of 203 inches (518 cm), 106.5 inches (271cm) wide, and a skew angle of 39° . The results showed that the anchored notch connection produced a high degree of composite action of the layered decks. For a point load placed in the middle of the decks, he reported composite efficiencies of 92.2% and 81.1% for the rectangular and skewed decks, respectively. Fast [2] performed cyclic load tests up to 21,600 cycles, ultimate load tests, and long-term

creep tests on beam specimens based on a beam configuration developed from results of the previous CSU research. His results indicated that the long-term load, leading to creep, has a greater effect on lowering the stiffness and composite action of the wood-concrete beam than cyclic loading does.

In recent years, with the development of new adhesives and gluing techniques, using adhesives as an interlayer shear connection in layered wood-concrete composites has been examined by Negrão et al. [37], Brunner and Gerber [38]. These techniques can lead to a high interaction between wood and concrete at a reasonable price. However, the research results performed by Negrão et al. showed that a glued connection is very brittle at failure.

In general, most wood-concrete structures are applied as floors in buildings or decks in short-span bridges, only few are used as beam structures. Some systems have a T-beam equivalent cross section; other systems have a rectangular cross section. The connections of wood-concrete composite structures can be categorized as following main groups: mechanical connection, glued connection, notched connection, and combinations from these three original connections. Dias [39] summarized the mechanics performance of the different types of connections; these characteristics can be easily seen in Figure 2.9 cited from his dissertation. This figure illustrates the general load-slip behavior observed in slip tests (also called “push out” tests) of the various connections under interlayer shear. Glued and notched joints have high strength and stiffness, with an almost linear behavior up to the failure which occurs at low value of deformation. The dowel only type fasteners have small strength and stiffness but have higher plastic deformation capacity. Other

types of connections are a compromise between strength, stiffness and plastic deformation.

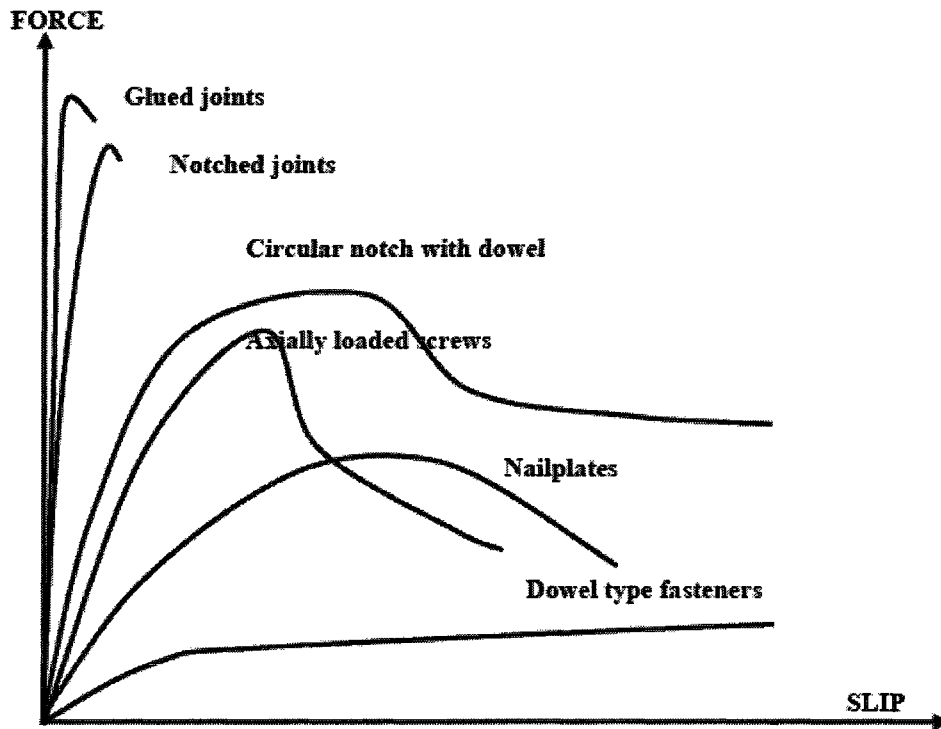


Figure 2.9 - Typical load-slip behaviors of different types of joint (adapted from Dias [39]).

2.2 Computational models

2.2.1 Development of structural computational models

Layered wood-concrete composite structures are systems combining two materials so as enable them to work together. The design engineer desires to achieve the highest degree of composite action, ideally a “fully composite”. However, this state cannot be achieved in real structures. Real composite structures are only “partially” composite. From a structural analysis standpoint, they perform between two limit states of layered composite structures, namely “fully composite” action and “fully non-composite” action. At the

fully composite limit state, as commonly defined, there is no interlayer slip and the cross section is monolithic. At the fully non-composite state, the two layers are not interconnected and the interlayer shear is only transmitted by friction in the interlayer contact region, and these characteristics lead to the occurrence of the highest interlayer slip. The methods of analysis are quite simple for those two limit cases. When the system is fully composite, the method of transformed sections applies; and when the system is fully non-composite, the stiffness is computed by simply adding the stiffness of the individual member sections. The actual behavior of a wood-concrete composite system is somewhere in between of the two limits and neither of the above methods of analysis is applicable. Obviously the analysis of partially composite wood-concrete structures becomes much more complex when restrained slip occurs between two layers.

Most of applications of wood-concrete composite structures are floors for buildings or decks for bridges. Thus, in reality they are stiffened plate systems. For that reason most pilot structures used in laboratory tests are beams. Consequently, in many cases the analytical model is based on isolating a portion of the stiffened plate as a T-beam, composed of a concrete flange and a wood web. In addition, using full-size physical floor or deck specimens is time-consuming and expensive. Use of a beam models in analysis is sometimes sufficient to comply with requirements of building codes.

The first analytical models of partially composite structures were in wood-wood and steel-concrete beams done by Clark [40] and Newmark et al. [41], respectively, in the 1950s. Similar models were developed by many other authors and then adapted to apply to wood-concrete composite structures. In 1992 Werner [27] introduced a linear elastic model taking into account the slip between wood and concrete based on previous works

by Newmark et al. [41] and Möhler [42]. Werner's model was based on the differential equation of equilibrium of the layered beam. The model is simple and easy to use, for those reasons it is widely used and presented in Annex B of Eurocode 5 [43] to analyze timber-timber composite structures. The same method was then extended by Ceccotti [44] to wood-concrete composite structures. However, there are some limitations when applying this model such as the geometry of elements, type of applied loads, and nature of interlayer connection, and materials. To overcome these limitations, Natterer and Hoeff (1992) [45] developed a model derived from the general differential equation to consider different loading conditions as well as the effective widths of the concrete slab.

Typically for wood-concrete composites in which the interlayer shear connection is composed of discrete mechanical connectors, the load-slip behavior of shear connectors is nonlinear. In addition, failure analysis often considers the nonlinearity of the materials. Using simplified or closed form analytical methods one often cannot include nonlinear connector behavior which leads to non-conservative results under certain conditions. Thus recently, the finite element method has been employed by several authors to overcome that limitation. Zakaria and Ghazali [46], Ahamdi and Saka [18], Van der Linden [26], and Dias [39] were among those authors to use finite element method in their research as a tool of analysis.

At CSU, from a development of Goodman [47, 48] about the mathematical theory of layered wood beams system and extended by Ko [49], a finite element program FEAFLO was developed by Thompson et al. [50, 51], Vanderbilt et al. [52], and Tremblay et al. [53] for modeling wood joist floor systems. The model adopted in the program was simplified by the assumption of linear load-slip behavior. A sub-program of

FEAFLO was FEABEA program used for modeling layered beam system. Later, Wheat [54] expanded FEAFLO to NONFLO, in which non-linear load-slip connection behavior was included. Both FEABEA and NONFLO were based on the use of the total potential energy expression for each element in functional form as:

$$\begin{aligned}
J_e = & \sum_{i=1}^{n_L} \int_0^{L_e} \left[\frac{1}{2} E_i I_i \left(\frac{d^2 y}{dx^2} \right)^2 + \frac{1}{2} E_i A_i \left(\frac{du_i^a}{dx} \right)^2 \right] dx \\
& + \sum_{i=1}^{n_L-1} \int_0^{L_e} \frac{1}{2} \left(\frac{k_i n_i}{s_i} \right) \left[\left(u_{i+1}^a - u_i^a \right) - \frac{1}{2} (h_{i+1} + h_i) \frac{dy}{dx} \right]^2 dx \\
& - \int_0^{L_e} w y dx
\end{aligned} \tag{2.1}$$

In which

L_e = length of element,

E_i = modulus of elasticity of layer i ,

I_i = moment of inertia of layer i about its own centroid,

n_L = number of layers,

y = vertical deflection,

A_i = cross-section area of layer i ,

u_i^a = axial deformation of layer i ,

k_i = connector stiffness between layer i and $i+1$,

n_i = number of rows of interlayer connectors between layer i and $i+1$,

s_i = spacing of interlayer connectors between layers i and $i+1$,

h_i = thickness of layer i , and

w = applied load per length of beam.

In Equation 2.1 the second term presents the total potential energy due to interlayer slip in all interlayers of an element.

Later, Chen et al. [55] utilized the FEABEA program to model layered wood-concrete T-beams in his research. He showed that a simple nailed (dowel type) interlayer connection produced extremely low efficiency of composite action. And then Koike [29] (1998) also adapted FEABEA to layered wood-concrete rectangular beams connected by notched shear keys.

In 2002, Wieligmann [56] used commercial FEM software, AxisVM [57], to model the slip test and beam specimens previously load tested by Brown [29]. He modeled Brown's connection detail by using plane stress element and gap elements to compare with the results of Brown's slip test. The failure mode in his results agreed with experimental results of the slip test. Wieligmann's FEM modeling of the slip test apparatus indicated that the measured slip modulus values reported by Brown were considerably smaller than the predicted values. He surmised that the device used may have been inaccurate due to possible misalignment of the heavy, bulky wood-concrete specimens and unintended relative movement of the device's component pieces. The device had been developed previously for much lighter wood-wood specimens. Also, his FEM model could not consider the drying and shrinkage effects of the concrete and wood that would create a gap between two layers and loosen the connections. To analyze the beams with notches, Wieligmann developed two models: 1) a beam model with node-to-node links at notch locations, and 2) beam model with detailed 2D plane stress FEM notch modeling. In the first model, notches were modeled by node-to-node link elements with stiffness in longitudinal direction of the beam taken from slip modulus. In the second model, notched area was modeled by using plane stress elements for wood and concrete, gap elements to model the interaction between two layers. Since the width of the notch in Brown's shear

test specimen was smaller than the width of his beam specimens the average stiffness from shear tests was used in the first beam model. This led to the conclusion that the deflection predicted by the first model was smaller than that of second model and of the Brown's beams. This also raises a curiosity about the effectiveness of the dowel as the width of the beam increases. The second FE beam model of Wieligmann was in a quite good agreement with experimental results, but it can only be used to model narrow beams because it was a 2D plane stress analysis.

2.2.2. Computational models for long-term analysis of wood and applications for layered wood-composite systems

Both wood and concrete are rheological materials, therefore time-dependent analysis plays an important role in understanding behavior of wood-concrete structures under long-term loading. Long-term effects on wood-concrete composite structures include:

1. Normal creep of wood and concrete. The normal creep is the variation of strains in time under non-zero constant stresses.
2. Shrinkage and swelling of the exposed wood and concrete. Shrinkage/swelling causes variation of strains in time even in absence of applied stresses.
3. Creep of the interlayer connection.
4. Repeated loading reduces stiffness and composite action of the whole structure (mainly because repeated loading reduces the "rigidity" of the interlayer connection).

5. “Mechano-sorptive” effect of wood. The mechano-sorptive effect is the increase of creep in time due to variations of timber moisture content.

Among these effects, the mechano-sorptive is rather complex. Several mechano-sorptive models for wood were proposed. The first model considering the effect of moisture content was proposed by Leicester in 1971 [58] when he studied deflections of a timber beam in a drying cycle. This simple model is similar to a Maxwell rheological model which contained two elements in series. Total deflection Δ was taken to be composed of an elastic component Δ_e and a mechano-sorptive component Δ_m that were related to the load parameter as

$$\Delta = \Delta_e + \Delta_m, \quad (2.2)$$

$$\Delta_e = KP, \quad (2.3)$$

$$\Delta_m = -\frac{d\Delta_m}{dm} = P \cdot f(m), \quad (2.4)$$

where m is the average moisture content of the beam, $f(m)$ is a function of moisture content. For ease of understanding, the model can be represented schematically as shown in Figure 2.10.

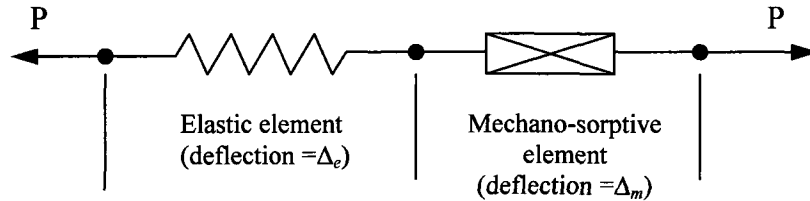


Figure 2.10 - The first approximation rheological model (Leicester [58]).

Ranta-Maunus (1975) [59] developed an alternative mechano-sorptive model for wood that considered the effect of variation of moisture content in both drying and wetting

changes. He referred to his development as the “theory of hydroviscoelasticity” since it based on a similar mathematical formulation of the theory of thermoviscoelasticity. The general and symbolic constitutive equation used by Ranta-Maunus can be expressed as

$$\varepsilon(t) = \int_0^t J(t-\tau) d\tau + \int_0^t \left\{ K(t-\tau)\sigma(\tau) + L(t-\tau)[\sigma(t) - \sigma(\tau)] [u(t) - u(\tau)] \right\} du(\tau), \quad (2.5)$$

where J is normal creep function; K relates to the creep that arises from a constant stress distribution; and L indicates a recovery phenomenon. u is the moisture content function.

In 1992 Mårtenson [60] introduced a constitutive model in rate form, i.e. the time derivatives of strain are function of stresses and moisture condition. In his model the strain rate $\dot{\varepsilon}$ is assumed to consist of four main parts, one elastic part, one part describing creep under constant humidity condition, one part describing the shrinkage-swelling behavior, and one the mechano-sorptive part. The general constitutive relation is of the form

$$\dot{\varepsilon} = \dot{\varepsilon}_e + \dot{\varepsilon}_c + \dot{\varepsilon}_{st} + \dot{\varepsilon}_{ms}, \quad (2.6)$$

where: $\dot{\varepsilon}_e = \frac{\dot{\sigma}}{E}$ is the elastic strain rate,

$$\dot{\varepsilon}_c = \frac{d}{dt} \left[\sum_{n=1}^N \int_0^t J_n \left[1 - \exp\left(-\frac{\xi(t) - \xi(t)}{\tau_n}\right) \right] d\sigma(t') \right] \text{ is the pure creep strain rate,}$$

$$\dot{\varepsilon}_{st} = (\alpha - \Delta\alpha)\dot{u} \text{ is the shrinkage-swelling strain rate,}$$

$$\dot{\varepsilon}_{ms} = m\sigma\dot{u} \text{ is the mechano-sorptive strain rate.}$$

In above equations, u is the moisture content, σ is the current stress, α is the shrinkage-swelling coefficient, E is the elastic modulus, and m is the mechano-sorptive parameter. The formulation of the creep strain rate is a conventional viscoelastic formulation with material parameter J_n , τ_n , and the material time ξ . All material parameters can be functions of the moisture content.

Also in 1992, Toratti [61] proposed mechano-sorptive models that fit his test results. The strain of wood when subjected to loading and moisture content variation is assumed to consist of the following additive parts: elastic strain, normal creep strain, mechano-sorptive creep strain, and free shrinkage strain.

$$\varepsilon(t) = \varepsilon_E + \varepsilon_{visk} + \varepsilon_{ms} + \varepsilon_u. \quad (2.7)$$

In equation (2.7), the elastic strain depends on both the elastic modulus and moisture content, as expressed in empirical form as

$$\varepsilon_E = \sigma J_0(u) = \frac{\sigma}{E_0(u)},$$

$$E_0(u) = \frac{1}{J_0(u)} = 14000(1 - 1.06u) \text{ [MPa]}, \quad (2.7a)$$

u : moisture content of wood [-].

The normal creep was modeled by six Kelvin rheological elements in series:

$$\varepsilon_{visk} = J_0(u_{ref}) \int_0^t \left\{ \sum_{n=1}^6 J_n \left(1 - e^{-\left(\frac{t-t'}{\tau_n}\right)}\right) \frac{d\sigma}{dt'} \right\} dt'. \quad (2.8)$$

$J_0(u_{\text{ref}})$ from Equation 2.7a with $u_{\text{ref}} = 0.2$ [-],

σ : stress [MPa],

t : time [days],

J_n [-] and τ_n [days] are pairs of pre-defined values.

The free shrinkage of wood parallel to grain is assumed to be dependent on the strain of wood:

$$\varepsilon_u = \{\alpha - b\varepsilon(t)\} \Delta u.$$

α : shrinkage coefficient parallel to grain,

$$b = 1.3 \text{ [-]},$$

Δu : moisture content increment.

For mechano-sorptive creep strain, Toratti proposed three models: linear model, creep limited model, and combined mechano-sorptive model. By comparing the test results with proposed mechano-sorptive model, he showed that the combined mechano-sorptive model described very well the creep and the recovery behavior in all cases. The formulations of the combined mechano-sorptive model are not the same for tension stress and compression stress. For tension stress:

$$\varepsilon_{ms} = J^\infty \int_0^t \left\{ 1 - \exp \left(-c \left(\sum_0^t |\Delta u| - \sum_0^{t'} |\Delta u| \right) \right) \right\} d\sigma(t'), \quad (2.9)$$

and for compression stress:

$$\varepsilon_{ms} = J^\infty \int_0^t \left\{ 1 - \exp \left(-c \left(\sum_0^t |\Delta u| - \sum_0^{t'} |\Delta u| \right) \right) \right\} d\sigma(t') + J_0(u_{ref}) e^{\int_0^t \sigma(t') |du(t')|}. \quad (2.10)$$

All the above expressions of mechano-sorptive phenomenon are linear models. In 1995, Hanhijärvi et al. [62, 63] introduced a non-linear model for viscoelastic and mechano-sorptive which can be expressed in a diagram as shown in Figure 2.11.

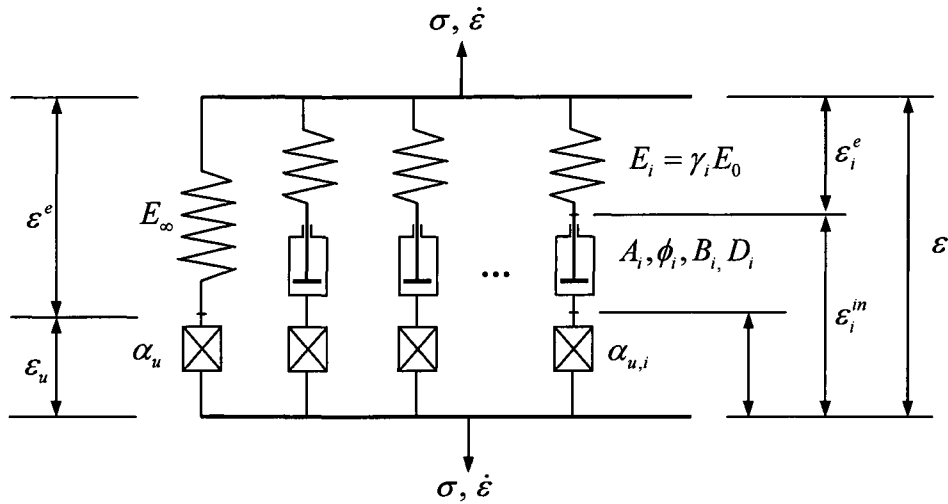


Figure 2.11 - Rheological model for coupled viscoelastic and mechano-sorptive creep of wood (Hanhijärvi [62]).

In this model, the total strain rate is expressed in the follow equation:

$$\dot{\varepsilon}_i = \frac{\dot{\sigma}_i}{E_i} + A_i \sinh[\phi_i \sigma_i + B_i \tanh(D_i \dot{u})] + \alpha_{u,i} \dot{u}. \quad (2.8)$$

A_i , ϕ_i , B_i , and $\alpha_{u,i}$ are material parameters satisfying $A_i B_i D_i + \alpha_{u,i} = \alpha_u$ (based on an assumption that all parallel elements have a common moisture expansion coefficient α_u in the case of slow moisture penetration). The model was then reformulated for three-dimensional states of stress by Helnwein and applied to FEM model of a bending beam and a wood joint structure [64]. Their three-dimensional analyses gave enhanced insight

to the interaction between sorption and the time-dependent mechanical behavior. The two example studies also proved the general applicability of their developed model.

The most recent model was introduced in 2003 by Bou-Saïd [65] and Chassagne et al. [66]. He presented a three-dimensional non-linear hydroviscoelastic model, combined with hygro-expansion effects. That model is able to describe creep and recovery phenomena of wood under variable humidity conditions. The stress and strain relation can be written in incremental form as:

$$\forall t, \Delta t : \quad \Delta \sigma_{ij} = \bar{E}_{ijkl} \Delta \varepsilon_{kl} + \sigma_{ij}^{hist}, \quad (2.9)$$

where

$$\bar{E}_{ijkl} = \frac{1}{\Delta t} \sum_{\mu=1}^m \left[\frac{E_{\mu,ijkl} \left(1 - e^{-a'_{\mu,ijkl} S_{\mu}(\bar{k}) \Delta t} \right)}{a'_{\mu,ijkl} S_{\mu}(\bar{k})} \right] + \sum_{\chi=m+1}^n \left[\frac{E_{\chi,ijkl} \left(1 - e^{-\frac{a_{\chi,ijkl} \Delta w}{(be^{-c \cdot w^{hist}} - d)} S_{\chi}(\bar{k})} \right)}{\frac{a_{\chi,ijkl} \Delta w}{(be^{-c \cdot w^{hist}} - d)} S_{\chi}(\bar{k})} \right] \quad (2.9a)$$

$$\begin{aligned} \sigma_{ij}^{hist} = & \sum_{\mu=1}^m \sum_{k=1}^3 \sum_{l=1}^3 \sigma_{\mu,ijkl}(t) (e^{-a'_{\mu,ijkl} S_{\mu}(\bar{k})} - 1) \\ & + \sum_{\chi=m+1}^n \sum_{k=1}^3 \sum_{l=1}^3 \sigma_{\chi,ijkl}(t) \left(e^{-\frac{a_{\chi,ijkl}}{(be^{-c \cdot w^{hist}} - d)} S_{\chi}(\bar{k})} - 1 \right) \end{aligned} \quad (2.9b)$$

\bar{E}_{ijkl} is a fictitious modulus tensor, σ_{ij}^{hist} represents the effect of the stress history on the current response. $\Delta \sigma_{ij}$ is the stress increment tensor, $\Delta \varepsilon_{ij}$ is the total strain incremental tensor minus the free strain increment tensor induced by shrinkage and thermal expansion, and $a'_{\mu,ijkl}$, $a_{\chi,ijkl}$ are constants. Shrinkage and swelling strains are assumed to be linear functions of the relative moisture variation. Although it is mathematically

complicated formulation, the Bou-Saïd et al. model basically contains an n Maxwell chain model, where m units represent normal creep; other $n-m$ units represent mechano-sorptive creep. The activation of m normal creep units depends on the stress level and is implemented by using rate-process theory. These units serve to describe the non-linear dependence of normal creep rate on stress. Otherwise, the activation of $n-m$ mechano-sorptive creep units depends on the rate of the relative moisture changes, the accumulated moisture history, and the stress level.

All of the preceding models that include mechano-sorptive were verified with experimental results obtained from laboratory tests conducted either by the original authors or by other researchers. Most experimental results were taken from bending tests of either small-scale or full-scale beams; consequently most models were used in the form of a uniaxial flexural stress state. Later Hanhijärvi and Bou-Saïd et al. applied their respective models to multiaxial stress states.

For structures exposed to the outdoor environment or the structures in high variation of moisture content, the long-term behavior of wood-concrete structures is rather complex. In such cases, a numerical procedure is employed in order to find accurate solutions. Few numerical approaches have been introduced to date. For example, Capretti [67] (1992) used Ranta Maunus [59] model to describe the rheological behavior of timber and connection of timber-concrete beams; Kulmann and Schänzlin [68] (2001) employed the Hanhijärvi [62] model for describing the mechano-sorptive creep of timber in their finite difference algorithm for beams; Fragiaco and Ceccotti [69, 70] (2006) employed Toratti's model [61] to verify the long-term behavior of several timber-concrete beams tested in Florence, Italy.

2.2.3 Creep and shrinkage prediction models for concrete

Concrete exhibits time-dependent strain due to shrinkage and creep. In actual structures, shrinkage and creep occur simultaneously and the treatment of two together is often convenient in practical engineering. The time-dependent deformation of concrete may severely affect the serviceability, durability, and stability of concrete structures or concrete composite structures.

Creep and shrinkage of concrete are affected by many factors such as strength of concrete, age of concrete at loading, type of curing conditions, ambient conditions, type of cement and aggregate, water/cement ratio, size and shape of member, type and duration of loading etc. The study of creep and shrinkage of concrete interested many researchers for a long time. A number of models to predict creep and shrinkage of concrete have been proposed. Early mathematical models were developed to facilitate structural analysis. The introduction of computer technology made it possible to use highly rigorous models, the recent modeling focus on predicting experimental data as closely as possible. Some analytical models have been standardized as code provisions for concrete structures design in practical engineering such as ACI-209R-92 model [71] and the CEB-FIP-1990 code model [72]. These models as well as other recent models like the B3 model [73], Müller et al. model [74], and GL2000 model [75, 76] are based on extensive research and experimental studies. All these models provide formulas for time-dependent modulus of elasticity, shrinkage, and creep compliance. The main formulations of ACI-209R-92 model and CEB-FIP-1990 are summarized in this section.

ACI-209R-92 code provisions

This provision provides a procedure for prediction of creep and shrinkage for normal weight and light weight concrete using both moist and steam curing, type I and III cement under standard conditions.

Modulus of elasticity

$$E_c(t) = 0.04326 \sqrt{\rho^3 f_{cm} \left(\frac{t}{a+bt} \right)} \quad (\text{MPa}) \quad (2.10)$$

where a , b are constant, which depend on type of cement and curing condition; ρ is the density; f_{cm} is the measured mean compressive strength at 28 days (MPa); and t is age of concrete (days).

Shrinkage

$$\varepsilon_{sh}(t, t_c) = \frac{(t - t_c)}{T_c + (t - t_c)} \varepsilon_{shu} \quad (2.11)$$

where $t_c = 7$ days for moist cured concrete and 1-3 days for steam cure concrete; $T_c = 35$ days for cured concrete and 55 days for steam cure concrete; ε_{shu} is ultimate shrinkage, $\varepsilon_{shu} = 780$ for standard conditions.

Creep

$$J(t, t_0) = \left[\frac{1 + \phi(t, t_0)}{E_c(t_0)} \right] \quad (2.12)$$

$$\phi(t, t_0) = \frac{v_u (t - t_0)^\psi}{d + (t - t_0)^\psi} \quad (2.13)$$

where v_u is the coefficient for age at application load; d is a constant, normally between 6 and 30 days; ψ is a constant, normally between 0.4 and 0.8; t_0 is age of concrete at time of loading (days)

CEB-FIP 1990 model

This model is restricted to apply for ordinary structural concrete, having 28 days mean cylinder compressive strength ranging between 12 and 80 MPa, mean relative humidity of environment ranging between 40% and 100% and mean temperature ranging between 5 °C and 30°C.

Modulus of elasticity

$$E(t_0) = E_c \sqrt{\exp \left\{ S \left(1 - \sqrt{\frac{28}{t_0}} \right) \right\}} \quad (2.14)$$

where E_c is modulus of elasticity of at the age of 28 days (MPa); S is a constant depends on the type of cement used.

Shrinkage

$$\varepsilon_{sh}(t, t_c) = [160 + 10\beta_{sc}(9 - 0.1f_{cm})] \times 10^{-6} \beta_{RH} \sqrt{\frac{(t - t_c)}{\left\{ 350 \left(\frac{2A_c}{100d} \right)^2 + (t - t_c) \right\}}} \quad (2.15)$$

where β_{sc} is a coefficient, depends on type of cement; β_{RH} is a coefficient, depends on relative humidity; A_c is the cross-sectional area in mm²; d is the perimeter of the member in contact with atmosphere (mm).

Creep

$$J(t, t_0) = \frac{1}{E_c(t_0)} + \frac{\phi(t, t_0)}{E_c} \quad (2.16)$$

$$\phi(t, t_0) = \left[1 + \frac{1-h}{0.46 \left(\frac{2A_c}{100d} \right)^{1/3}} \right] \left[\frac{5.3}{\sqrt{0.1f_{cm}}} \right] \left[\frac{1}{0.1 + (t_0)^{0.2}} \right] \times \left[\frac{(t-t_0)}{[\beta_H + (t-t_0)]} \right]^{0.3} \quad (2.17)$$

where

$$\beta_H = 150 \left[1 + (1.2h)^{18} \right] \left(\frac{2A_c}{100d} \right) + 250 \leq 1500 ;$$

and h is the relative humidity of the ambient environment in decimal form.

2.2.4 Reasons for a new computational model for the layered wood-concrete composite structures with notched shear keys

From the preceding literature review, layered wood-concrete composite structure with notched shear keys would be a candidate for a potential market of residential buildings and short-span bridges. However, to apply this type of structure commonly as a commercial product, especially for short-span bridges, some important further investigation was necessary.

In the system with pre-tensioned dowels, the tensile load of the dowel will affect the local and overall behavior of the structure. In the pilot wood-concrete composite structures built at CSU, after curing of the concrete, the dowels are tightened, but it is not known

how much and how far away the tightened dowel affects the contact region between wood and concrete layers around that dowel. Studies relating to the tensile load of the dowel, quantity and positional distribution of the dowels on the floor/deck structures would be useful.

The shear transition mechanisms in the wood-concrete composite with notched shear keys is somehow different from other systems that have continuous shear connectors or evenly distributed shear connectors. Using a simplified model such as a beam line element model does not fully reflect behavior of the layered wood-concrete composite floor/deck system with notched shear keys, as the 1D model cannot discretize the notch. Furthermore, a one-dimensional model uses the concept of a “slip modulus” which is highly variable and difficult to measure in physical tests. The “slip modulus” is obtained by direct measurement of the slip from small composite blocks loaded with shear, the “push-out” specimens. As evident in equation (2.1) the slip modulus is theoretically a pure inter shear based material constant. Physical slip tests do not replicate that condition, due to various factors, such as difficulty in eliminating eccentricity of the applied load. The “push-out” test also does not fully represent the way interconnection works in a bending beam which has combined shear + flexure, thus curvature. Thus the improved way to incorporate the connection is to employ the general theory of solid mechanics to solve it. But with a complex system like wood-concrete composite beam with notched shear keys, it is not feasible to find a closed form solution by mean of the general theory of solid mechanics. In this case, the finite element method with 3D elements offers the advantage of discretization of the notch and more complete mechanics representation of the layered beam. In the service life, wood-concrete composite structures will be exposed

to different environmental conditions. As shown by previous researchers, the mechano-sorptive phenomenon happens with all wood and wood-base structures in conditions of relative humidity variations. Any rigorous studies of long-term structural behavior of layered wood-concrete composite beams with notched shear keys under moisture content variation conditions should be done by means of theoretical methods verified by experimental tests. Successful numerical models can help to reduce the expensive experimental tests.

Chapter 3

Related physical phenomena in the research

3.1. Introduction

Wood-concrete composite flexural structures are composed of wood, concrete and an interlayer connection. Connections directly affect the composite efficiency of structures while long-term behavior of wood and concrete as materials affect the long-term behavior of the overall composite structure as well as long-term composite efficiency. Beside normal applied loads that create normal creep for wood and concrete, the changing of weather condition creates the changing of relative humidity and temperature of environment around structures. Relative humidity changing causes the moisture content inside the wood to change, and the variations of moisture content in wood create shrinkage/swelling in wood layer. This variation also directly affects the mechanical properties of wood as well as causing the mechano-sorptive phenomenon in wood material. In addition, a layered wood-concrete beam is an internally statically indeterminate structure where the shear force in the shear-key anchor connection detail is unknown. Since wood and concrete have different thermal expansion coefficients, changing temperature in time makes the composite beam deform over time and the thermal stress fields created within the materials vary with time.

In general, relations between physical phenomena affecting the time-dependent behavior of the wood-concrete composite structures can be schematized as shown in Figure 3.1. At the material level, the long-term behavior of wood depends upon creep, mechano-sorptive creep and shrinkage/swelling phenomena. The long-term behavior of concrete

involves creep and shrinkage/swelling while steel has no creep and shrinkage at normal service conditions. The moisture diffusion process happens in the wood material and the heat transfer process happens in all three materials. At the structural level, because three materials work compositely, any time-dependent phenomenon occurring at the material level will affect the time-dependent behavior of the composite structure. The first part of this chapter considers two physical phenomena due to exposure that affect the long-term behavior of wood-concrete composite beam structures: diffusion of moisture content in wood and heat transfer in both wood and concrete. The second part summarizes basic of the rheological characteristics and the third part describes the numerical approach to solve constitutive equations for rheological materials which is then applied in the succeeding chapters.

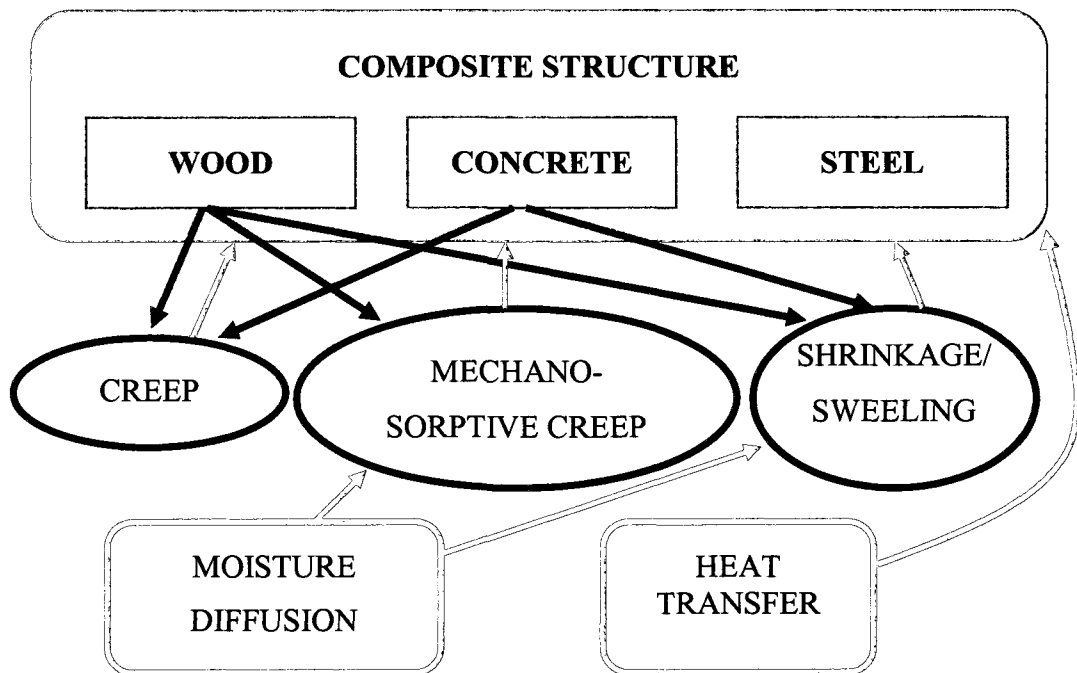


Figure 3.1 Physical phenomena affecting time-dependent behavior of the wood-concrete composite structures.

3.2. Moisture diffusion and heat transfer

In its natural state, wood contains cell wall substance, imbibed and free water, internal voids and extraneous materials including extractives. Although most wood species are commonly thought of as solid and compact materials, because of their cellular structure, they are actually quite porous materials. The relative and absolute amounts of wood substance, imbibed and free water and void space present in wood have a direct effect on the physical and mechanical properties of wood and also upon its seasoning characteristics. In practical engineering, the amount of water present in wood is called “moisture content”, which is defined as the ratio between the weight of the water in wood and the weight of the “oven-dry” wood. To consider the effects of moisture content on long-term behavior of wood, one should take into account moisture content over time of each point in material but not in average sense. These necessitate solving a non-steady state diffusion problem to find the variation of moisture content field in wood over the service time. Similarly, the temperature fields in wood and concrete must be found over time to consider the effect of thermal expansion.

Although the heat transfer and diffusion are expressed by two different groups of equations, namely Fourier’s equations and Fick’s equations, they are mathematically similar. In next section, the mathematical expression of the heat transfer and diffusion problems are summarized and presented side by side.

3.2.1 Mathematical expression of heat transfer and diffusion problem

Steady-state heat transfer and diffusion problem

The 1st Fourier's law

If there is a temperature gradient within a body, heat energy will flow from the region of high temperature to the region of low temperature. The heat flux is proportional with a coefficient that depends on material property.

The 1st Fick's law

If there is a diffusion substance (e.g. moisture content in this research problem) gradient within a body, diffusion substance will move from the region of high diffusion substance density to the region of low diffusion substance density. The diffusion substance flux is proportional with a coefficient that depends on material property.

In general, the 1st Fourier's law and the 1st Fick's law are represented as:

$$\mathbf{q}_T = -\mathbf{k} \frac{\partial T}{\partial \mathbf{x}}, \quad (3.1a)$$

$$\mathbf{q}_w = -\mathbf{D} \frac{\partial w}{\partial \mathbf{x}}, \quad (3.1b)$$

where \mathbf{q}_T is the heat flux vector, dimension of [Joule/(m²·s)].

\mathbf{k} is the thermal conductivity matrix, dimension of [Joule/(m·s°C)].

T is the temperature field, dimension of [°C].

where is \mathbf{q}_w the diffusion substance flux vector, in this case it is moisture content flux, dimension of [kg/(m²·s)].

\mathbf{D} is the diffusivity matrix, dimension of [m²/s].

w is the concentration of diffusion

substance, in this case it is concentration of water in wood, dimension of [kg/m³].

Non-steady state of heat transfer and diffusion problem

The 2nd Fourier's law

The 2nd Fick's law

Or Heat Equation

The temperature profile within a body depends on the rate of its internally-generated heat, its capacity to store some of this heat, and its rate of thermal conduction to its boundaries. The whole process can be expressed by the Heat Equation which is derived from the conservation of energy and the 1st Fourier's law.

The concentration of diffusion substance profile within a body depends on the capacity to store the diffusion substance of the dissolve body, and the rate of diffusion flux through the body. This process can be expressed by the non-steady state diffusion equation which is derived from the conservation of mass and the 1st Fick's law.

Net heat conduct through the boundaries	=	Heat generated within	-	Change in energy stored within
--	---	-----------------------------	---	---

Net diffusion substance transported through the boundaries	=	Change in mass of diffusion substance stored within
--	---	--

Mathematically, this equation can be expressed as:

Above physical process can be expressed as:

$$\frac{\partial q_T}{\partial x} = q_{gen} - \frac{de}{dt} \quad (3.2.a)$$

$$\frac{\partial w}{\partial t} = \frac{\partial q_w}{\partial x} \quad (3.2.b)$$

In wood - concrete composite beam Substitute the concentration flux in right

problem, there is no heat generated within any material after the concrete finishes curing, or $q_{gen} = 0$. The change in internal energy e is related to the body's ability to store heat by raising its temperature, given by:

$$\frac{de}{dt} = \rho c \frac{dT}{dt} \quad (3.3)$$

Substitute the heat flux in right hand side of equation (3.3) by using the 1st Fourier law above to arrive the Heat Equation:

$$\rho c \frac{dT}{dt} = \frac{\partial}{\partial \mathbf{x}} \left(\mathbf{k} \frac{\partial T}{\partial \mathbf{x}} \right) \quad (3.4.a)$$

where :

ρ is the material density, c is the heat specific of material.

Boundary Condition:

In service life, wood-concrete composite beam is exposed to the surrounding environment. If we ignore the radiation heat from the sun (day time, top surface only) then the dominant boundary

Boundary Condition:

The moisture flux through the boundary can be determined by:

$$q_w = S.(w_{eq} - w_{surface}) \quad (3.5.b)$$

where

condition is the heat flux due to heat convection between the solid materials and the air. In that case, the boundary condition can be expressed as:

$$q_{conv} = h(T_{surf} - T_{amb}) \quad (3.5.a)$$

Where

h is the convection heat transfer coefficient.

T_{surf} is the temperature of surface of solid material.

T_{amb} is the temperature of ambient air.

w_{eq} is the equilibrium moisture content in wood. Equilibrium moisture content is defined as that moisture content at which wood is neither gaining nor losing moisture. This equilibrium can be reached if wood stays in an unchanged environmental condition (constant temperature and relative humidity) for a period of time.

$w_{surface}$ is the moisture in the surface of wood.

S is the emission coefficient (m/s^2).

3.2.2 Finite element method to solve heat transfer and diffusion

In this research, the heat transfer and diffusion problem of wood – concrete composite beam are solved by finite element method implemented in the ABAQUS software [77]. Basic derivations of finite element method equations for heat transfer and diffusion are summarized as follows.

A variational statement for the Heat equation is obtained directly from the standard Galerkin approach as:

$$\int_V \delta T \left\{ \frac{\partial}{\partial \mathbf{x}} \left[\mathbf{k} \frac{\partial T}{\partial \mathbf{x}} \right] \right\} dV = \int_V \delta T \rho c \frac{\partial T}{\partial t} dV. \quad (3.6)$$

Applying the Green's lemma for the right hand side of equation 3.6 leads:

$$\int_V \frac{\partial \delta T}{\partial \mathbf{x}} \cdot \mathbf{k} \cdot \frac{\partial T}{\partial \mathbf{x}} dV - \int_S \delta T q dS = \int_V \delta T \rho c \frac{\partial T}{\partial t} dV \quad (3.7)$$

Consider $\dot{T} = \frac{\partial T}{\partial t}$ and use the same finite element approximation for both T and \dot{T}

$$T = N^N(\mathbf{x})T^N \quad (a)$$

$$\dot{T} = N^N(\mathbf{x})\dot{T}^N \quad (b)$$

The Galerkin approach assumes that δT , the variational field, is interpolated by the same function:

$$\delta T = N^N(\mathbf{x})\delta T^N, \quad (c)$$

where T^N , \dot{T}^N , and δT^N are temperature, temperature change rate and variational temperature at nodes. Substitute (a), (b), and (c) into equation (3.7):

$$\delta T^N \left\{ \int_V \frac{\partial N^N}{\partial \mathbf{x}} \cdot \mathbf{k} \cdot \frac{\partial T}{\partial \mathbf{x}} dV - \int_S N^N q dS - \int_V N^N \rho c \dot{T} dV \right\} = 0 \quad (3.8)$$

Because δT^N are arbitrarily chosen, this gives the system of equations:

$$\int_V \frac{\partial N^N}{\partial \mathbf{x}} \cdot \mathbf{k} \cdot \frac{\partial T}{\partial \mathbf{x}} dV - \int_S N^N q dS - \int_V N^N \rho c \dot{T} dV = 0 \quad (3.9.a)$$

A same derivation is applied to the diffusion equation to get the final finite element equation of diffusion problem:

$$\int_V \frac{\partial N^N}{\partial \mathbf{x}} \cdot \mathbf{D} \cdot \frac{\partial w}{\partial \mathbf{x}} dV - \int_S N^N q dS - \int_V N^N \dot{w} dV = 0 \quad (3.9.b)$$

In the general matrix form, both equations (3.9.a) and (3.9.b) can be expressed as:

$$[K]\{\Phi\} + [C]\{\dot{\Phi}\} = \{Q\} \quad (3.10)$$

In ABAQUS, the backward difference algorithm is chosen to solve the time-history problem. Discrete the time domain with time step Δt , and write equation 3.10 at time $t + \Delta t$:

$$\begin{aligned} [K]\{\Phi\}_{t+\Delta t} + [C]\{\dot{\Phi}\}_{t+\Delta t} &= \{Q\}_{t+\Delta t} \\ [C]\{\dot{\Phi}\}_{t+\Delta t} &= \{Q\}_{t+\Delta t} - [K]\{\Phi\}_{t+\Delta t} \end{aligned} \quad (3.11)$$

Now consider the finite element expression $\{\dot{\Phi}\}$ as a backward difference at time $t + \Delta t$:

$$\{\dot{\Phi}\} = \frac{1}{\Delta t} (\{\Phi\}_{t+\Delta t} - \{\Phi\}_t) \quad (3.12)$$

Substitute equation (3.12) into (3.11) to obtain:

$$[C] \frac{1}{\Delta t} (\{\Phi\}_{t+\Delta t} - \{\Phi\}_t) = \{Q\}_{t+\Delta t} - [K]\{\Phi\}_{t+\Delta t} \quad (3.13)$$

Rewrite equation 3.13 for unknown $\{\Phi\}_{t+\Delta t}$:

$$\left(\frac{1}{\Delta t} [C] + [K] \right) \{\Phi\}_{t+\Delta t} = \{Q\}_{t+\Delta t} - \frac{1}{\Delta t} [C] \{\Phi\}_t \quad (3.14)$$

In equation (3.14), all parameters used in the calculation of $[K]$ and $[C]$ need to be evaluated at time $t + \Delta t$.

3.3. Basic of rheological characteristics

3.3.1. Introduction

Under the long-term load in normal service conditions, both wood and concrete behave as rheological materials. Time-dependent behavior of wood and concrete is complex. However, in engineering practice, the long-term behavior of wood and concrete can be assumed as linear visco-elastic. This assumption is acceptable if the level of long-term stress is not high. In this part, some basic concepts of visco-elasticity of the axial stress state are summarized.

Visco-elastic creep phenomenon: when subjected to a step constant stress, the visco-elastic materials experience a time-dependent increase in strain. The creep phenomenon can be observed from creep test in which strain is recorded while applied stress is kept as a constant value.

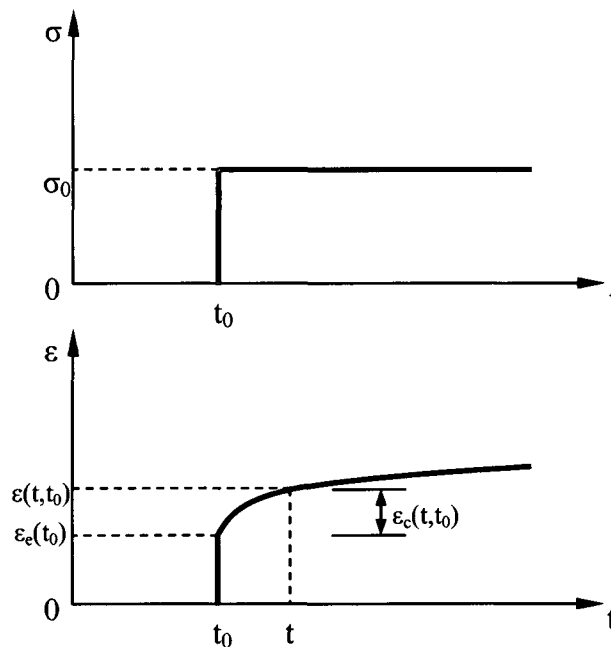


Figure 3.2 Creep phenomenon.

For generalized purpose, call $\sigma(t)$ function of input stress, then it can be expressed as:

$$\sigma(t) = \sigma_0 H(t - t_0) \quad (3.15)$$

Where $H(t - t_0)$ is the Heaviside step function.

$$H(t - t_0) = \begin{cases} 0 & \forall t < t_0 \\ 1 & \forall t \geq t_0 \end{cases} \quad (3.16)$$

The strain at time $t > t_0$ includes two parts: elastic strain and viscous or creep strain.

Mathematically, this strain can be expressed as

$$\varepsilon(t, t_0) = \varepsilon_e(t_0) + \varepsilon_c(t, t_0) \quad (3.17)$$

Relaxation phenomenon: when subjected to a step constant strain, the visco-elastic material experiences time-dependent decrease in stress. Relaxation can be observed from a relaxation test in which the stress is recorded as the strain held constant. Similar to creep phenomenon, express the strain as $\varepsilon(t) = \varepsilon_0 H(t - t_0)$, then the stress at time $t > t_0$ also includes two parts: instant elastic stress $\sigma(t_0)$ and delayed stress induced by relaxation $\sigma_r(t, t_0)$.

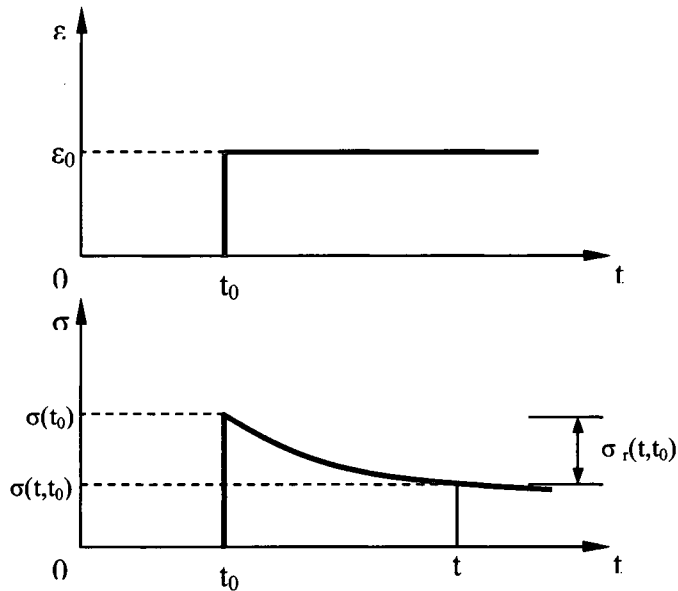


Figure 3.3 Relaxation phenomena.

Shrinkage: Concrete changes its volume even without applying load, this phenomenon is called shrinkage. The concrete shrinkage includes drying shrinkage and “autogenous” shrinkage. Drying shrinkage is caused by losing water mass to the environment from the concrete, this process makes concrete undergo a volumetric change. Autogenous shrinkage is defined as a concrete volume change occurring without moisture transfer to the environment. Autogeneous shrinkage is merely a result of the internal chemical and structural reactions of the concrete components. Practical observations show that in typical mixture concrete, contribution of autogenous is insignificant due to the dominant role of drying shrinkage. The shrinkage causes cracks in concrete if the volume cannot deform freely.

3.3.2 Constitutive models of linear visco-elastic material

In this research, wood and concrete are considered to be linear visco-elastic materials. With wood-concrete composite beam structure used in a residential building or a short span bridge, the long-term load is a small proportion of the total load and creates a relatively small stress level. In that case, using linear visco-elastic theory to determine long-term behavior of structure is reasonable. Classical linear visco-elasticity is characterized by two properties, “proportionality” and “superposition”, which are best explained by considering a strain response to a stress excitation.

- Proportionality: Over time the strain response is proportional to the amplitude of a constant stress step which is applied at $t = t_0$: $\epsilon_i(t, t_0) = \sigma_i J(t - t_0)$ for $t > t_0$.

For a unit step stress at $t = 0$, the strain response is identified as creep function $J(t)$.

- Superposition: The strain response to two subsequently applied constant amplitude stress steps equals the sum of the strain response induced by each excitation as depicted in Fig. 3.4. Mathematically, this statement can be expressed as:

$$\varepsilon(t) = \sigma_0 J(t-t_0) + \sigma_1 J(t-t_1) \quad (3.18)$$

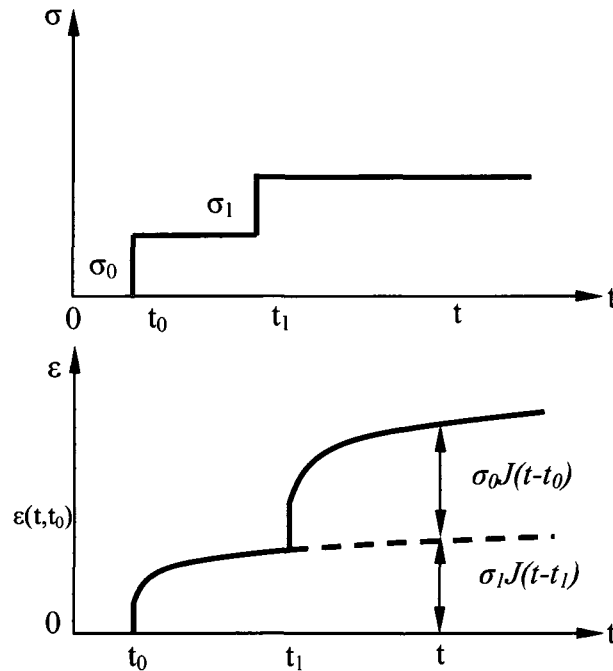


Figure 3.4 Superposition of the creep deformation.

Creep Compliance

In a creep test a constant stress σ_0 is applied at the beginning time t_0 and the time-dependent strain $\varepsilon(t)$, for $t > t_0$, is measured. For linear visco-elastic materials, the relationship between stress and strain can be represented as

$$\varepsilon(t, t_0) = J(t, t_0) H(t, t_0) \sigma_0 \quad (3.19)$$

The function $J(t, t_0)$ is called the “creep compliance” or “creep function” which is the creep strain per unit of applied stress. Creep compliance is a material property, which means each material has its own value of creep compliance.

In engineering practice, the creep function can be expressed as:

$$J(t, t_0) = J_0(t_0) + J_{ref}\varphi(t, t_0) \quad (3.20)$$

where $J_0(t_0)$ is the elastic deformability of the material at the time of load application.

J_{ref} is the elastic deformability at a reference time.

$\varphi(t, t_0)$ is the creep coefficient at time t due to the load applied at t_0 .

Equation (3.20) allows one to separate the time-dependent strain into two components, elastic strain (time-independent) and creep strain (time-dependent).

$$\varepsilon(t, t_0) = \varepsilon_e(t_0) + \varepsilon_c(t, t_0) \quad (3.21)$$

where $\varepsilon_e(t_0) = J(t_0)H\sigma_0$

$$\varepsilon_c(t, t_0) = J_{ref}\varphi(t, t_0)H\sigma_0$$

Relaxation modulus

In a relaxation test a constant strain ε_0 is applied at the beginning time t_0 and the time-dependent stress $\sigma(t)$ is measured for $t > t_0$. This stress also depends on the time of application of the strain, t_0 . For linear visco-elastic materials, the relationship between strain and stress can be expressed as

$$\sigma(t, t_0) = R(t, t_0)H(t, t_0)\varepsilon_0 \quad (3.22)$$

where

$\sigma(t, t_0)$ is the stress function due to constant strain applied at t_0 .

$H(t, t_0)$ is the Heaviside step function.

$R(t, t_0)$ is the relaxation function.

Similar to the creep function, the relaxation can be expressed as

$$R(t, t_0) = E_0(t_0) - E_{ref}\psi(t, t_0) \quad (3.23)$$

where

$E_0(t_0)$ is the elastic modulus of material at the time of load application t_0 .

E_{ref} is the elastic modulus of material at the reference time.

$\psi(t, t_0)$ is the relaxation coefficient at time t due to the load applied at t_0 .

Substituting equation (3.23) to equation (3.22), the relation between stress and strain is obtained in form of elastic stress and relaxation stress

$$\sigma(t, t_0) = \sigma_e(t_0) - \sigma_r(t, t_0) \quad (3.24)$$

where

$$\sigma_e(t_0) = E_0(t_0)H\varepsilon_0$$

$$\sigma_r(t, t_0) = E_{ref}\psi(t, t_0)H\varepsilon_0$$

The integral representation

For any visco-elastic material, if either the creep function $J(t, t_0)$ or the relaxation function $R(t, t_0)$ is known then the corresponding history of stress or strain can be determined. However, equations (3.19) and (3.22) are applied for input excitation as a constant stress or strain. In a case where the input excitation is an arbitrary function, the relation between stress and strain can be expanded and represented in integral forms by applying the superposition principle. For simplicity, only an integral representation of the creep phenomenon is derived.

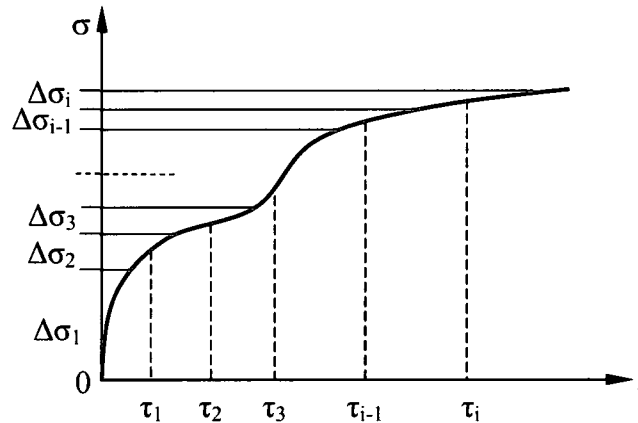


Fig. 3.5 Arbitrary stress input approximated by the sum of a series of constant stress increment.

Any arbitrary function of stress input can be approximated by the sum of a series of constant stress input, $\Delta\sigma_1, \Delta\sigma_2, \dots$, as shown in Fig. 3.5 and mathematically described by:

$$\sigma(t) = \sum_{i=1}^n \Delta\sigma_i H(t - \tau_i) \quad (3.25)$$

By applying the superposition principle (as first introduced by Boltzmann in 1876), the sum of the strain outputs resulting from each component of stress input is the same as the strain output resulting from the combined stress input. There, the strain output due to variable stress $\sigma(t)$ equals:

$$\varepsilon(t) = \sum_{i=1}^n \varepsilon_i(t - \tau_i) = \sum_{i=1}^n \Delta\sigma_i J(t - \tau_i) H(t - \tau_i)$$

If the number of step goes to infinity, the total strain can be expressed by an integral representation as:

$$\varepsilon(t) = \int_0^t J(t - \tau) H(t - \tau) d[\sigma(\tau)] \quad (3.26)$$

This is a Stieltjes integral. Since the dummy variable τ is always less than or equal to t , the function $H(t - \tau)$ is always unity in the range of integration, and if the stress is differentiable then equation (3.26) reduces to the first kind of Volterra integral equation, namely

$$\varepsilon(t) = \int_0^t J(t - \tau) \frac{\partial \sigma(\tau)}{\partial \tau} d\tau \quad (3.27)$$

In this formula, time τ may be taken as the independent variable. If the creep compliance $J(t)$ is separated into a time-independent compliance J_0 and a time-dependent creep function $\varphi(t)$, the equation (3.27) becomes the second kind of Volterra integral equation, namely

$$\varepsilon(t) = J_0 \sigma(t) + \int_0^t \varphi(t - \tau) \frac{\partial \sigma(\tau)}{\partial \tau} d\tau \quad (3.28)$$

In case of relaxation, by applying superposition and above arguments a set of similar equations can be derived where the input excitation is strain instead of stress.

$$\sigma(t) = \int_0^t R(t-\tau) d\varepsilon(\tau) \quad (3.29)$$

$$\sigma(t) = \int_0^t R(t-\tau) \frac{\partial \varepsilon(\tau)}{\partial \tau} d\tau \quad (3.30)$$

And

$$\sigma(t) = E_0 \varepsilon(t) + \int_0^t \psi(t-\tau) \frac{\partial \varepsilon(\tau)}{\partial \tau} d\tau \quad (3.31)$$

Where $\psi(t)$ is relaxation coefficient function, E_0 is the elastic modulus at $t = t_0$.

If a constant load is applied from $t = t_0$ to create a constant stress $\sigma(t) = \sigma_0$ or $\varepsilon(t) = \varepsilon_0$ and there is no stress or strain at $t < t_0$, the above equations can be expressed as

$$\varepsilon(t, t_0) = J(t, t_0) \sigma_0 + \int_{t_0}^t J(t, \tau) \frac{\partial \sigma(\tau)}{\partial \tau} d\tau \quad (3.32)$$

$$\sigma(t, t_0) = R(t, t_0) \varepsilon_0 + \int_{t_0}^t R(t, \tau) \frac{\partial \varepsilon(\tau)}{\partial \tau} d\tau \quad (3.33)$$

Relation between Creep Compliance and Relaxation Modulus

Creep and relaxation phenomena are two aspects of the same visco-elastic behavior of materials so there is a relation between creep compliance and relaxation modulus. In other words, one should be predicable if the other is known. By applying the Laplace transform and inverse Laplace transform (Findley et al. [78]) with equations (3.27) and (3.30), the relation between creep compliance and relaxation modulus is:

$$\int_0^t J(t-\tau)R(\tau)d\tau = t \quad (3.34)$$

or

$$\int_0^t R(t-\tau)J(\tau)d\tau = t \quad (3.35)$$

In practical engineering, a creep test is easier to conduct than a relaxation test. Thus, the relaxation modulus can be obtained based on the above interrelationship, by measuring creep compliance in a creep test.

3.3 Rate-type constitutive equation

Equations (3.32) and (3.33) are constitutive equations in mechanics problems involving visco-elastic materials. Closed form solutions for Volterra integral equations such as equations (3.32) and (3.33) can be found only in cases where the creep compliance and relaxation modulus are simple functions of time. For general mechanic computations, the stress or strain history is not known in advance. Therefore a step-by-step solution algorithm needs to be implemented in which the computation is discretized into finite time increments. The integral formulations then are replaced by finite sums. Such a formulation, however, has the inconvenient feature that the strain (or stress) increment at any new time step is computed as a function of the entire previous stress (or strain) history. This is impractical for long-term computation because the whole stress (or strain) history must be stored for each computational point and excessively long sum of strain (or stress) values must be computed at each time step. That would require an immense storage capacity and an extremely long computational time.

An alternative formulation is preferable where by the stress increment at a new time step can be computed from strain increment and a finite number of state variables, all of which are known at the beginning of the time step. The relaxation and creep function need to be rewritten into a form which enables one to formulate such an algorithm. In general, the relaxation and creep functions are rewritten as sums of real exponential functions (these equations are explained subsequently in this chapter) as follows

$$R(t, t_0) = \sum_{n=0}^N E_n(t_0) e^{\left(\frac{t-t_0}{\tau_n}\right)} \quad (3.36)$$

$$J(t, t_0) = \sum_{n=0}^N J_n(t_0) \left[1 - e^{\left(\frac{t-t_0}{\tau_n}\right)} \right] \quad (3.37)$$

Mathematically, equations (3.36) and (3.37) are the approximation of the relaxation function and creep compliance by a Dirichlet series. And physically, they are governing equations of the generalized Maxwell and the generalized Kelvin models.

Basis visco-elastic models

Linear visco-elastic materials have both linear elastic and linear viscous behavior. Graphically, this material can be represented as a combination of linear spring and linear viscous dashpot elements. The two simplest models of visco-elastic material based on spring and dashpot element are the Maxwell model and the Kelvin model. The Maxwell model contains a linear spring element and a linear dashpot element connected in series as shown in Fig. 3.6(a) The Kelvin model is shown in Fig 3.6(b) where a spring element and a dashpot element are connected in parallel. Hereafter, in this text, the simple

Maxwell model and the simple Kelvin model shown in Fig. 3.6 will be called a Maxwell body and a Kelvin body, respectively.

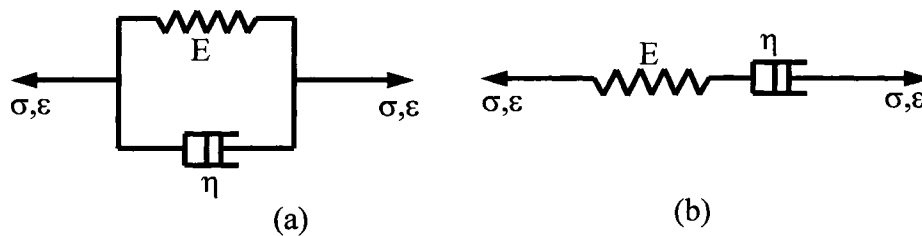


Figure 3.6 Kelvin body (a) and Maxwell body (b).

In general, creep compliance (or relaxation modulus) is obtained by fitting a mathematical curve to the experimental data obtained from a creep test (or a relaxation test). The most typical models to represent creep compliance and relaxation modulus use the generalized Kelvin model (Kelvin bodies connected in series) and the generalized Maxwell model (Maxwell bodies connected in parallel). Generalized Kelvin and generalized Maxwell models are easy to fit closely with any experimental creep compliance function or relaxation modulus function based on enough number of Kelvin bodies or Maxwell bodies.

Generalized Kelvin model

The generalized Kelvin model consists of a number of Kelvin bodies and one linear spring element connected in series as shown in Fig. 3.7.

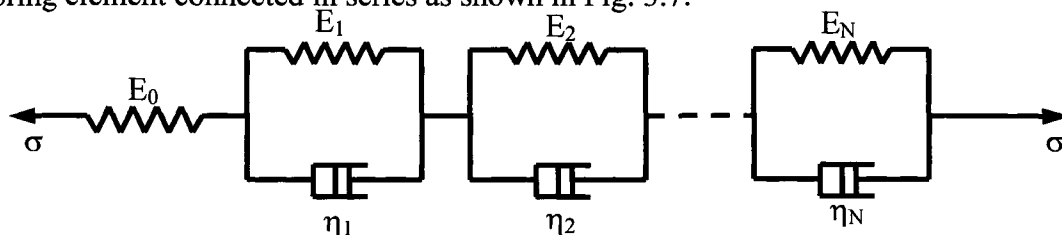


Figure 3.7 Generalized Kelvin model.

The first spring element with instantaneous elastic modulus E_0 represents instantaneous deformation. The n^{th} Kelvin element has spring stiffness E_n and coefficient of viscosity η_n where $\eta_n = E_n \tau_n$ where τ_n is the retardation time. The creep compliance function of generalized Kelvin model can be expressed as

$$J(t, t_0) = J_0 + \sum_{n=1}^N J_n \left[1 - e^{-\left(\frac{t-t_0}{\tau_n}\right)} \right] \quad (3.36)$$

Where $J_0 = \frac{1}{E_0}$ and $J_n = \frac{1}{E_n}$. It is assumed that J_n is independent of the loading time t_0 ,

the creep compliance function $J(t, t_0)$ will be in hereditary type or $J(t, t_0) = J(t-t_0)$.

Replacing equation (3.36) with equation (3.26), the strain-stress relation of visco-elastic material is

$$\varepsilon(t) = \int_0^t \left\{ J_0 + \sum_{n=1}^N J_n \left[1 - e^{-\left(\frac{t-\tau}{\tau_n}\right)} \right] \right\} d\sigma(\tau) \quad (3.37)$$

The total strain for visco-elastic material at time $t + \Delta t$ will be

$$\varepsilon(t + \Delta t) = \int_0^{t+\Delta t} \left\{ J_0 + \sum_{n=1}^N J_n \left[1 - e^{-\left(\frac{t+\Delta t-\tau}{\tau_n}\right)} \right] \right\} d\sigma(\tau) \quad (3.38)$$

The increment of total strain of an intermediate step $k[t_{k-1}, t_k]$, where $t_{k-1} = t$, $t_k = t + \Delta t$

and $\Delta t_k = t_k - t_{k-1} = \Delta t$, will be determined as

$$\begin{aligned} \Delta \varepsilon_k = & \int_0^{t_{k-1}+\Delta t} \left\{ J_0 + \sum_{n=1}^N J_n \left[1 - e^{\left(\frac{-t_{k-1}+\Delta t-\tau}{\tau_n} \right)} \right] \right\} d\sigma(\tau) - \\ & \int_0^{t_{k-1}} \left\{ J_0 + \sum_{n=1}^N J_n \left[1 - e^{\left(\frac{-t_{k-1}-\tau}{\tau_n} \right)} \right] \right\} d\sigma(\tau) \end{aligned} \quad (3.39)$$

$\Delta \varepsilon_{vis}$ can also be expressed in the form

$$\Delta \varepsilon_k = \Delta \bar{\varepsilon}_{ek} + \Delta \bar{\varepsilon}_{ck} \quad (3.40)$$

Where

$$\Delta \bar{\varepsilon}_{ek} = \int_0^{t_{k-1}+\Delta t} J_0 d\sigma(\tau) - \int_0^{t_{k-1}} J_0 d\sigma(\tau) \quad (3.41)$$

$$\Delta \bar{\varepsilon}_{ck} = \int_0^{t_{k-1}+\Delta t} \sum_{n=1}^N J_n \left[1 - e^{\left(\frac{-t_{k-1}+\Delta t-\tau}{\tau_n} \right)} \right] d\sigma(\tau) - \int_0^{t_{k-1}} \sum_{n=1}^N J_n \left[1 - e^{\left(\frac{-t_{k-1}-\tau}{\tau_n} \right)} \right] d\sigma(\tau) \quad (3.42)$$

Applying the trapezoidal rule, the elastic strain can be expressed as

$$\Delta \bar{\varepsilon}_{ek} = J_0 \Delta \sigma_k \quad (3.43)$$

Where $\Delta \sigma_k = \sigma_k - \sigma_{k-1}$ is the stress increment in step k.

Equation (3.42) represents the increment of the viscous strain in step k and can be expanded as

$$\begin{aligned} \Delta \bar{\varepsilon}_{ck} = & \int_0^{t_{k-1}} \sum_{n=1}^N J_n \left[1 - e^{\left(\frac{-t_{k-1}-\tau}{\tau_n} \right)} \right] d\sigma(\tau) + \int_{t_{k-1}}^{t_{k-1}+\Delta t} \sum_{n=1}^N J_n \left[1 - e^{\left(\frac{-t_{k-1}+\Delta t-\tau}{\tau_n} \right)} \right] d\sigma(\tau) \\ & - \int_0^{t_{k-1}} \sum_{n=1}^N J_n \left[1 - e^{\left(\frac{-t_{k-1}-\tau}{\tau_n} \right)} \right] d\sigma(\tau) \end{aligned} \quad (3.44)$$

Applying the trapezoidal rule again to evaluate the integration between t_{k-1} and $t_{k-1} + \Delta t$ to obtain

$$\Delta \bar{\varepsilon}_{ck} = \int_0^{t_{k-1}} \sum_{n=1}^N J_n e^{\left(\frac{t_{k-1}-\tau}{\tau_n}\right)} \left[1 - e^{\left(\frac{\Delta t_k}{\tau_n}\right)} \right] d\sigma(\tau) + \sum_{n=1}^N J_n \left[1 - e^{\left(\frac{\Delta t_k}{\tau_n}\right)} \right] \frac{\Delta \sigma_k}{2} \quad (3.45)$$

Or rewritten in other form

$$\Delta \bar{\varepsilon}_{ck} = \sum_{n=1}^N J_n \left[1 - e^{\left(\frac{\Delta t_k}{\tau_n}\right)} \right] \left(\frac{\Delta \sigma_k}{2} + \sigma_{nk-1}^{hist} \right) \quad (3.46)$$

Where

$$\sigma_{nk-1}^{hist} = \int_0^{t_{k-1}} e^{\left(\frac{t_{k-1}-\tau}{\tau_n}\right)} d\sigma(\tau) \quad (3.47)$$

The determination of σ_{nk}^{hist} can be done by a recurrence formula obtained from applying the trapezoidal rule [79, 2]

$$\sigma_{nk}^{hist} = \int_0^{t_{k-1}+\Delta t} e^{\left(\frac{t_{k-1}+\Delta t-\tau}{\tau_n}\right)} d\sigma(\tau) \quad (3.48)$$

$$\sigma_{nk}^{hist} = e^{\left(\frac{\Delta t}{\tau_n}\right)} \int_0^{t_{k-1}} e^{\left(\frac{t_{k-1}-\tau}{\tau_n}\right)} d\sigma(\tau) + \int_{t_{k-1}}^{t_{k-1}+\Delta t} e^{\left(\frac{t_{k-1}+\Delta t-\tau}{\tau_n}\right)} d\sigma(\tau) \quad (3.49)$$

$$\sigma_{nk}^{hist} = \left[\sigma_{nk-1}^{hist} + \frac{\Delta \sigma_k}{2} \right] e^{\left(\frac{\Delta t}{\tau_n}\right)} + \frac{\Delta \sigma_k}{2} \quad (3.50)$$

Substituting equations (3.43) and (3.46) into equation (3.40), one obtains the incremental form of strain and stress relation of viscoelastic material, equation (3.51) in which the increment of strain can be determined from the history of stress.

$$\Delta \varepsilon_k = J_0 \Delta \sigma_k + \sum_{n=1}^N J_n \left[1 - e^{\left(\frac{-\Delta t}{\tau_n} \right)} \right] \left(\frac{\Delta \sigma_k}{2} + \sigma_{nk-1}^{hist} \right) \quad (3.51)$$

It is necessary to write the algebraic form of stress-strain relation so that the increment of stress can be determined if the history of strain is known. Rearranging equation (3.51) gives

$$\Delta \varepsilon_k = \left(J_0 + \frac{1}{2} \sum_{n=1}^N J_n \left[1 - e^{\left(\frac{-\Delta t}{\tau_n} \right)} \right] \right) \Delta \sigma_k + \sum_{n=1}^N J_n \left[1 - e^{\left(\frac{-\Delta t}{\tau_n} \right)} \right] \sigma_{nk-1}^{hist} \quad (3.52)$$

Or

$$\Delta \sigma_k = \frac{1}{\left(J_0 + \frac{1}{2} \sum_{n=1}^N J_n \left[1 - e^{\left(\frac{-\Delta t}{\tau_n} \right)} \right] \right)} \left(\Delta \varepsilon_k - \sum_{n=1}^N J_n \left[1 - e^{\left(\frac{-\Delta t}{\tau_n} \right)} \right] \sigma_{nk-1}^{hist} \right) \quad (3.53)$$

This equation can be rewritten in a compact form

$$\Delta \sigma_k = \overline{E}_k (\Delta \varepsilon_k - \Delta \varepsilon_{ck}) \quad (3.54)$$

Where

$$\overline{E}_k = \frac{2}{\left(2J_0 + \sum_{n=1}^N J_n \left[1 - e^{\left(\frac{-\Delta t}{\tau_n} \right)} \right] \right)} \quad (3.55)$$

And

$$\Delta \varepsilon_{ck} = \sum_{n=1}^N J_n \left[1 - e^{\left(\frac{-\Delta t}{\tau_n} \right)} \right] \sigma_{nk-1}^{hist} \quad (3.56)$$

Generalized Maxwell model

The mechanical representation of generalized Maxwell model is shown in the Fig. 3.8.

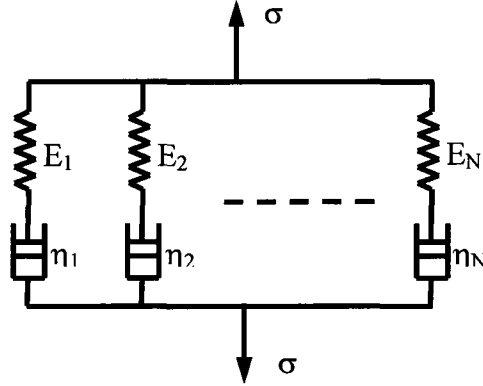


Figure 3.8 Generalized Maxwell model.

The generalized Maxwell model consists N Maxwell bodies connected in parallel, the stiffness of spring element is E_n and the viscous coefficient of dashpot element is η_n . For an aging material like concrete which has modulus of elasticity changing over time, the relaxation modulus in generalized Maxwell model then can be expressed as

$$R(t, t_0) = \sum_{n=1}^N E_n(t_0) e^{\left(\frac{t-t_0}{\tau_n}\right)} \quad (3.58)$$

Where τ_n is the relaxation time of the n -th Maxwell body and defined as

$$\tau_n = \frac{E_n(t_0)}{\eta_n(t_0)} \quad (3.59)$$

Replacing (3.58) into (3.29), the stress at time t due to input excitation strain is

$$\sigma(t) = \int_0^t \sum_{n=1}^N E_n(\tau) e^{\left(\frac{t-\tau}{\tau_n}\right)} d\varepsilon(\tau) \quad (3.60)$$

From equation (3.60), the stress at time $t + \Delta t$ can be written as

$$\sigma(t + \Delta t) = \int_0^{t+\Delta t} \sum_{n=1}^N E_n(\tau) e^{\left(\frac{t+\Delta t-\tau}{\tau_n}\right)} d\varepsilon(\tau) \quad (3.61)$$

Therefore stress increment of a general intermediate step k $[t_{k-1}, t_k]$ with $t_{k-1} = t$, $t_k = t + \Delta t$ or $\Delta t_k = t_k - t_{k-1} = \Delta t$ can be determined as

$$\Delta\sigma_k = \sigma(t_k + \Delta t) - \sigma(t_k) = \sigma_k - \sigma_{k-1} \quad (3.62)$$

Substituting equations (3.60) and (3.61) into equation (3.62) gives

$$\Delta\sigma_k = \sum_{n=1}^N e^{\left(\frac{-t_k}{\tau_n}\right)} \int_0^{t_k} E_n(\tau) e^{\left(\frac{\tau}{\tau_n}\right)} d\varepsilon(\tau) - \sum_{n=1}^N e^{\left(\frac{-t_{k-1}}{\tau_n}\right)} \int_0^{t_{k-1}} E_n(\tau) e^{\left(\frac{\tau}{\tau_n}\right)} d\varepsilon(\tau) \quad (3.63)$$

$$\begin{aligned} \Delta\sigma_k = & \sum_{n=1}^N \left[e^{\left(\frac{-t_{k-1}}{\tau_n}\right)} \int_0^{t_{k-1}} E_n(\tau) e^{\left(\frac{\tau}{\tau_n}\right)} d\varepsilon(\tau) \right] \left[e^{\left(\frac{-\Delta t_k}{\tau_n}\right)} - 1 \right] + \\ & + \sum_{n=1}^N e^{\left(\frac{-t_k}{\tau_n}\right)} \int_{t_{k-1}}^{t_k} E_n(\tau) e^{\left(\frac{\tau}{\tau_n}\right)} d\varepsilon(\tau) \end{aligned} \quad (3.64)$$

Calling the whole term in the first square bracket σ_{nk-1}^{hist} and applying the trapezoidal rule for the second term leads to

$$\Delta\sigma_k = - \sum_{n=1}^N \sigma_{nk-1}^{hist} \left[1 - e^{\left(\frac{-\Delta t}{\tau_n}\right)} \right] + \sum_{n=1}^N e^{\left(\frac{-\Delta t}{\tau_n}\right)} \frac{1}{2} \left[E_n(t_{k-1}) + E_n(t_k) e^{\left(\frac{\Delta t}{\tau_n}\right)} \right] \Delta\varepsilon_k \quad (3.65)$$

Equation (3.65) can be expressed in a compact form as

$$\Delta\sigma_k = \bar{E}_k (\Delta\varepsilon_k - \Delta\varepsilon_{ck}) \quad (3.66)$$

Where

$$\bar{E}_k = \sum_{n=1}^N \frac{1}{2} \left[E_n(t_k) + E_n(t_{k-1}) e^{\left(\frac{-\Delta t}{\tau_n}\right)} \right] \quad (3.67)$$

$$\Delta \varepsilon_{ck} = \frac{1}{\bar{E}_k} \sum_{n=1}^N \sigma_{nk-1}^{hist} \left[1 - e^{\left(\frac{-\Delta t}{\tau_n}\right)} \right] \quad (3.68)$$

The stress history can be determined by means of recurrence formula [79, 2] which similar to equation from (3.48) to (3.50):

$$\sigma_{nk}^{hist} = e^{\left(\frac{-t_{k-1} + \Delta t}{\tau_n}\right)} \int_0^{t_{k-1} + \Delta t} E_n(\tau) e^{\left(\frac{\tau}{\tau_n}\right)} d\varepsilon(\tau), \quad (3.69)$$

$$\sigma_{nk}^{hist} = e^{\left(\frac{-t_{k-1}}{\tau_n}\right)} e^{\left(\frac{-\Delta t}{\tau_n}\right)} \left[\int_0^{t_{k-1}} E_n(\tau) e^{\left(\frac{\tau}{\tau_n}\right)} d\varepsilon(\tau) + \int_{t_{k-1}}^{t_k} E_n(\tau) e^{\left(\frac{\tau}{\tau_n}\right)} d\varepsilon(\tau) \right]. \quad (3.70)$$

Using the trapezoidal rule to calculate the last integration and observing that the first integration represents the term σ_{nk-1}^{hist} yields

$$\sigma_{nk}^{hist} = \sigma_{nk-1}^{hist} e^{\left(\frac{-\Delta t}{\tau_n}\right)} + \frac{1}{2} \left[E_n(t_k) + E_n(t_{k-1}) e^{\left(\frac{-\Delta t}{\tau_n}\right)} \right] \Delta \varepsilon_k. \quad (3.71)$$

In case of non-aging material which has constant modulus of elasticity over time, formulas (3.67) and (3.71) can be simplified as

$$\bar{E}_k = \frac{1}{2} \sum_{n=1}^N E_n \left[1 + e^{\left(\frac{-\Delta t}{\tau_n}\right)} \right], \quad (3.72)$$

and

$$\sigma_{nk}^{hist} = \sigma_{nk-1}^{hist} e^{\left(\frac{-\Delta t}{\tau_n}\right)} + \frac{E_n}{2} \left[1 + e^{\left(\frac{-\Delta t}{\tau_n}\right)} \right] \Delta \varepsilon_k. \quad (3.73)$$

Determination of chain parameters

Parameters of the generalized Kelvin model are determined based on fitting mathematical expression to the creep data while parameters of the generalized Maxwell model are determined based on fitting mathematical expressions to the relaxation data. Relaxation tests are often harder to do thus the relaxation function is often not available. But the creep compliances are more readily available from creep tests. In that case, creep curves have to be transformed into relaxation curves (Bažant and Wu 1974 [80]). If the creep test data is not available, the creep compliance can be taken from available theoretical models.

The stiffness of the single spring element can be determined directly for both models. In the Kelvin chain model E_0 is the elastic modulus at time t_0 , while in Maxwell chain model, E_0 is equal to the asymptotic final value of the relaxation curve. The elastic moduli of other chain elements and the relaxation or retardation times are obtained by a nonlinear least squares method minimizing the sum of quadratic differences between the theoretical curve and the approximating curve at a number of discrete sampling load durations. The above statement can be expressed mathematically for creep compliance case and relaxation case as

$$\Phi_J = \sum_{q=1}^p \left[J(t_q, t_0) - \tilde{J}(t_q, t_0) \right]^2 \quad (3.75)$$

$$\Phi_R = \sum_{q=1}^p \left[R(t_q, t_0) - \tilde{R}(t_q, t_0) \right]^2 \quad (3.76)$$

In equations (3.75) and (3.76), J and R represent values of approximating function while \tilde{J} and \tilde{R} represent value from experimental curve or proposed theoretical curve.

For an aging material like concrete, several factors can affect the visco-elastic behavior. These factors include the type of concrete, the relative humidity, the compressive strength, the effective thickness of concrete, and the loading time t_0 . In order to take into account those effects, many set of chain parameters must be determined. The relaxation or retardation time remains fixed while the elastic moduli are determined at number of sampling load ages. In Chapter 5, the detailed procedure to determine Maxwell chain parameters for concrete based on the proposed CEB-FIP 1990 relaxation function are presented.

Chapter 4

Mathematical model for long-term structural behavior of wood

4.1 Introduction

Wood is an orthotropic material in nature and its physical and mechanical properties vary greatly depending on species. Considerable research has been done to study physical and mechanical properties of wood species in different regions thus the material parameters needed for short-term analysis are readily available. However, the wood physical and mechanical properties of wood can change over the time if ambient environmental conditions such as relative humidity and temperature change. For long-term analysis, in normal service condition the mechanical behavior of wood is highly complex when compared with other building materials.

Long-term structural behavior includes the following phenomena which occur simultaneously.

- Normal creep.
- Mechano-sorptive creep.
- Modulus of elasticity varies with moisture content.
- Thermal expansion.
- Shrinkage and swelling induced by change of moisture content.

For wood material, normal creep (i.e. visco-elastic creep) was defined earlier as a phenomenon in which the deformation increases under a constant applied load while the moisture content inside is held constant. The rate and magnitude of normal creep increase when the constant applied stress is increased. Observed normal creep is linear at low

stress levels but changes to non-linear as stress level increases. The linear limit occurs when stress level reaches about 30-50% of short-term ultimate strength, depending on load type, moisture content, and temperature. High moisture content and temperature reduce this limit (Schniewind 1968 [81], Le Govic 1994[82], Morlier & Palka 1994 [83]).

When the relative humidity of ambient environment of a creep test specimen changes, the moisture content in specimen will change as a result of the diffusion process. Under this circumstance total normal creep deformation is higher than that occurring under a condition of constant moisture content. The difference in creep between the two cases (constant vs. changing moisture content during a creep test) is caused by the changing of moisture content and is termed mechano-sorptive creep.

Mechano-sorptive creep is an accumulation process of creep deformation over each changing moisture content cycle. A changing moisture cycle includes two periods: wetting and drying (or drying and wetting). The total strain increases during the drying periods and decreases during the wetting periods. Like normal creep, the mechano-sorptive behavior is linear at low stress levels, and it increases in rate and magnitude and its behavior becomes nonlinear at high stress level. The level of stress at which the mechano-sorptive creep behavior changes to nonlinear is not firmly established. Nonlinearity initiating at a stress level of 30-40% of short-term ultimate strength was observed by Hunt and Shelton (1988) [84], Hearmon and Paton (1964) [85], and also by Gril (1988) [86]. Toratti (1988) [87] observed nonlinear mechano-sorptive creep initiating at stress levels ranging between 12.5% and 37.5% of short-term ultimate strength.

Figs. 4.1 and 4.2 show typical behavior of mechano-sorptive phenomenon. Mohagher 1987 [88] presents measured creep data for a specific beam subjected to 4-point bending in Fig. 4.1. The beam was extremely small, specifically 10 mm x 10 mm in cross-section with a span of 300 mm. The relative humidity was varied as a pulse function (rectangular function) with the period of 20 days. The applied stress levels shown are at the extreme (bottom and top) fibers of the beam. At an applied stress level of 10 MPa, in the period of observation of 600 days, there was no tertiary creep. At the 20 MPa and 30 MPa stress levels, the primary creep and secondary creep stages were shorter; the tertiary creep stage appeared and led the specimens to rupture at about 550 days and 300 days, respectively.

Hearmon and Paton 1964 [85] present the normal creep and mechano-sorptive creep data for another specific beam subjected to 3-point bending in Fig. 4.2. The beam was 2 mm x 2 mm in cross-section and had a span of 60mm. The upper value of the relative humidity pulse function was 93% but the lower value and the period of this function were not reported. Thus the figure only shows the principal long-term behavior of wood under constant load and cyclic relative humidity variation. The solid line curve shows the normal creep of the test specimen subjected to the load level of 3/8 of maximum load and the constant relative humidity of 93%. Two other curves show the total creep when the specimens were subjected to the two different load levels and the same pulse function of relative humidity.

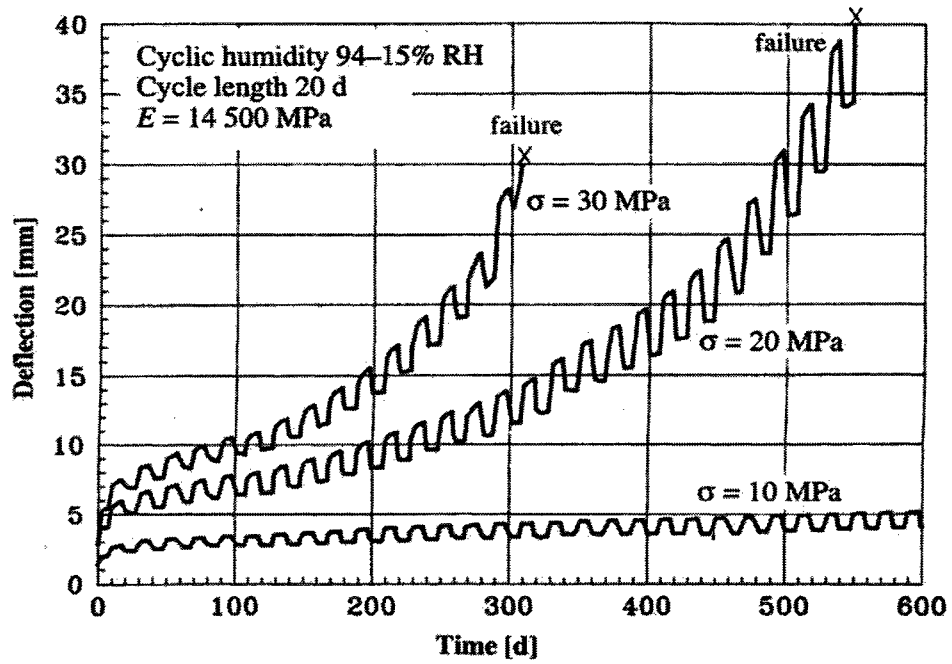


Figure 4.1 Creep of wood beams under constant load subjected to cyclic change of relative humidity.

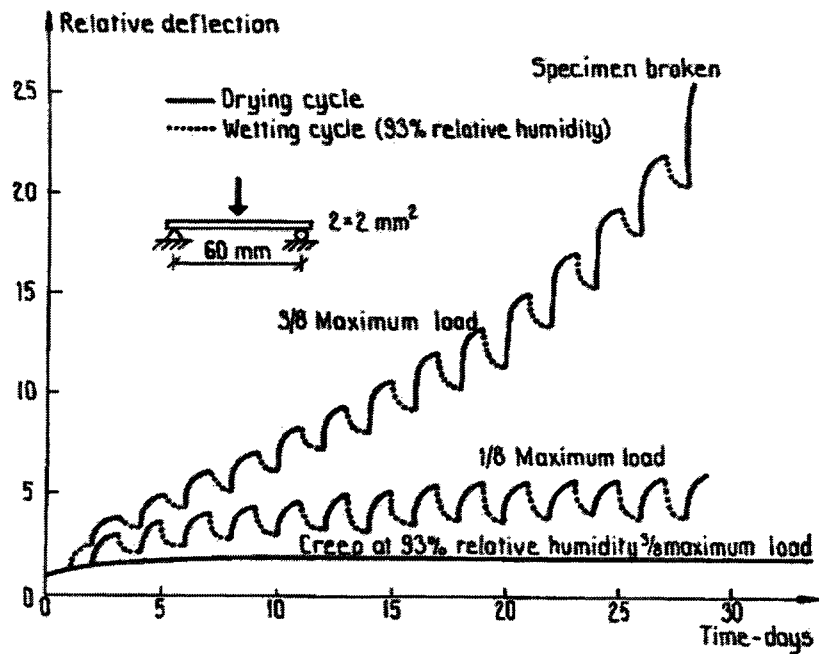


Figure 4.2 Normal and mechano-sorptive creeps in a bending beam test (Hearmon and Paton 1964).

The mechanisms of mechano-sorptive were proposed and explained by some authors such as Van Der Put (1989) [89], Gril (1988) [86], Boyd (1992) [90], Mukudai and Yata (1986, 1987, 1988) [91, 92, 93], Hoffemeyer and Davidson (1989) [94].

4.2 Hypothesis

Long-term behavior of wood is complex and affected by many factors. Several computational models for long-term behavior of wood and wood based structures proposed by other researchers were reviewed in Chapter 2. The basic approaches of different authors are quite different so they have evolved into various different computational models. The objective of this author's dissertation research is to understand the long-term behavior of one specific type of wood-concrete composite structure, not to focus on modeling long-term behavior of wood only. For that reason, the author has adopted the Toratti model [61]. Originally, the Toratti model was developed to model creep deformation of wood beams. Fragiacommo [4, 5] later applied the Toratti model for wood in computing long-term deflection of a wood-concrete beam by the finite element method. The formulations of Toratti model and Fragiacommo expansion of this model both applied the finite element method to a uniaxial stress state. Each is summarized in section 4.3. Then the formulation is expanded by the author to apply to a multiaxial stress state.

Two important assumptions apply for the Toratti model. First, the superposition principle is assumed to be valid, and second, both normal creep and mechano-sorptive creep are assumed to be linear. For both the above assumptions to hold the long-term stress level must be low. In wood and wood-composite structures, long-term static load often creates a low stress level (about 30% of short-term ultimate strength of wood). In common

design codes of practice the long-term static load corresponds to the quasi-permanent load combination, where the permanent load is considered applied together with only a part (usually 30-40%) of the non-permanent imposed load. Such a load combination is significantly lower than the ultimate limit state load combination, where both permanent and imposed loads are multiplied by factors greater than 1 (typically 1.2 to 1.5). Further, safety coefficients are also applied at the material level. For these reasons under long-term loading the stress level is unlikely to be greater than 30% of the short-term ultimate strength of wood.

4.3 Toratti model formulations

By using the principle of superposition, the total strain can be separated into a sum of three components: normal creep strain $\varepsilon_{vis}(t)$, mechano-sorptive strain $\varepsilon_{ms}(t)$, and moisture expansion strain $\varepsilon_u(t)$, i.e.

$$\varepsilon(t) = \varepsilon_{vis}(t) + \varepsilon_{ms}(t) + \varepsilon_u(t) \quad (4.1)$$

Toratti neglected the thermal expansion strain because his model was applied to a simply supported solid wood beam. In wood-concrete composite beam, the thermal expansion coefficients of wood and concrete are different. When the temperature changes, the layers are not freely expanding due to the constraint of interlayer connection. Thus, the total strain must include the thermal expansion strain. Equation (4.1) need to be rewritten as:

$$\varepsilon(t) = \varepsilon_{vis}(t) + \varepsilon_{ms}(t) + \varepsilon_u(t) + \varepsilon_T(t) \quad (4.2)$$

where $\varepsilon_T(t)$ is the thermal expansion strain.

Creep compliance function and normal creep strains

Toratti assumed the following creep function for wood:

$$J_w(t, u) = J_{w0}(u) + J_{w0}(u_{ref})\varphi_w(t) \quad (4.3)$$

where: $J_{w0}(u)$ is the elastic compliance with the moisture content u ;

$J_{w0}(u_{ref})$ is the elastic compliance at a referential moisture content;

$\varphi_w(t)$ is the creep coefficient function.

Using the “power-type” creep coefficient with two parameters, the formulation for creep compliance is obtained as

$$J_w(t, u) = J_{w0}(u) + J_{w0}(u_{ref})\left(\frac{t}{t_d}\right)^k \quad (4.4)$$

Fitting the creep function (4.4) to the creep test data, Toratti obtained values of $t_d = 29500$ days (double of the creep time), $k = 0.21$, and $u_{ref} = 0.2$ for his model.

The elastic compliance can be computed from modulus of elasticity which is dependent on moisture content in accordance with

$$J_{w0}(u) = \frac{1}{E_w(u)} \quad (4.5)$$

$$E_w(u) = E_{w0}(1 - 1.06u) \quad (4.6)$$

E_{w0} is the initial modulus of elasticity of wood.

Another way to represent the creep compliance function is to use the generalized Kelvin series model. From a computational point of view, the advantages of using generalized Kelvin model in exponential form were discussed in Chapter 3. Unlike concrete, the

creep compliance function of wood does not depend on the time of load application but instead depends on the interior moisture content. The formulation of creep compliance function in equation (3.36) can be rewritten for wood as:

$$J_w(t, u) = J_{w0}(u) + J_{w0}(u_{ref}) \sum_{n=1}^N J_n \left(1 - e^{-\left(\frac{t}{\tau_n}\right)} \right) \quad (4.7)$$

The creep compliance in power type in (4.4) can be converted to the generalized Kelvin formulation in equation (4.7) by using the nonlinear least square method to get the Kelvin parameters listed in Table 4.1.

Table 4.1 Parameters of generalized Kelvin model for wood.

n	J_n	τ_n (days)
1	0.0686	0.01
2	-0.0056	0.1
3	0.0716	1
4	0.0404	10
5	0.2073	100
6	0.5503	5000

In equation (4.2), the normal creep strain can be separated into time-independent and time-dependent components as:

$$\varepsilon_{vis}(t) = \int_0^t J_w(\tau, u) d\sigma_w(\tau) = \varepsilon_E + \varepsilon_c \quad (4.8)$$

Substituting equation (4.7) into equation (4.8), one obtains

$$\varepsilon_{vis}(t) = \int_0^t \left[J_{w0}(u) + J_{w0}(u_{ref}) \sum_{n=1}^N J_n \left(1 - e^{\left(\frac{-\tau}{\tau_n} \right)} \right) \right] d\sigma(\tau) \quad (4.9)$$

or

$$\varepsilon_{vis}(t) = \int_0^t J_{w0}(u) d\sigma(\tau) + \int_0^t \left[J_{w0}(u_{ref}) \sum_{n=1}^N J_n \left(1 - e^{\left(\frac{-\tau}{\tau_n} \right)} \right) \right] d\sigma(\tau) \quad (4.10)$$

Elastic strain

If there is no variation of environmental conditions, $J_{w0}(u) = J_{w0} = \text{constant}$ and the elastic strain depends on only the history of stress. Consequently,

$$\varepsilon_E(t) = J_{w0} \int_0^t d\sigma(\tau) \quad (4.11)$$

If the environmental conditions change with time, the change of elastic modulus being dependent on moisture content also creates a component of elastic strains. In that situation, the equation of elastic strain becomes:

$$\varepsilon_E(t) = \int_0^t J_{w0}(u) d\sigma(\tau) + \int_0^t \sigma(\tau) dJ_{w0}(u) = \varepsilon_E' + \varepsilon_E'' \quad (4.12)$$

where ε_E' is the elastic strain induced by the history of stress, $\sigma = \sigma(t)$; and ε_E'' is the elastic strain induced by the history of moisture content, $u = u(t)$.

Mechano-sorptive creep strain

The mechano-sorptive strain of wood is defined as

$$\varepsilon_{ms}(t) = J^\infty \int_0^t \left\{ 1 - e^{\left[-c \int_\tau^t du(\tau_1) \right]} \right\} d\sigma(\tau) \quad (4.13)$$

where J^∞ is the compliance at mechano-sorptive creep limit.

Moisture expansion strain

The moisture expansion strain of wood is defined as

$$\varepsilon_u(t) = \int_0^t [\alpha_u - b\varepsilon(\tau)] du(\tau) \quad (4.14)$$

where α_u and b are material parameters.

Thermal expansion strain

The thermal expansion strain of wood is defined as

$$\varepsilon_T(t) = \int_0^t \alpha_T dT(\tau) \quad (4.15)$$

where α_T is the coefficient of thermal expansion.

4.4 Incremental form of the constitutive equation for wood

By employing the procedure presented in Chapter 3, the constitutive equation in integral form can be converted to algebraic form to enable a solution to be obtained by numerical methods. The total time of analysis $[0, t]$ is discretized into a finite number of time increments. Consider a general intermediate step k with $\Delta t_k = t_k - t_{k-1} = \Delta t$ and increment of stress and strains in the form:

$$\left. \begin{aligned} \Delta\sigma_k &= \sigma_k - \sigma_{k-1} = \sigma(t_k) - \sigma(t_{k-1}) \\ \Delta\varepsilon_k &= \varepsilon_k - \varepsilon_{k-1} = \varepsilon(t_k) - \varepsilon(t_{k-1}) \end{aligned} \right\} \quad (4.16)$$

In algebraic form, the increment of total strain at the k^{th} step is:

$$\Delta\varepsilon_k = \Delta\varepsilon_{visk} + \Delta\varepsilon_{msk} + \Delta\varepsilon_{uk} + \Delta\varepsilon_{Tk} \quad (4.17)$$

For each strain component presented in equations (4.10) to (4.15), by writing the strains at time t_k and time t_{k-1} , and then taking the difference between those two strains and finally applying the trapezoidal rule for incremental strain formulas [74, 2], one obtains incremental strain components in equation (4.17) as follows.

Incremental elastic strain

$$\Delta\varepsilon_{Ek} = \frac{J_0(u_{k-1}) + J_0(u_k)}{2} \Delta\sigma_k + \frac{\sigma_{k-1} + \sigma_k}{2} \Delta J_0(u_k) \quad (4.18)$$

where $\Delta J_0(u_k) = J_0(u_k) - J_0(u_{k-1})$.

Incremental creep strain

$$\Delta\varepsilon_{ck} = J_0(u_{ref}) \sum_{n=1}^N J_n \left[1 - e^{\left(\frac{-\Delta t}{\tau_n} \right)} \right] \left(\frac{\Delta\sigma_k}{2} + \sigma_{nk-1}^{hist} \right) \quad (4.19)$$

where σ_{nk}^{hist} is history stress computed by the recurrent formula:

$$\sigma_{nk}^{hist} = \left[\sigma_{nk-1}^{hist} + \frac{\Delta\sigma_k}{2} \right] e^{\left(\frac{-\Delta t}{\tau_n} \right)} + \frac{\Delta\sigma_k}{2}. \quad (4.20)$$

Incremental mechano-sorptive strain

$$\Delta\varepsilon_{msk} = J^\infty \left[1 - e^{(-c|\Delta u_k|)} \right] \left(\frac{\Delta\sigma_k}{2} + \sigma_{msk-1}^{hist} \right) \quad (4.21)$$

where

$$\sigma_{msk}^{hist} = \left(\sigma_{msk-1}^{hist} + \frac{\Delta\sigma_k}{2} \right) e^{(-c|\Delta u_k|)} + \frac{\Delta\sigma_k}{2} \quad (4.22)$$

Incremental moisture expansion strain

$$\Delta\varepsilon_{uk} = \alpha_u \Delta u_k - b\varepsilon_{k-1} \Delta u_k - \frac{b\Delta\varepsilon_k}{2} \Delta u_k \quad (4.23)$$

where $\Delta u_k = u_k - u_{k-1}$.

Incremental thermal expansion strain

$$\Delta\varepsilon_{Tk} = \alpha_T \Delta T_k \quad (4.24)$$

where $\Delta T_k = T_k - T_{k-1}$.

Substituting equations (4.18), (4.19), (4.21), (4.23), and (4.24) into equation (4.17) and rearranging terms one obtains the incremental stress in term of incremental strains:

$$\Delta\sigma_k = \bar{E}_k \left[\lambda_{uk} \Delta\varepsilon_k - \Delta\varepsilon_{Euk} - \Delta\varepsilon_{Ck} - \Delta\varepsilon_{MSk} - \Delta\varepsilon_{Uk} - \Delta\varepsilon_{Tk} \right] \quad (4.25)$$

where:

\bar{E}_k is the “fictitious” modulus of wood in step the k^{th} , given by

$$\bar{E}_k = \frac{1}{J_{0k} + J_{ck} + J_{msk}} \quad (4.26)$$

in which:

$$J_{0k} = \frac{1}{E(u(t_k))} \quad (4.27)$$

$$J_{ck} = \frac{J_0(u_{ref})}{2} \sum_{n=1}^N J_n \left[1 - e^{\left(\frac{-\Delta t}{\tau_n} \right)} \right] \quad (4.28)$$

$$J_{msk} = \frac{J^\infty}{2} \left[1 - e^{(-c|\Delta u_k|)} \right] \quad (4.29)$$

$$\lambda_{uk} = 1 + \frac{b\Delta u_k}{2}, \quad (4.30)$$

$\Delta \varepsilon_{Euk}$ represents the incremental elastic strain induced by humidity variation, given by

$$\Delta \varepsilon_{Euk} = \sigma_{k-1} [J_0(t_k) - J_0(t_{k-1})], \quad (4.31)$$

$\Delta \varepsilon_{Ck}$ is the incremental strain due to normal creep phenomenon, given by

$$\Delta \varepsilon_{Ck} = J_0(u_{ref}) \left\{ \sum_{n=1}^N J_n \left[1 - e^{\left(\frac{-\Delta t_k}{\tau_n} \right)} \right] \sigma_{nk-1}^{hist} \right\}, \quad (4.32)$$

$\Delta \varepsilon_{MSk}$ is the incremental strain due to mechano-sorptive phenomenon, given by

$$\Delta \varepsilon_{MSk} = J^\infty \left[1 - e^{(-c|\Delta u_k|)} \right] \sigma_{k-1}^{ms,hist}, \quad (4.33)$$

$\Delta \varepsilon_{Uk}$ is the incremental strain due to moisture expansion, given by

$$\Delta \varepsilon_{Uk} = (\alpha_u - b\varepsilon_{k-1}) \Delta u_k, \quad (4.34)$$

and $\Delta \varepsilon_{Tk}$ is the incremental strain due to thermal expansion as defined in equation (4.24).

If there is no variation of relative humidity over time, Δu can be taken as zero. In that case, the equation (4.25) simplifies to:

$$\Delta\sigma_k = \bar{E}_k [\Delta\varepsilon_k - \Delta\varepsilon_{Ck} - \Delta\varepsilon_{Tk}] \quad (4.35)$$

where

$$\bar{E}_k = \frac{1}{J_{0k} + J_{ck}} \quad (4.36)$$

$$J_{0k} = \frac{1}{E(t_k)} \quad (4.37)$$

Equation (4.35) is the standard form for any material that has a normal creep phenomenon.

4.5 Expansion of the constitutive equation to three-dimensional analysis

In this research, the time-dependent behavior of a wood-concrete composite beam with notched shear keys will be investigated based on developing a three-dimensional finite element model so the usage of three-dimensional constitutive equations for wood and concrete is an obligation. Although there are some three-dimensional models for time-dependent behavior of wood such as those of Helnwein [64], Bou-Saïd et al. [65, 66], Svenson and Toratti [95] etc., those models focus on the time-dependent behavior of wood in some extreme conditions of load and environment. The use of a rigorous model for wood would require experimentally determining material parameters, but that determination is beyond scope of the research. The main goal of the research is to understand the time-dependent behavior of the wood-concrete composite structure, but not to focus on studying the time-dependent behavior of wood by itself. Using rigorous models for the wood material is unnecessary in that goal and would be a time consuming solution. As mentioned earlier if the long-term static load is low magnitude then long-

term behavior of wood can be assumed as linear. Thus, expanding of Toratti's model to use in three-dimensional finite element is adopted in the research.

One problem of expanding a one-dimensional model to a three-dimensional model is to select the material parameters for the three-dimensional model. As mentioned above, this research does not focus on experimentally studying material parameters affecting the long-term behavior of the wood material. When those parameters are not available, some assumptions must to be adopted. In 2008, Davies and Fragiacomio [96] reported the total creep perpendicular to the grain of small blocks of laminated veneer lumber (LVL) is about four times larger than the total creep parallel to the grain. As summarized by Mirianon et al. in 2008 [97], four of six Poisson ratios of softwoods are small. Based on those results, the following assumptions were initially adopted in this research:

- *The creep in the parallel to grain direction is adopted from Toratti's model. The creep perpendicular to the grain is taken to be four times larger than the creep in parallel to the grain direction.*
- *1, 2, and 3 are principal directions of a composite beam, where the 1 direction is the longitudinal axis of the beam, then $\nu_{13} = \nu_{31} = \nu_{12} = \nu_{21} = 0$.*

With above assumption, constitutive equation (4.25) can be expanded into the three-dimensional form:

$$\Delta\sigma_k = \bar{C}_k [\Delta\epsilon_k - \Delta\epsilon_{Eu_k} - \Delta\epsilon_{Ck} - \Delta\epsilon_{MSk} - \Delta\epsilon_{Uk} - \Delta\epsilon_{Tk}] \quad (4.38)$$

Or in matrix form:

$$\{\Delta\sigma\}_k = [\bar{C}]_k \left(\{\Delta\epsilon\}_k - \{\Delta\epsilon_{Eu}\}_k - \{\Delta\epsilon_C\}_k - \{\Delta\epsilon_{MS}\}_k - \{\Delta\epsilon_U\}_k - \{\Delta\epsilon_T\}_k \right) \quad (4.39)$$

where

$$[\bar{C}]_k = \begin{bmatrix} \bar{C}_{11k} & \bar{C}_{12k} & \bar{C}_{13k} & 0 & 0 & 0 \\ \bar{C}_{21k} & \bar{C}_{22k} & \bar{C}_{23k} & 0 & 0 & 0 \\ \bar{C}_{31k} & \bar{C}_{32k} & \bar{C}_{33k} & 0 & 0 & 0 \\ 0 & 0 & 0 & C_{44} & 0 & 0 \\ 0 & 0 & 0 & 0 & C_{55} & 0 \\ 0 & 0 & 0 & 0 & 0 & C_{66} \end{bmatrix} \quad (4.40)$$

with

$$\begin{aligned} \bar{C}_{11k} &= \frac{\bar{E}_{11k} (1 - \nu_{23}\nu_{32})}{(1 - 2\nu_{21}\nu_{32}\nu_{13} - \nu_{31}\nu_{13} - \nu_{32}\nu_{23} - \nu_{21}\nu_{12})} \\ \bar{C}_{22k} &= \frac{\bar{E}_{22k} (1 - \nu_{13}\nu_{31})}{(1 - 2\nu_{21}\nu_{32}\nu_{13} - \nu_{31}\nu_{13} - \nu_{32}\nu_{23} - \nu_{21}\nu_{12})} \\ \bar{C}_{22k} &= \frac{\bar{E}_{33k} (1 - \nu_{21}\nu_{12})}{(1 - 2\nu_{21}\nu_{32}\nu_{13} - \nu_{31}\nu_{13} - \nu_{32}\nu_{23} - \nu_{21}\nu_{12})} \\ \bar{C}_{12k} = \bar{C}_{21k} &= \frac{\bar{E}_{11k} (\nu_{21} + \nu_{23}\nu_{31})}{(1 - 2\nu_{21}\nu_{32}\nu_{13} - \nu_{31}\nu_{13} - \nu_{32}\nu_{23} - \nu_{21}\nu_{12})} \\ \bar{C}_{13k} = \bar{C}_{31k} &= \frac{\bar{E}_{11k} (\nu_{31} + \nu_{21}\nu_{32})}{(1 - 2\nu_{21}\nu_{32}\nu_{13} - \nu_{31}\nu_{13} - \nu_{32}\nu_{23} - \nu_{21}\nu_{12})} \\ \bar{C}_{23k} = \bar{C}_{32k} &= \frac{\bar{E}_{33k} (\nu_{23} + \nu_{21}\nu_{13})}{(1 - 2\nu_{21}\nu_{32}\nu_{13} - \nu_{31}\nu_{13} - \nu_{32}\nu_{23} - \nu_{21}\nu_{12})} \\ C_{44} &= 2G_{44} \\ C_{55} &= 2G_{55} \\ C_{66} &= 2G_{66} \end{aligned} \quad (4.41)$$

and

$$\bar{E}_{11k} = \frac{1}{J_{011k} + J_{ck} + J_{msk}} \quad (4.42a)$$

$$\bar{E}_{22k} = \frac{1}{J_{022k} + 4J_{ck} + 4J_{msk}} \quad (4.42b)$$

$$\bar{E}_{33k} = \frac{1}{J_{033k} + 4J_{ck} + 4J_{msk}} \quad (4.42c)$$

$$J_{011k} = \frac{1}{E_{11}(u(t_k))} \quad (4.43a)$$

$$J_{022k} = \frac{1}{E_{22}(u(t_k))} \quad (4.43b)$$

$$J_{033k} = \frac{1}{E_{33}(u(t_k))} \quad (4.43c)$$

J_{ck} and J_{msk} in equation (4.42) are computed using equations (4.28) and (4.29). In formulations (4.41) and (4.43) all material properties such as Young's moduli, shear moduli and Poisson ratios are taken as the properties used in short-term analysis.

In the formulation for three-dimensional analysis, the moisture expansion strain component is modified from equation (4.14) to a simple form which was introduced by Ranta-Maunus [59] as shown in equation (4.44). Fragiaco [4, 69] used equation (4.14) in his model but he noticed that the change of the second coefficient did not yield a significant change of the moisture expansion strains, thus in this research equation (4.22) is reduced to:

$$\varepsilon_u(t) = \int_0^t \alpha_u du(\tau) \quad (4.44)$$

This simplification means that the moisture expansion phenomenon is modeled as thermal expansion:

$$\{\varepsilon_U\}_k = \{\alpha_u\} \Delta u_k \quad (4.45)$$

$$\{\varepsilon_T\}_k = \{\alpha_T\} \Delta T_k \quad (4.46)$$

where $\{\alpha_u\}$ and $\{\alpha_T\}$ are vectors of moisture expansion coefficient and thermal expansion coefficient:

$$\{\alpha_u\} = [\alpha_{u1} \quad \alpha_{u2} \quad \alpha_{u3} \quad 0 \quad 0 \quad 0]^T \quad (4.47)$$

$$\{\alpha_T\} = [\alpha_{T1} \quad \alpha_{T2} \quad \alpha_{T3} \quad 0 \quad 0 \quad 0]^T \quad (4.48)$$

Other incremental stress and strain components are defined as follows:

$$\text{Incremental strain components: } \{\Delta\varepsilon\}_k = [\Delta\varepsilon_{11} \quad \Delta\varepsilon_{22} \quad \Delta\varepsilon_{33} \quad \Delta\varepsilon_{23} \quad \Delta\varepsilon_{13} \quad \Delta\varepsilon_{12}]_k^T.$$

$$\text{Incremental stress: } \{\Delta\sigma\}_k = [\Delta\sigma_{11} \quad \Delta\sigma_{22} \quad \Delta\sigma_{33} \quad \Delta\sigma_{23} \quad \Delta\sigma_{13} \quad \Delta\sigma_{12}]_k^T.$$

With incremental strain vectors induced by normal creep and mechano-sorptive phenomena, only the first three elements in these vectors are non-zero and are computed by formulations similar to equations (4.19), (4.20), (4.21), and (4.22); namely:

$$\Delta\varepsilon_{11ck} = J_0(u_{ref}) \sum_{n=1}^N J_n \left[1 - e^{\left(\frac{-\Delta t}{\tau_n}\right)} \right] \left(\frac{\Delta\sigma_{11k}}{2} + \sigma_{11nk-1}^{hist} \right) \quad (4.49a)$$

$$\Delta\varepsilon_{22ck} = 4J_0(u_{ref}) \sum_{n=1}^N J_n \left[1 - e^{\left(\frac{-\Delta t}{\tau_n}\right)} \right] \left(\frac{\Delta\sigma_{22k}}{2} + \sigma_{22nk-1}^{hist} \right) \quad (4.49b)$$

$$\Delta\varepsilon_{33ck} = 4J_0(u_{ref}) \sum_{n=1}^N J_n \left[1 - e^{\left(\frac{-\Delta t}{\tau_n}\right)} \right] \left(\frac{\Delta\sigma_{33k}}{2} + \sigma_{33nk-1}^{hist} \right) \quad (4.49c)$$

$$\sigma_{11nk}^{hist} = \left[\sigma_{11nk-1}^{hist} + \frac{\Delta\sigma_{11k}}{2} \right] e^{\left(\frac{\Delta t}{\tau_n}\right)} + \frac{\Delta\sigma_{11k}}{2} \quad (4.50a)$$

$$\sigma_{22nk}^{hist} = \left[\sigma_{22nk-1}^{hist} + \frac{\Delta\sigma_{22k}}{2} \right] e^{\left(\frac{\Delta t}{\tau_n}\right)} + \frac{\Delta\sigma_{22k}}{2} \quad (4.50b)$$

$$\sigma_{33nk}^{hist} = \left[\sigma_{33nk-1}^{hist} + \frac{\Delta\sigma_{33k}}{2} \right] e^{\left(\frac{\Delta t}{\tau_n}\right)} + \frac{\Delta\sigma_{33k}}{2} \quad (4.50c)$$

$$\Delta\epsilon_{11msk} = J^\infty \left[1 - e^{(-c|\Delta u_k|)} \right] \left(\frac{\Delta\sigma_{11k}}{2} + \sigma_{11msk-1}^{hist} \right) \quad (4.51a)$$

$$\Delta\epsilon_{22msk} = 4J^\infty \left[1 - e^{(-c|\Delta u_k|)} \right] \left(\frac{\Delta\sigma_{22k}}{2} + \sigma_{22msk-1}^{hist} \right) \quad (4.51b)$$

$$\Delta\epsilon_{33msk} = 4J^\infty \left[1 - e^{(-c|\Delta u_k|)} \right] \left(\frac{\Delta\sigma_{33k}}{2} + \sigma_{33msk-1}^{hist} \right) \quad (4.51c)$$

$$\sigma_{11msk}^{hist} = \left(\sigma_{11msk-1}^{hist} + \frac{\Delta\sigma_{11k}}{2} \right) e^{(-c|\Delta u_k|)} + \frac{\Delta\sigma_{11k}}{2} \quad (4.52a)$$

$$\sigma_{22msk}^{hist} = \left(\sigma_{22msk-1}^{hist} + \frac{\Delta\sigma_{22k}}{2} \right) e^{(-c|\Delta u_k|)} + \frac{\Delta\sigma_{22k}}{2} \quad (4.52b)$$

$$\sigma_{33msk}^{hist} = \left(\sigma_{33msk-1}^{hist} + \frac{\Delta\sigma_{33k}}{2} \right) e^{(-c|\Delta u_k|)} + \frac{\Delta\sigma_{33k}}{2} \quad (4.52c)$$

Chapter 5

Mathematical model for long-term structural behavior of concrete

5.1 Introduction

Shrinkage and creep of the concrete are two phenomena that affect the long-term structural behavior of wood-concrete composite structures. The creep phenomenon occurs when there is a non-zero stress field in concrete. Shrinkage of the concrete occurs even without the presence of a stress field. Unlike the creep in wood, which depends mostly on the load level and the duration of loading, creep in concrete also depends on the age of the concrete at that time the long-term load is applied. Shrinkage and creep result from internal chemical reactions and the lost of water from concrete volume to the ambient environment. Shrinkage and creep of concrete are affected by many factors as mentioned in Chapter 2. Creep in concrete behaves non-linearly at high stress levels or at elevated temperatures. However, at stress levels below 40% of short-term ultimate failure stress (compressive) and normal environmental exposure conditions for civil engineering structures like buildings and bridges, the creep is linear. For that reason, most proposed models of concrete creep assume linear behavior.

Shrinkage and creep of concrete can have considerable influence on the serviceability, durability, and stability of wood-concrete composite structures. To model the long-term structural behavior of a wood-concrete composite beam with notched shear keys, the modeling of shrinkage and creep of concrete must be included. However, the approach

taken in this research is neither to study the shrinkage and creep of concrete nor to propose a new model for it but rather to select a reasonable model from those available, and expand the equations of that model so that they can be applied in a 3D finite element model. Two models, ACI-209R-92 [71] and CEB-FIP 1990 [72], were considered. In expanding the two formulations for 3D finite element method analysis, the author selected the shrinkage model from ACI-209R-92 and the creep model from CEB-FIP 1990. A comparative study by Goel et al. [98] shows that the shrinkage models of both ACI-209R-92 and CEB-FIP 1990 are reasonably consistent with each other, but the formulations in ACI-209R-92 are simpler and easier to use. Lacidogna et al. [99, 100] improved a procedure proposed by Bazant and Wu (1974) [101] to determine Maxwell chain parameters based on the creep model in CEB-FIP 1990. Lacidogna's procedure was used by Fragiacommo (2000) [4, 5] for uniaxial stress state. The approach used in this dissertation work is to expand Fragiacommo's development to 3D formulations for creep based on CEB-FIP 1990.

Two assumptions are employed for using the creep model in three-dimension formulations: 1) visco-elastic behavior is linear and 2) concrete is considered as an isotropic material. As discussed in earlier chapters, the low magnitude of long-term static loading and normal environmental service conditions ensure that the first assumption is valid. For plain concrete, the second assumption is widely accepted. In case of wood-concrete composite beam, although there is nominal temperature and shrinkage steel reinforcement in the concrete layer, it costs execution time and memory to model the rebar inside concrete layer by solid elements. Instead, in this research, the concrete layer with rebar inside is modeled as an isotropic solid media.

5.2. Shrinkage formulation based on ACI-209R-92

The concrete shrinkage prediction mode recommended by ACI-209R-92 after 7 days for moist cured concrete is given by the following equations:

$$(\varepsilon_{sh})_t = \frac{t}{35+t} (\varepsilon_{sh})_u \quad (5.1)$$

where:

$(\varepsilon_{sh})_t$ is the shrinkage strain at time t ;

$(\varepsilon_{sh})_u$ is the ultimate shrinkage strain.

t is the time in days after shrinkage is considered, that is, after the end of the initial wet curing.

If there is no specific shrinkage data for local aggregates and conditions, the ultimate shrinkage strain can be determined from ACI-209R-92 from the following equation:

$$(\varepsilon_{sh})_u = 780\gamma_{sh} \times 10^{-6} \quad (5.2)$$

where:

γ_{sh} is a product of all applicable correction factors for the testing conditions other than the standard condition,

$\gamma_{sh} = 1$ under standard testing condition. The correction factors for γ_{sh} include:

- (1) Correction factor for the effect of initial moist curing: this factor equal to 1.0 for concrete that moist cured for 7 days and equal to 0.93 for concrete that moist cured for 14 days.

- (2) Correction factor for the effect of ambient relative humidity: this factor is used when the ambient relative humidity is greater than 40%:

$$\gamma_{\lambda} = 1.4 - 0.0102\lambda \text{ for } 40 \leq \lambda \leq 80$$

$$\gamma_{\lambda} = 3 - 0.030\lambda \text{ for } 80 \leq \lambda \leq 100, \text{ where } \lambda \text{ is the ambient relative humidity.}$$

- (3) Correction factor for the effect of specimen size is given by the following equation:

$$\lambda_{vs} = 1.2 \exp\left(-0.12 \frac{v}{s}\right) \text{ where } \frac{v}{s} \text{ is the volume-surface area ratio of the}$$

specimen in inches.

- (4) Correction factor for concrete composite: various equations for calculating the correction factor for the effects of the slump of fresh concrete, aggregate content, cement content, and air content in the concrete are recommended in the code, but in most cases, these correction factors can be neglected.

5.3 Creep formulation based on CEB-FIP 1990

In the CEB-FIP 1990 formulations, the creep of concrete depends on the modulus of elasticity and compressive strength that develops in time after the concrete is cast. Before presenting creep formulations, it is necessary to present the formulations of the modulus of elasticity and compressive strength of concrete. The compressive strength of concrete at a specific time after 28 day is determined by the following equation:

$$f_{cm}(t) = \beta_{cc}(t) \cdot f_{cm} \quad (5.3)$$

where

$f_{cm}(t)$ is the average compressive strength of a standard cylinder test.

$\beta_{cc}(t)$ is the coefficient considering the age of concrete, given by the following equation:

$$\beta_{cc}(t) = e^{s\left(1-\sqrt{\frac{28}{t}}\right)} \quad (5.4)$$

where s is a coefficient depending on type of concrete. For normal concrete $s=0.25$.

$f_{cm} = f_{ck} + 8$, where f_{ck} is the characteristic strength of concrete at the age of 28 days (in MPa).

The time-dependent modulus of elasticity is recommended by the following equation:

$$E_c(t) = \beta_E(t)E_c \quad (5.5)$$

where

$E_c(t)$ is the modulus of concrete at time t (days);

E_c is the modulus of concrete at age of 28 days, determined from the compressive strength by equation:

$$E_c = 21500 \sqrt[3]{\frac{f_{cm}}{10}} \text{ [MPa]} \quad (5.6)$$

$\beta_E(t)$ is a coefficient that describes the evolution of modulus of elasticity in time, given from equation:

$$\beta_E(t) = \sqrt{\beta_{cc}(t)}, \text{ where } \beta_{cc}(t) \text{ is defined in equation (5.4).}$$

The creep prediction model in CEB-FIP 1990 is valid for normal weight concrete, when the compressive stress is over 40% of compressive strength, and concrete is exposed to

the environmental condition in which temperature ranges between 5°C and 30°C and relative humidity ranges between 40% and 100%. The creep compliance function was presented earlier as equation (2.16) which is repeated below as equation (5.7)

$$J(t, t_0) = J_0(t_0) + J_{ref} \phi(t, t_0) \quad (5.7)$$

where

$$J_0(t_0) = \frac{1}{E_c(t_0)} \quad (5.8)$$

$$J_{ref} = \frac{1}{E_c} \quad (5.9)$$

The creep coefficient function $\phi(t, t_0)$ is determined from the following equations:

$$\phi(t, t_0) = \phi_0 \beta_c(t - t_0) \quad (5.10)$$

where

ϕ_0 is the creep coefficient at the time of loading t_0 ;

β_c is the coefficient to describe the development of creep in time after loading;

t is the age of concrete at the time that creep is considered;

t_0 is the age of concrete at the time that load is applied.

The creep coefficient ϕ_0 can be estimated by the following expression:

$$\phi_0 = \phi_{RH} \cdot \beta(f_{cm}) \cdot \beta(t_0) \quad (5.11)$$

where

$$\phi_{RH} = 1 + \frac{1 - \frac{RH}{100}}{0.463 \sqrt{\frac{h_0}{h_0}}} \quad (5.12)$$

$$\beta(f_{cm}) = \frac{5.3}{\sqrt{\frac{f_{cm}}{f_{cm0}}}} \quad (5.13)$$

$$\beta(t_0) = \frac{1}{0.1 + t_0^{0.2}} \quad (5.14)$$

In equations from (5.12) to (5.14), new parameters are defined as follows:

$h_0 = \frac{2A_c}{u}$ is the notational size of the member in *mm*, where A_c is the cross-section

of concrete and u is the perimeter of cross-section that contacts with the air;

$$\bar{h}_0 = 100 \text{ mm};$$

$$f_{cm0} = 10 \text{ MPa};$$

RH is the relative humidity of the ambient air in %.

The coefficient of development of creep in time is given by the expression:

$$\beta_c(t-t_0) = \left(\frac{t-t_0}{\beta_H + t-t_0} \right)^{0.3} \quad (5.15)$$

where

$$\beta_H = 150 \left[1 + \left(1.2 \frac{RH}{100} \right)^{18} \right] \frac{h_0}{\bar{h}_0} + 250 \leq 1500 \quad (5.16)$$

5.4 Determination of parameters of generalized Maxwell model for creep of concrete based on CEB-FIP 1990

The use of the generalized Maxwell model is favorable in numerical methods because it is not necessary to retain the entire prior history of stress or strain over each calculation step; indeed the retention of the stress or strain history is virtually impossible after a finite number of steps of analysis. In general, parameters of Maxwell chain are determined by

fitting experimental relaxation curve by using the non-linear least squares method. Most long-term material tests provide experimental creep curves and code provisions provide prediction creep compliance functions so in these cases the creep curves or creep functions must be converted to relaxation curves or to a relaxation function (Bažant and Wu 1974 [101]).

In the case of concrete, the visco-elastic behavior cannot be represented as a single creep curve but requires a series of creep curves to take into account the effects of aging and other factors. To determine the Maxwell chain model for an aging material like concrete, the relaxation or retardation times are often fixed while the elastic moduli are determined at a number of sampling loading ages. The elastic moduli at intermediate loading ages are then determined by multi-linear interpolation.

A procedure to determine the Maxwell chain parameters for concrete based on prediction creep function of CEB-FIP 1990 was developed by Lacidogna [99, 100]. In this procedure, the generalized Maxwell model has seven branches; the relaxation function of the generalized Maxwell model as presented in equation (3.58) can be rewritten as:

$$R(t, t_0) = \sum_{n=1}^7 E_n(t_0) e^{\left(\frac{t-t_0}{\tau_n} \right)} \quad (5.17)$$

The last relaxation time is selected to be much larger than the interested duration of analysis so that $\frac{t-t_0}{\tau_7} \approx 0$ therefore the last elastic modulus E_7 can be determined from the last value of relaxation function. The mechanical representation of the generalized Maxwell model with seven branches in this case is shown in Fig. 5.1.

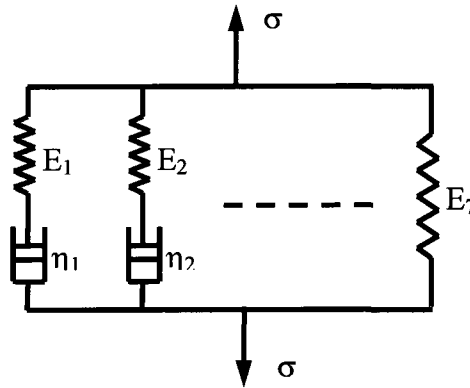


Figure 3.7 Generalized Maxwell model used by Lacidogna.

Other relaxation times are fixed as shown in Table 5.1 and the intervals between two consecutive relaxation times are uniform in logarithmic scale.

The detailed procedure to determine the elastic moduli, which depend on the parameters RH , f_{ck} , and h_0 at any loading ages, was presented in Fragiacommo 2000 [4] for concrete in uniaxial stress state. This research also employs Lacidogna procedure, but Fragiacommo's detailed procedure is not presented herein.

Table 5.1 Relaxation times for concrete

n	τ_n (days)
1	0.075
2	0.75
3	7.5
4	75
5	750
6	7500
7	10^{30}

5.5 Incremental form of constitutive equation for concrete

As represented in Chapter 3, the incremental form of constitutive equation for a visco-elastic material using the generalized Maxwell model is equation (3.66) (for a uniaxial stress state). In case of concrete in wood-concrete composite structures, besides the normal creep strain one must take into account the shrinkage and thermal expansion strains. The total strain is expressed as:

$$\varepsilon(t) = \varepsilon_c(t) + \varepsilon_{sh}(t) + \varepsilon_T(t) \quad (5.18)$$

where: $\varepsilon_c(t)$ is the creep strain; $\varepsilon_{sh}(t)$ is the shrinkage strain; and $\varepsilon_T(t)$ is the thermal expansion strain.

Using the same derivation leading to the equation (3.66) in Chapter 3, the incremental form of constitutive equation for concrete is:

$$\Delta\sigma_k = \bar{E}_k (\Delta\varepsilon_k - \Delta\varepsilon_{ck} - \Delta\varepsilon_{shk} - \Delta\varepsilon_{Tk}) \quad (5.19)$$

where:

$$\bar{E}_k = \sum_{n=1}^7 \frac{1}{2} \left[E_n(t_k) + E_n(t_{k-1}) e^{\left(\frac{-\Delta t}{\tau_n}\right)} \right] \quad (5.20)$$

$$\Delta\varepsilon_{ck} = \frac{1}{E_k} \sum_{n=1}^7 \sigma_{nk-1}^{hist} \left[1 - e^{\left(\frac{-\Delta t}{\tau_n}\right)} \right] \quad (5.21)$$

$$\sigma_{nk}^{hist} = \sigma_{nk-1}^{hist} e^{\left(\frac{-\Delta t}{\tau_n}\right)} + \frac{1}{2} \left[E_n(t_k) + E_n(t_{k-1}) e^{\left(\frac{-\Delta t}{\tau_n}\right)} \right] \Delta\varepsilon_k \quad (5.22)$$

In equations (5.20) to (5.22), elastic moduli $E_n(t_k)$ are determined by Lacidogna's procedure.

Two other incremental strains are calculated as follows:

$$\Delta \varepsilon_{shk} = \varepsilon_{shk} - \varepsilon_{shk-1} = \varepsilon_{sh}(t_k) - \varepsilon_{sh}(t_{k-1}) \quad (5.23)$$

$$\Delta \varepsilon_{Tk} = \alpha_T \Delta T_k = \alpha_T [T(t_k) - T(t_{k-1})] \quad (5.24)$$

where ε_{sh} is the shrinkage strain in equation (5.1), $T(t)$ is the temperature, and α_T is the thermal expansion coefficient of concrete.

5.6 Expansion of the constitutive equation of concrete to three-dimensional analysis

The equations in the previous section for uniaxial stress can be applied directly for one-dimensional problems. To implement the constitutive equation for concrete in ABAQUS using solid elements, the incremental form of constitutive equation must be expanded to 3D form. Mechanical properties of concrete (modulus of elasticity, shear modulus and Poisson ratio etc.) are time-dependent but there are neither data nor models available for these properties in triaxial stress state. Thus in this research it is assumed only the elastic modulus and shear modulus are time-dependent, while Poisson's ratio is a constant in long-term analysis. As applied with wood material, the expansion can be started from equation (5.19) by rewriting it as [102]:

$$\Delta \sigma_k = \bar{C}_k (\Delta \varepsilon_k - \Delta \varepsilon_{ck} - \Delta \varepsilon_{shk} - \Delta \varepsilon_{Tk}) \quad (5.25)$$

or in matrix form:

$$\{\Delta \sigma\}_k = [\bar{C}]_k (\{\Delta \varepsilon\}_k - \{\Delta \varepsilon_c\}_k - \{\Delta \varepsilon_{sh}\}_k - \{\Delta \varepsilon_T\}_k) \quad (5.26)$$

where:

$$\left[\bar{C} \right]_k = \bar{E}_k \begin{bmatrix} \frac{(\nu-1)}{2\nu^2+\nu-1} & \frac{-\nu}{2\nu^2+\nu-1} & \frac{-\nu}{2\nu^2+\nu-1} & 0 & 0 & 0 \\ \frac{-\nu}{2\nu^2+\nu-1} & \frac{(\nu-1)}{2\nu^2+\nu-1} & \frac{-\nu}{2\nu^2+\nu-1} & 0 & 0 & 0 \\ \frac{-\nu}{2\nu^2+\nu-1} & \frac{-\nu}{2\nu^2+\nu-1} & \frac{(\nu-1)}{2\nu^2+\nu-1} & 0 & 0 & 0 \\ 0 & 0 & 0 & \frac{1}{2(1+\nu)} & 0 & 0 \\ 0 & 0 & 0 & 0 & \frac{1}{2(1+\nu)} & 0 \\ 0 & 0 & 0 & 0 & 0 & \frac{1}{2(1+\nu)} \end{bmatrix} \quad (5.27)$$

\bar{E}_k in equation (5.27) is computed as in equation (5.20); ν is Poisson ratio of concrete.

$$\left\{ \Delta \varepsilon_{ck} \right\} = \frac{1}{\bar{E}_k} \left\{ \begin{array}{l} \sum_{n=1}^7 \sigma_{11k-1}^{hist} \left[1 - e^{\left(\frac{-\Delta t}{\tau_n} \right)} \right] \\ \sum_{n=1}^7 \sigma_{22k-1}^{hist} \left[1 - e^{\left(\frac{-\Delta t}{\tau_n} \right)} \right] \\ \sum_{n=1}^7 \sigma_{33k-1}^{hist} \left[1 - e^{\left(\frac{-\Delta t}{\tau_n} \right)} \right] \\ \sum_{n=1}^7 \sigma_{23k-1}^{hist} \left[1 - e^{\left(\frac{-\Delta t}{\tau_n} \right)} \right] \\ \sum_{n=1}^7 \sigma_{13k-1}^{hist} \left[1 - e^{\left(\frac{-\Delta t}{\tau_n} \right)} \right] \\ \sum_{n=1}^7 \sigma_{12k-1}^{hist} \left[1 - e^{\left(\frac{-\Delta t}{\tau_n} \right)} \right] \end{array} \right\} = \frac{1}{\bar{E}_k} \left\{ \sum_{n=1}^7 \sigma_{k-1}^{hist} \left[1 - e^{\left(\frac{-\Delta t}{\tau_n} \right)} \right] \right\} \quad (5.28)$$

$$\left\{ \sigma_{k-1}^{hist} \right\} = \left\{ \sigma_{k-2}^{hist} \right\} e^{\left(\frac{-\Delta t}{\tau_n} \right)} + \bar{E}_{k-1} \left(\left\{ \Delta \varepsilon \right\}_{k-1} - \left\{ \Delta \varepsilon_{sh} \right\}_{k-1} - \left\{ \Delta \varepsilon_T \right\}_{k-1} \right) \quad (5.29)$$

With the assumption that concrete is isotropic material, the shrinkage strain vector in three-dimension case can be represented as:

$$\{\varepsilon_{sh}\}_t = \left[\frac{t}{35+t}(\varepsilon_{sh})_u \quad \frac{t}{35+t}(\varepsilon_{sh})_u \quad \frac{t}{35+t}(\varepsilon_{sh})_u \quad 0 \quad 0 \quad 0 \right]^T \quad (5.30)$$

And the thermal strain vector is expanded from one-dimensional case as follow:

$$\{\Delta\varepsilon_T\} = \{\alpha_T\} \Delta T \quad (5.31)$$

where $\{\alpha_T\} = [\alpha \quad \alpha \quad \alpha \quad 0 \quad 0 \quad 0]^T$ is the vector of coefficient of thermal expansion.

Chapter 6

Finite element implementations in ABAQUS

6.1 Basic equations of finite element method for solid mechanics

In general, the problem of solid mechanics is to find the solution for displacements, strains, stresses or other state variables in a solid body that is subjected to some history of loading and/or body forces. The exact solution requires that both force and moment equilibrium be maintained at all times over any point in the whole volume of the body so that the exact solution is not easy to find in case of complex geometry and boundary conditions. The displacement method of finite element analysis is based on approximating the equilibrium requirements by replacing it with a weaker requirement, that equilibrium must be maintained in an average sense over a finite number of divisions of the volume of the body. The basic equation of finite element method is often developed from the exact equilibrium statement in form of virtual work. The derivation of the basic equations of the finite element method for solid mechanics has been presented in many well known text books on the finite element method and solid mechanics books e.g. [78, 104, 105, 106].

Let V denote a volume occupied by a part of the body in the current configuration, and let S be the surface bounding this volume. Here we are adopting a Lagrangian view point: the volume being considered is a volume of material in the body, V is the volume of space occupied by this material at the “current” point in time. Let \mathbf{t} be the traction force per unit of current area, and let the body force at any point within the volume of the material

under consideration be \mathbf{f} per unit of current volume. Force equilibrium for the volume is then.

$$\int_S \mathbf{t} dS + \int_V \mathbf{f} dV = 0. \quad (6.1)$$

The relation between \mathbf{t} and Cauchy stress matrix $\boldsymbol{\sigma}$, unit outward normal vector \mathbf{n} to S at the point is $\mathbf{t} = \mathbf{n} \cdot \boldsymbol{\sigma}$ (6.2). Apply this definition

$$\int_S \mathbf{n} \cdot \boldsymbol{\sigma} dS + \int_V \mathbf{f} dV = 0.$$

Then apply the Gauss's theorem to rewrite the surface integral as a volume integral:

$$\int_V \left(\frac{\partial}{\partial \mathbf{x}} \right) \cdot \boldsymbol{\sigma} dV + \int_V \mathbf{f} dV = 0.$$

Since the volume is arbitrary, above equation must apply pointwise in the body, thus providing the differential equation of translational equilibrium:

$$\left(\frac{\partial}{\partial \mathbf{x}} \right) \cdot \boldsymbol{\sigma} + \mathbf{f} = 0. \quad (6.3)$$

Similarly, by writing moment equilibrium and then applying the Gauss's theorem with that equation leads to the results that the Cauchy stress matrix must be symmetric:

$$\boldsymbol{\sigma} = \boldsymbol{\sigma}^T \quad (6.4)$$

The basis for the development of a displacement-interpolation finite element model is the introduction of some locally based spatial approximation to parts of the solution. To develop such an approximation, we replace three equilibrium equations (6.3) by an equivalent “weak form” – a single scalar equation over the entire body, which is obtained

by multiplying the pointwise differential equation by a chosen trial function, over the entire volume, and integrating. As the test function is quite arbitrary, the differential equilibrium statement in any particular direction at any point can always be recovered by choosing the test function to be nonzero only in that direction at that point. For this case of equilibrium with general stress matrix, this equivalent “weak form” is the virtual work principle. The test function can be imagined to be a “virtual” velocity field, $\delta \mathbf{v}$, which is completely arbitrary except that it must obey all prescribed kinematic constraints and have sufficient continuity: the dot product of this test function with the equilibrium force field represents the “virtual” work rate.

Taking dot product of equation (3.3) with $\delta \mathbf{v}$ results in a single scalar equation at each material point that is then integrated over the entire body to give:

$$\int_V \left[\left(\frac{\partial}{\partial \mathbf{x}} \right) \cdot \boldsymbol{\sigma} + \mathbf{f} \right] \cdot \delta \mathbf{v} dV = 0 \quad (6.5)$$

Applying the chain rule to equation (6.5) yields:

$$\begin{aligned} \left(\frac{\partial}{\partial \mathbf{x}} \right) \cdot (\boldsymbol{\sigma} \cdot \delta \mathbf{v}) &= \left[\left(\frac{\partial}{\partial \mathbf{x}} \right) \cdot \boldsymbol{\sigma} \right] \cdot \delta \mathbf{v} + \boldsymbol{\sigma} : \left(\frac{\partial \delta \mathbf{v}}{\partial \mathbf{x}} \right), \text{ so that} \\ \int_V \left[\left(\frac{\partial}{\partial \mathbf{x}} \right) \cdot \boldsymbol{\sigma} + \mathbf{f} \right] \cdot \delta \mathbf{v} dV &= \int_V \left[\left(\frac{\partial}{\partial \mathbf{x}} \right) \cdot (\boldsymbol{\sigma} \cdot \delta \mathbf{v}) - \boldsymbol{\sigma} : \left(\frac{\partial \delta \mathbf{v}}{\partial \mathbf{x}} \right) \right] dV \\ &= \int_S \mathbf{n} \cdot \boldsymbol{\sigma} \cdot \delta \mathbf{v} dS - \int_V \boldsymbol{\sigma} : \left(\frac{\partial \delta \mathbf{v}}{\partial \mathbf{x}} \right) dV \\ &= \int_S \mathbf{t} \cdot \delta \mathbf{v} dS - \int_V \boldsymbol{\sigma} : \left(\frac{\partial \delta \mathbf{v}}{\partial \mathbf{x}} \right) dV \end{aligned}$$

Now the virtual work statement can be rewritten as:

$$\int_S \mathbf{t} \cdot \delta \mathbf{v} dS + \int_V \mathbf{f} \cdot \delta \mathbf{v} dV = \int_V \boldsymbol{\sigma} : \left(\frac{\partial \delta \mathbf{v}}{\partial \mathbf{x}} \right) dV$$

One can define $\frac{\partial \delta \mathbf{v}}{\partial \mathbf{x}} = \delta \mathbf{L} = \delta \mathbf{D} + \delta \mathbf{W}$, where $\delta \mathbf{L}$ is virtual velocity gradient in the current configuration, $\delta \mathbf{D}$ is symmetric part and $\delta \mathbf{W}$ is anti-symmetric part of $\delta \mathbf{L}$. With these definitions:

$$\boldsymbol{\sigma} : \delta \mathbf{L} = \boldsymbol{\sigma} : \delta \mathbf{D} + \boldsymbol{\sigma} : \delta \mathbf{W}.$$

Since $\boldsymbol{\sigma}$ is symmetric,

$$\boldsymbol{\sigma} : \delta \mathbf{W} = \frac{1}{2} \boldsymbol{\sigma} : \delta \mathbf{L} - \frac{1}{2} \boldsymbol{\sigma} : \delta \mathbf{L}^T = \frac{1}{2} \boldsymbol{\sigma} : \delta \mathbf{L} - \frac{1}{2} \boldsymbol{\sigma} : \delta \mathbf{L} = \mathbf{0}$$

Then the classical form of the virtual work equation can be written as:

$$\int_V \boldsymbol{\sigma} : \delta \mathbf{D} dV = \int_S \delta \mathbf{v} \cdot \mathbf{t} dS + \int_V \delta \mathbf{v} \cdot \mathbf{f} dV \quad (6.6)$$

Recall that \mathbf{t} , \mathbf{f} , and $\boldsymbol{\sigma}$ are an equilibrium set,

$$\mathbf{t} = \mathbf{n} \cdot \boldsymbol{\sigma}, \quad \left(\frac{\partial}{\partial \mathbf{x}} \right) \cdot \boldsymbol{\sigma} + \mathbf{f} = \mathbf{0}, \quad \boldsymbol{\sigma} = \boldsymbol{\sigma}^T;$$

and that $\delta \mathbf{D}$ and $\delta \mathbf{v}$ are compatible,

$$\delta \mathbf{D} = \frac{1}{2} \left(\left[\frac{\partial \delta \mathbf{v}}{\partial \mathbf{x}} \right] + \left[\frac{\partial \delta \mathbf{v}}{\partial \mathbf{x}} \right]^T \right);$$

This virtual work statement has a simple physical meaning: rate of external work done by the external forces subjected to any virtual velocity field is equal to the rate of virtual work done by the equilibrating stresses on the rate of deformation of the same virtual velocity field.

The left-hand side of the equation (3.6) can be replaced with the integral over the reference volume of the virtual work rate per reference volume defined by any conjugate pairing of stress and strain:

$$\int_{V^0} \boldsymbol{\tau}^c : \delta \boldsymbol{\varepsilon} dV^0 = \int_S \mathbf{t}^T \cdot \delta \mathbf{v} dS + \int_V \mathbf{f}^T \cdot \delta \mathbf{v} dV, \quad (6.7)$$

where $\boldsymbol{\tau}^c$ and $\boldsymbol{\varepsilon}$ are any conjugate pairing of material stress and strain measures.

The finite element interpolator can be written in general as

$$\mathbf{u} = \mathbf{N}_N \mathbf{u}^N, \quad (6.8)$$

where \mathbf{N}_N are interpolation functions that depend on some material coordinate system, \mathbf{u}^N are nodal variables (summation convention is adopted). Thus:

$$\delta \mathbf{v} = \mathbf{N}_N \delta \mathbf{v}^N$$

The virtual rate of material strain $\delta \boldsymbol{\varepsilon}$, associated with $\delta \mathbf{v}$ is rate form. Thus, it must be linear in $\delta \mathbf{v}$, so one can write it in the form:

$$\delta \boldsymbol{\varepsilon} = \boldsymbol{\beta}_N \delta \mathbf{v}^N$$

where $\boldsymbol{\beta}_N$ is a matrix that depends on the current position \mathbf{x} of the material point being considered. Without loss of generality one can write $\boldsymbol{\beta}_N = \boldsymbol{\beta}_N(\mathbf{x}, \mathbf{N}_N)$. Substituting the virtual components into (3.7), the equilibrium equation is approximated as

$$\delta \mathbf{v}^N \int_{V^0} \boldsymbol{\beta}_N : \boldsymbol{\tau}^c dV^0 = \delta \mathbf{v}^N \left[\int_S \mathbf{t}^T \cdot \delta \mathbf{v} dS + \int_V \mathbf{f}^T \cdot \delta \mathbf{v} dV \right];$$

since $\delta \mathbf{v}^N$ are independent variables, one can choose each one to be nonzero and all others zero in turn, to arrive at a system of nonlinear equilibrium equations:

$$\int_{V^0} \boldsymbol{\beta}_N : \boldsymbol{\tau}^c dV^0 = \int_S \mathbf{t}^T \cdot \delta \mathbf{v} dS + \int_V \mathbf{f}^T \cdot \delta \mathbf{v} dV. \quad (6.9)$$

This system of equation forms the basis for the assumed displacement finite element analysis procedure and can be written symbolically as

$$F^N(\mathbf{u}^M) = 0. \quad (6.10)$$

Where F^N is the force component to the N^{th} variable in the problem and \mathbf{u}^M is the value of the M^{th} . The basic problem is to solve \mathbf{u}^M throughout the history of interest.

6.2 Modeling of time-dependent behavior of wood-concrete composite beam with ABAQUS

To analyze the time-dependent structural behavior of layered wood-concrete structures by the finite element method for solid mechanics, the author has three options: 1) develop a specific FEM program (must include solid elements) to solve the problem; or 2) based on applicable open-source FEM programs, add specific modules to solve the problem; or 3) use applicable commercial FEM software which implements solid elements and permit new types of material. The first option permits a highest customization for the developer, but it takes time to develop the program. In addition, writing pre-processing, post-processing modules such as mesh generation for solid bodies, visualization results etc. is time consuming and unnecessary given the other two options are available. The second option helps to reduce the time to write the program if subsequent developers are familiar with open-source FEM programs. However, open source FEM programs often don't

support pre-processing and post-processing abilities. Using commercial FEM software with open-source abilities seems to be the best option for the author at present. To pursue this option the software must be applicable to the problem and available to access.

In this project, the commercial FEM software ABAQUS [78] is chosen as a computational tool. ABAQUS is a general purpose, production-oriented finite element analysis product designed especially for advanced applications. Its powerful modeling tools can be used to solve a wide range of problems from linear static and dynamic analysis to complex nonlinear coupled physic analyses. The following features were considered when choosing ABAQUS as the needed computational tool:

- Ability to solve all related physical problems in the research: diffusion, heat transfer, and stress analysis.
- Provides a robust algorithm to solve contact problem, a key feature permits to model the interaction between two layers in partly composite structures.
- Permits implementation of user-defined subroutines. In this research, subroutine DFLUX is used to define time-dependent load in diffusion and heat transfer analyses; subroutine UMAT is used to implement constitutive model for wood, concrete, and steel.

ABAQUS/Standard provides 46 user subroutines written in FORTRAN to permit ABAQUS users to customize the software for particular applications which cannot be solved directly. Each user subroutine has its own interface which the users have to follow strictly. In particular, user subroutine UMAT allows constitutive models to be added to the program for stress analysis problems, while user subroutine DLUX allows defining a

non-uniform distributed flux as a function of position, time, temperature, element number etc. in heat transfer or mass diffusion analysis.

The time-dependent behavior of wood-concrete composite beam is analyzed in ABAQUS in a two step procedure. The first step includes two independent analyses due to the two types of exposure involved: the diffusion analysis (only moisture diffusion in the wood layer is considered) and the heat transfer analysis. The result of the diffusion analysis is the changing moisture content profile in the wood layer over the analysis time. The input data for the diffusion analysis include the geometric parameters of the wood layer and diffusion coefficient of wood (to build the stiffness matrix), emissivity and the relative humidity history (to build the load vectors). Similarly, the result of the heat transfer analysis is the changing temperature profile in the wood, concrete layers and in the dowels. The input data are geometric parameters, heat conduct coefficients, heat specifics (to build the stiffness matrix), and coefficient of convection heat transfer and temperature history (to build the load vectors).

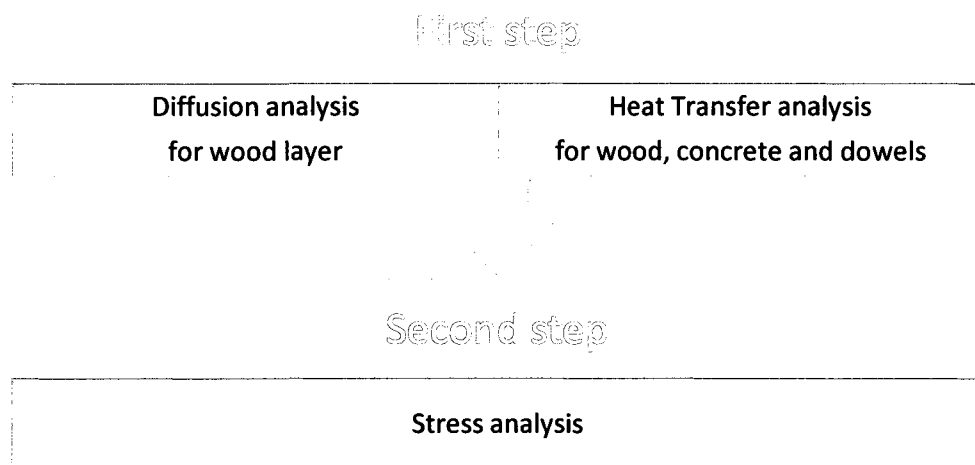


Figure 6.1 Long-term structural behavior analysis of wood-concrete composite beam.

The second step is the stress analysis. In this step, input data include geometric parameters, mechanical properties (elastic moduli, Poisson's ratio, Maxwell chain parameter for concrete, Kelvin chain parameter for wood, moisture expansion coefficients for wood, thermal expansion coefficients for all materials etc.), moisture content profile for the wood layer, temperature profiles for all layers and dowels, long-term static loads, and history of changing load.

To apply the two-step procedure, the geometric meshes in the diffusion analysis, heat transfer analysis, and the stress analysis must be the same coincident nodes although element types are different. The mesh sizes and element types used in analyses are detailed in a following section.

6.2.1 Implementation of the diffusion and heat transfer analyses

The diffusion and heat transfer phenomena are similar in mathematical expression, as presented in Chapter 3, thus they are also similar in the finite element implementation. In ABAQUS, the diffusion of the moisture content in the wood layer can be modeled by choosing the "mass diffusion analysis" type while the heat transfer problem of whole composite beam can be modeled by choosing the "heat transfer analysis" type. The distribution of moisture content in the wood layer varies over the time due to the change of the ambient relative humidity. Similarly, the temperature field in the wood, concrete layers and the dowels vary over the time, so that the type of analysis is transient or non-steady state.

In the moisture diffusion process, the variation of the ambient relative humidity creates a distributed flux of moisture either moving into or out off the exposed surfaces of the wood layer. In the heat transfer process, the variation of the ambient temperature creates

a distributed flux of heat moving through the exposed surfaces of the beam into the interior of the materials. To define the distributed flux, the user subroutine DFLUX is used. Although the DFLUX subroutine permits a non-uniform distributed flux over the body surface, in this research it is assumed that the flux of moisture (diffusion analysis) and the flux of heat (heat transfer analysis) are uniform.

Diffusion analysis

In diffusion analysis, the diffusion coefficient in the perpendicular to grain direction and the surface emissivity of wood proposed by Toratti (1990) are adopted as the following:

$$D_p = 0.432e^{2.28u} \text{ mm}^2/\text{h} \quad (6.11)$$

$$S = 0.468 \text{ mm/h} \quad (6.12)$$

Based on the research of Cai 2005 [107] diffusion coefficient in parallel to grain direction (longitudinal axis of the beam) is about 7-19 times as large as that in the perpendicular to grain directions. In this research the diffusion coefficient in the longitudinal axis of the beam is calculated based on the diffusion coefficient in the transverse direction shown in the equation (6.13) while the surface emissivity proposed by Toratti is applied for all exposed surfaces.

$$D_L = 10D_p \quad (6.13)$$

In equation determining the moisture flux moving through the exposed surfaces (3.5.b), w_{eq} is the equilibrium moisture content in the wood under a specific atmosphere condition. Various formulas to determine the equilibrium moisture content of the wood material have been proposed in the literature. For example, Toratti (1990) assumed that

the equilibrium moisture content depends only on the relative humidity by using equation:

$$w_{eq} = \frac{0.01RH}{(-0.00084823RH^2 + 0.11665RH + 0.38522)} \quad (6.14)$$

where RH is the environmental relative humidity in percentage.

Avramidis [108] and the Wood Hand Book [109] also offer equations for determining the equilibrium moisture content of wood which consider the effects of both environmental relative humidity and temperature. The equilibrium moisture content proposed by Avramidis (1989) is shown in equation (6.15).

$$w_{eq} = 0.01 \left(\frac{-T \ln(1-h)}{0.13(1-T/647.1)^{-6.46}} \right)^{\frac{1}{110T^{-0.75}}} \quad (6.15)$$

where h is the relative humidity in decimal; T is the temperature in Kelvin.

The equilibrium moisture content equation in the Wood Hand Book is represented in equation (6.16) as

$$w_{eq} = \frac{1,800}{W} \left[\frac{Kh}{1-Kh} + \frac{K_1Kh + 2K_1K_2K^2h^2}{1 + K_1Kh + 2K_1K_2K^2h^2} \right] \quad (6.16)$$

where h is the relative humidity in decimal form [%/100].

And for temperature T in Celsius,

$$\begin{aligned} W &= 349 + 1.29T + 0.0135T^2 \\ K &= 0.805 + 0.000736T - 0.00000273T^2 \\ K_1 &= 6.27 - 0.00938T - 0.000303T^2 \\ K_2 &= 1.91 + 0.0407T - 0.000293T^2 \end{aligned}$$

Fig. 6.1 compares the calculated equilibrium moisture content based on the three proposed equations with the monitored relative humidity and temperature from the first seven days of the author's creep test. Moisture content computed by three different equations varies in the same pattern as the variation of the relative humidity. Because Toratti's equation neglected the effect of temperature while the other two equations included the effect of temperature, the results suggest that the equilibrium moisture content depends mostly on the ambient relative humidity, i.e. temperature level is insignificant; all results vary in the same pattern as the variation of the relative humidity. The equilibrium moisture content based on the equation of the Wood Hand Book is almost the same as that based on the equation proposed by Avramidis. The results based on Toratti adoption is about 10-20% higher. The measured moisture content by Fast [2] was closer to the results computed by the Wood Hand Book and Avramidis equations so that in this research the equation in Wood Hand Book is used.

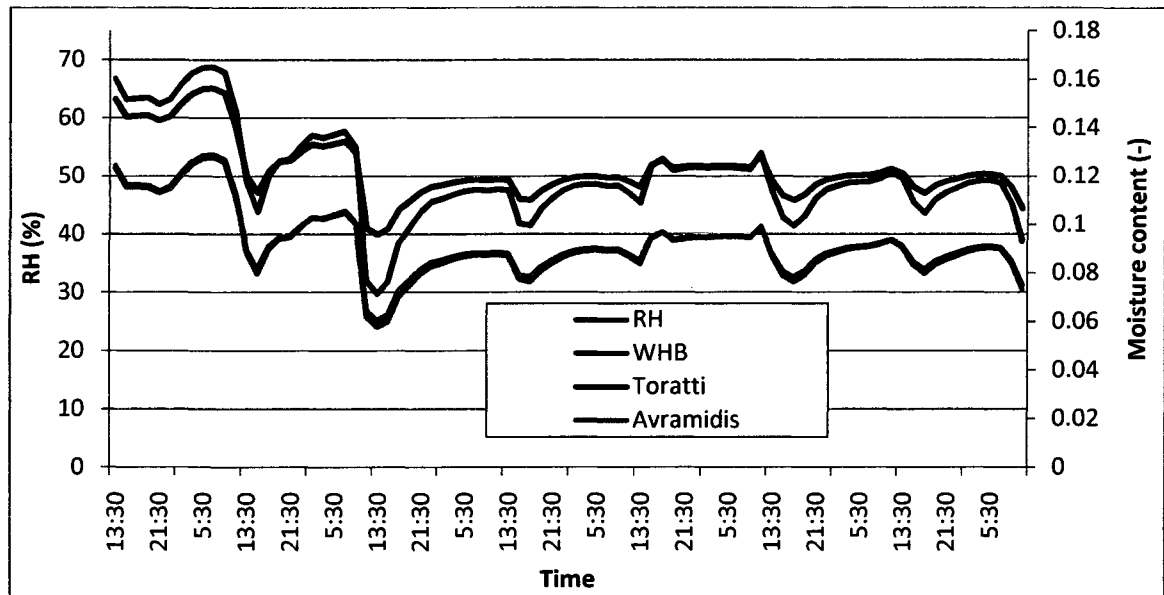


Figure 6.1 The measured relative humidity and the calculated equilibrium moisture content for the first 7 days in the creep test.

Heat transfer analysis

The heat transfer analysis is applied for the wood, concrete layers and dowels. The general thermal properties of three materials are tabulated in the Table 6.1 [104].

Table 6.1 Thermal properties used in the heat transfer analysis.

Materials \ Thermal properties	Heat conductivity k J/(h.mm.°C)	Heat specific c [Joule/(kg.°C)]	Thin film coefficient h J/(h.mm ² .°C)
Wood	0.423	420	0.18
Concrete	6.12	880	0.18
Steel	28.8	450	0.18

6.2.2 Implementation of the stress/displacement analysis

The constitutive equations of wood and concrete materials presented in Chapter 4 and Chapter 5 are implemented in the stress analysis of the wood-concrete beam in the ABAQUS by the user subroutine UMAT. The interface of subroutine as presented in *ABAQUS User Subroutines Reference Manual* [78] is:

```
SUBROUTINE UMAT (STRESS, STATEV, DDSdde, SSE, SPD, SCD,  
 1 RPL, DDSDDT, DRPLDE, DRPLDT,  
 2 STRAN, DSTRAN, TIME, DTIME, TEMP, DTEMP, PREDEF, DPRED, CMNAME,  
 3 NDI, NSHR, NTENS, NSTATV, PROPS, NPROPS, COORDS, DROT, PNEWDT,  
 4 CELENT, DFGRD0, DFGRD1, NOEL, NPT, LAYER, KSPT, KSTEP, KINC)  
C  
  INCLUDE 'ABA_PARAM.INC'  
C  
  CHARACTER*80 CMNAME  
  DIMENSION STRESS (NTENS), STATEV (NSTATV),  
 1 DDSdde (NTENS, NTENS), DDSDDT (NTENS), DRPLDE (NTENS),
```

```

2 STRAN (NTENS), DSTRAN (NTENS), TIME (2), PREDEF (1), DPRED (1),
3 PROPS (NPROPS), COORDS (3), DROT (3, 3), DFGRD0 (3, 3), DFGRD1 (3, 3)

```

*user coding to define DDSDE, STRESS, STATEV, SSE, SPD, SCD
and, if necessary, RPL, DDSDDT, DRPLDE, DRPLDT, PNEWDT*

```

RETURN
END

```

The detailed explanation for the interface can be found in the reference [78], only the most important variables that were updated or modified at each time increment are explained here.

STRESS: This array is passed in as the stress tensor at the beginning of the increment and must be updated in this routine to be the stress tensor at the end of the increment.

DDSDE: Jacobian matrix of the constitutive model, $\frac{\partial \Delta \sigma}{\partial \Delta \varepsilon}$, where $\Delta \sigma$ are the stress increments and $\Delta \varepsilon$ are the strain increments. $DDSDE(I, J)$ defines the change in the I th stress component at the end of the time increment caused by an infinitesimal perturbation of the J th component of the strain increment array.

DSTRAN: Array of strain increments. To update the stress tensor, the array of stress increment is computed based on the array of strain increment.

6.2.3 Element types, mesh sizes, and time steps

The choices for element types, mesh sizes and time step affect the accuracy and computational time of the overall analysis. The selection of the element types, mesh sizes and time steps for the implemented model must balance between the accuracy and practical computational time. The overall problem consists of three field analysis stages and the final analysis stage uses results of two previous analysis stages. The selection of

the mesh sizes and time steps must ensure spatial and time compatibility between the first two analyses and the last analysis.

Although quadratic solid (continuum) elements are available in the ABAQUS, only the 8-node linear brick element was used in the analyses. Specifically, the heat transfer analysis and diffusion analysis used the diffusive heat transfer element DC3D8 while the stress analysis used the stress/displacement element C3D8. To consider the effect of the mesh size to the overall convergence and accuracy, three different mesh sizes were applied for an analysis of short duration. The detail of this analysis is presented in the Appendix B. Based on the results of this analysis, one mesh size was chosen and applied for all analyses.

Beside the mesh size of the element, time step is another important factor that affects the computational time. For model verification analysis, the total time of the experimental test used is short (123 days for longest verification analysis) so selected time steps were one hour or two hours. For prediction analysis (duration of 5 years), a time step of one day was used. The use of a longer time step (for example 24 hours) will leave out the daily variation effect of the relative humidity. However, as shown in the diffusion analysis results in the Chapter 7, the daily variation of relative humidity affects to the variation of the moisture content of only a thin outer shell of the wood layer, so its effect the total creep of the wood layer is small.

Chapter 7

Creep Test and Model Verifications

7.1. Creep Test

A set of creep tests on wood-concrete composite beams with notched shear keys was previously performed by Fast [2] at CSU, but the lack of detailed monitored data on environmental conditions to accompany the deflection readings taken precluded using the outcomes to verify the mathematical model developed herein. Consequently, another long-term creep test program was specially designed in this research to provide thorough data to verify the theoretical model. The ongoing test program involves monitoring the long-term deflection and ambient environmental conditions for two replicate wood-concrete beams with notched shear keys. Each beam was placed in a small wood house without heat and air-conditioning systems. The doors of the houses are opened at daytime so that the environmental conditions inside are almost the same as the conditions outside without getting direct radiation from the sun (see Fig. 7.1). For security reasons, the doors are locked overnight and some weekend days.



Figure 7.1 Tested beams are located in two small wood houses with opened doors at daytime

7.1.1 Beam parameters and material properties

The configuration of the long-term creep test beams is the same as configuration of Fast's beams which is the outcome of many past studies done at CSU. Geometric parameters of the beam are depicted in Fig. 7.2. Each beam was constructed using four notched shear key connections of the geometry shown in Chapter 1 (Fig 1.1). The beam has a total length of 146 inches (3708 mm) and a clear span of 144 inches (3658 mm).

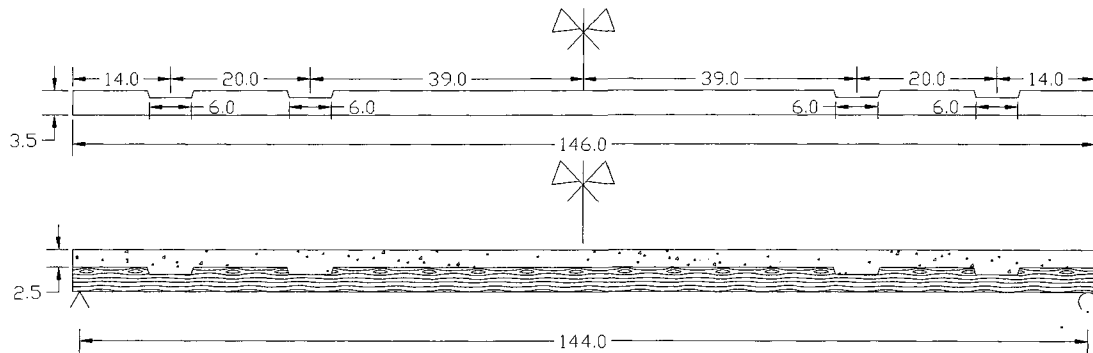


Figure 7.2 Geometric parameters of wood layer and wood-concrete beam. Length unit is in inch.

The wood layer was first pre-assembled from five nominal 2"x4" (actual size 1.5"x3.5" (38mmx89mm)) dimension lumber members placed vertically side by side. They were laterally interconnected by nailing (nail sized d40 at spacing 6 inches (152 mm)); and 0.5 inch (12.7 mm) of camber for wood layer was also created. The detailed procedure to create the camber was introduced by Leborgne and Gutkowski [111]. Then the notches were cut and a steel dowel was installed with epoxy at the center of each notch. To create a good contact between the beam and the supports, each end of the wood layer was covered by a piece of C-channel. The top surface of wood layer was painted by a waterproof paint to minimize moisture moving between the wood layer and the concrete

layer at least at the time of placing the concrete. After preparing the formwork and reinforcing bars, the wood layer was positioned on the supports and left unshored.

Commercial concrete provided by a local company was used for the concrete layer. A superplasticizer was added to the concrete mix before pouring to create a slump of 9 inches (228.6 mm). After placement, the concrete mix was vibrated to remove the air from concrete before curing. The formwork was removed about 24 hours after placing the concrete. Six standard cylinder specimens and two 12"x12"x 6" (304.8 mm x 304.8 mm x 152.4 mm) blocks were cast using the same concrete mix as used for the beams. The cylinder specimens served to determine the modulus of elasticity and the block specimens served to determine the shrinkage of the concrete mix.

The modulus of elasticity of each separate dimension lumber member is different, but the modulus of elasticity of whole wood layer was determined after the wood layer was assembled and before the notches were cut. A bending test was carried out to determine the modulus of elasticity of the wood layer. The wood layer was load tested as a simply supported beam with one point load at center. Three load increments of 52 lbs (230.3 N) were applied, and the corresponding midspan deflection was measured for each 52 lb increment. The modulus of elasticity, E_w was calculated using the following equations:

$$\overline{\Delta v} = \frac{\overline{\Delta P} l^3}{48 E_w I} \rightarrow E_w = \frac{\overline{\Delta P} l^3}{48 I \overline{\Delta v}} \quad (7.1)$$

where

$\overline{\Delta P}$ is the average of load increments = 52 lbs;

$\overline{\Delta v}$ is the average of midspan deflections;

$l=144$ inches (3658 mm) is the span of the beam;

$$I = \frac{bh^3}{12} = \frac{7.5 \times 2.5^3}{12} = 26.80 \text{ in}^4 (1115.5 \text{ cm}^4)$$

is the moment of inertia of wood cross-section.

The moduli of elasticity obtained were 1,780,000 *lbs/in²* (12,300 *N/mm²*) for the first wood beam and 1,670,000 *lbs/in²* (11,500 *N/mm²*) for the second wood beam. The deflection due to shear deformation is ignored when using equation (7.1), but the deflection due to shear deformation is only about 0.3% of the bending deflection in this case.

To determine the modulus of elasticity of the concrete, a standard uniaxial compression test was completed in accordance with ASTM C192-95 and ASTM C39-94. Three cylinders were tested at the 28th day. The initial modulus of elasticity was determined by using equation (7.2) suggested in section 8.5.1 of building code ACI 318-02[112]:

$$E_c = 57000 \sqrt{f'_c} \tag{7.2}$$

where f'_c is the 28-day compressive strength in psi. The average value of modulus of elasticity for three cylinders was 3,970,000 *psi* (27,400 *N/mm²*).

The reinforcement used in the concrete layer consisted of two no. 3 standard deformed steel bars. The main purpose of the rebar is to minimize cracking due to thermal expansion and shrinkage. The possible occurrence of cracking is not considered in the model.

The steel dowel has the following standard mechanical properties:

Modulus of elasticity $E = 30,500 \text{ ksi}$ (210,000 *N/mm²*).

Poisson ratio $\nu = 0.3$.

7.1.2 Long-term static loads

The wood-concrete composite beam begins to respond immediately after the concrete is placed. The stress and strain at any particular time after that casting time depend on the history of loading. For long-term analysis, only long-term loads such as self weight of the beam and self weight of other structural components transferred to the beam during its service life are considered. At the time of placing the concrete, only the wood layer is resisting the load which is only the weight of the concrete layer. Then as the concrete cures and develops strength both layers with interconnection will begin to work together as a composite cross-section. In general, normal weight concrete develops sufficient strength after 28 days of curing for new long-term loads to be applied on the beams. These loads can be the weight of the pavement layer in case of bridge structures, or the weight of the floor covering and furnishings in case of building structures. In the curing time, shrinkage of the concrete layer creates a gap between two layers. After 28 day and before applying any load to the beam, the dowels are tighten to reduce the gap and improve shear stiffness of the notches. In the creep test, each dowel was tightened with a torque of 50 Nm using a torque wrench at day 28. In the numerical model presented later, the dowel tightening process was not modeled because at the current version of ABAQUS, the bolt load can be modeled at the first step only.

In the creep test, two long-term loads are considered: the self weight of the concrete layer and the sustained live load which was applied at the 29th day after placing concrete. The self weight of concrete layer is calculated from concrete density $\rho_c = 147 \text{ lbs} / \text{ft}^3$ (measured from weight of concrete block specimens). The long-term load is created by

weight of concrete blocks as shown in Figs. 7.3 and 7.4. The concrete blocks were weighted and grouped to have two equal sets of weights $P=284 \text{ lbs}$ (1263 N).

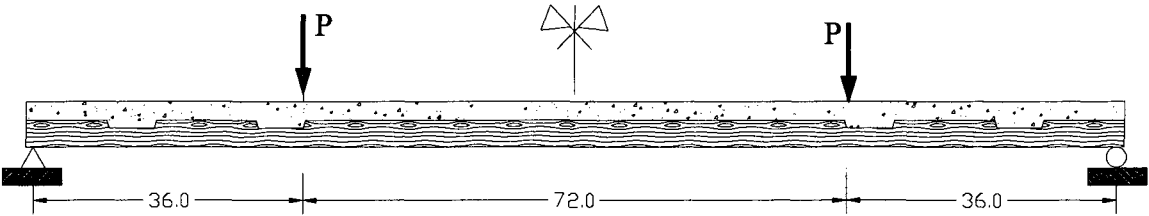


Figure 7.3 Load diagram of wood-composite beam with notched shear keys.



Figure 7.4 Wood-concrete concrete beam 1 and beam 2 with concrete blocks loads

7.1.3 Monitoring and measurements

To capture the long-term structural behavior of a load tested wood-concrete composite beam with notched shear keys, two of most interesting data are beam deflection and slip between the two layers. In addition, the variation of ambient environmental conditions (temperature and relative humidity) needs to be monitored to provide input data for long-term analysis. Real-time data of beam deflections, temperature and relative humidity in the test houses are being measured with appropriate sensors and recorded by a CR-1000 Datalogger, a product of Campbell Scientific Inc..

For the first specimen (wood-concrete beam1), three linear position transducers (string pots) were installed to monitor the deflections at L/4 and midspan of the beam. Two string pots monitoring the deflection at L/4 of the first specimen were then removed after 86 days of the test to be used in another project. At that point in time the data was not critical to the assessment of behavior of the specimen. For the second beam (wood-concrete beam2), only one string pot was installed to monitor deflection at midspan position. The relative humidity in two houses is recorded by two temperature/humidity sensors (the HTM2500 manufactured by Humirel Company). The temperature in first house is recorded by temperature sensor inside the datalogger; and a temperature and humidity datalogger (the RHT10 manufactured by Extech) was used to track both temperature and relative humidity in the second house. For the first six months following casting of the concrete, the datalogger is programmed to scan signal from sensors at every minute and then take average and record the average signal after every 10 minutes. After six months, the interval between two scanning and recording will be increased to keep a longer time of recording.

The slip between two layers is measured by a mechanical Whittemore gage as shown in Fig. 7.5. Four measured points were installed on each beam, two on each side of the beam. To reduce the error due to deformations, a steel bar is used at each measured point to extend the distance between two measured points as shown in Fig. 7.6. One end of the steel bar was rigidly attached to the measured point in the wood layer so that the whole steel bar moves as a rigid body together the measured point in the wood layer when there is slip between two layers. A small cylindrical hole was drilled at the other end of the steel bar (point A in the Figure 7.6). After the steel bar was attached to the wood layer, a small plug with a cylindrical hole on it was located and attached rigidly (point B in the Figure 7.6) to the concrete layer by glue. The distance between two cylindrical holes, one in the steel bar (point A) and one in the small plug (point B), was equal to the base length of the Whittemore gage. This distance changes when there is slip between two layers and the gage measures the change in length of this distance. Slip measurements are taken once per day starting when the beams were first loaded with the long-term load.

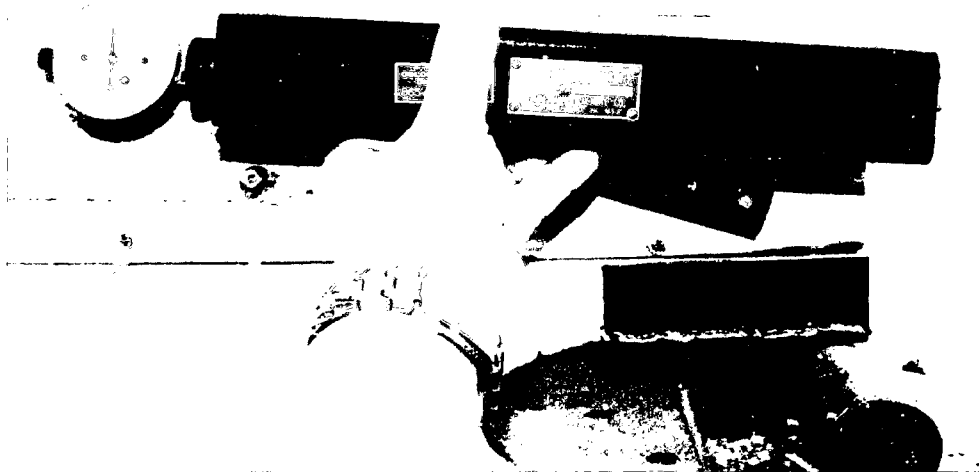


Figure 7.5 Slip measurements by Whittemore gage.

The mechanical Whittemore gage is also used to measure the shrinkage on two 12"x12"x6" concrete block specimens as shown in Fig. 7.7. On each block, two measurement points were attached in two perpendicular directions. The shrinkage measurements are also taken daily.



Figure 7.6 Beam end with apparatus to measure the interlayer slip.

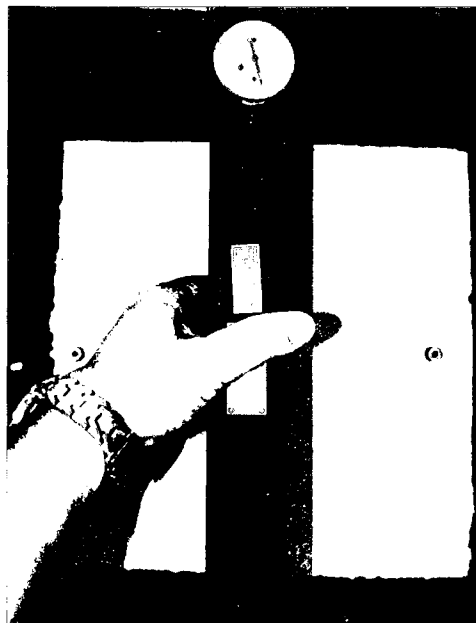


Figure 7.7 Shrinkage measurements by Whittemore gage.

The plugs with a cylindrical hole to measure concrete shrinkage were attached one day after the concrete was placed. A mathematical expression similar to the ACI-219R-92 shrinkage formulation was fitted to the shrinkage data taken in the first 7 days, namely:

$$\varepsilon_{sh}(t) = \frac{t}{t+8} \times 520 \text{ (} 10^{-6} \text{)} \quad (7.3)$$

where t is time in days and $t < 7$ days.

The measured shrinkage and mathematically approximate shrinkage are presented in Fig. 7.8.

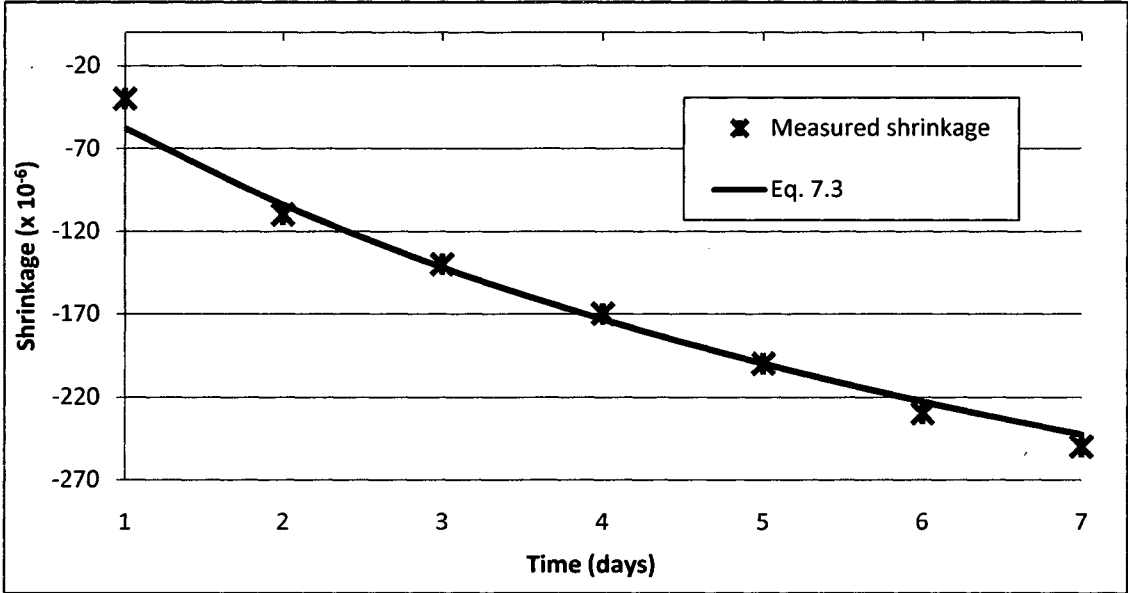


Figure 7.8 Measured shrinkage and fitting shrinkage for first 7 days of the concrete.

7.2 Model verifications and prediction analysis

The aforementioned two-step procedure was applied to analyze the time-dependent behavior of one of the two test specimens (termed “Beam 1”). The first step included the moisture diffusion analysis and the heat transfer analysis. The second step was the stress analysis. Three analyses were conducted. Two analyses were for model verification and

the other analysis was a prediction of time-dependent behavior over a time period of 5 years.

The first model verification analysis (Analysis State 1) is for the duration of first 7 days after the concrete is placed. The reason for doing this analysis is the lack of an empirical shrinkage formulation in the applicable specification codes (ACI-219R-92 and CEB-FIP 1990) for this time period. Thus, equation (7.3) was used in this analysis. The time step in this analysis was 1 hour. The effects of mesh sizes were studied in this analysis state and presented in the Appendix B. The results of mesh size studies led the author to select the Mesh Size 2 to apply for all subsequent analyses. In addition, the heat transfer analysis results in this stage showed that the temperature differential on each layer are small, i.e. almost a uniform; this means that the heat transfer analysis can be ignored if a time step bigger than 2 hours is applied in analysis. The second verification analysis (Analysis State 2) is for the duration of first 123 days i.e. until 93 days after the application of the long-term load. The time step used in this analysis was two hours.

An analysis to predict the time-dependent behavior over a five year period was performed for the Beam 1. The relative humidity and temperature used in the prediction analysis was generated (by replicating) from one year record of a weather station in Fort Collins. The time step used in this analysis was 24 hours.

The results of the diffusion and heat transfer analyses reveal that the characteristics of the variation of the environmental conditions (temperature and relative humidity in the ambient environment) can affect the long-term structural behavior of the wood-concrete composite beam. So some characteristics of the natural temperature and relative humidity records are considered in the Appendix A.

7.2.1 Diffusion and heat transfer analysis results

Diffusion analysis results

Because the daily variation of the relative humidity has a pattern roughly similar to a sine/cosine function, an additional diffusion analysis was performed with a sine function of the relative humidity. Figure 7.9 plots the variations of the relative humidity and the calculated moisture content of five chosen node points (depicted in the Figure 7.10) on the midspan cross-section over a period of five days. The relative humidity varies as a sine function with a period of 24 hours and amplitude of 25% and 75%. The results of this analysis show that when the period of the relative humidity function is as short as one day, the variation of the relative humidity affects only the variation of the moisture content of a thin outer shell of the wood layer. The implication is that the fluctuation of the relative humidity with high frequency (more than one period per day) does not affect the variation of moisture content at inner points. The moisture content of inner points remains unchanged over the time or varies linearly and reaches an equilibrium value after a period of time. There is a phase difference between the relative humidity and moisture content. The magnitude of a phase difference depends on the distance from that point to the exposed surface. For example, the phase difference of node 47 (on the exposure surface) was about six hours while the phase difference of node 420 (0.875 inches (22.26 mm) from the exposure surface) was about twelve hours.

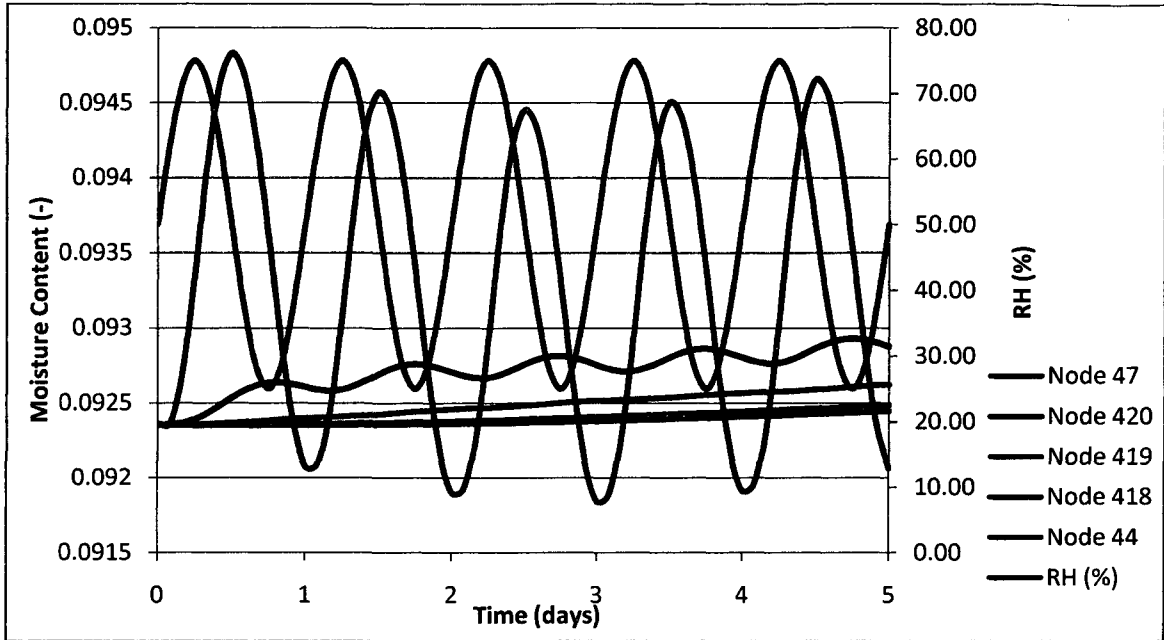


Figure 7.9 Relative humidity and calculated moisture content variation in 5 days.

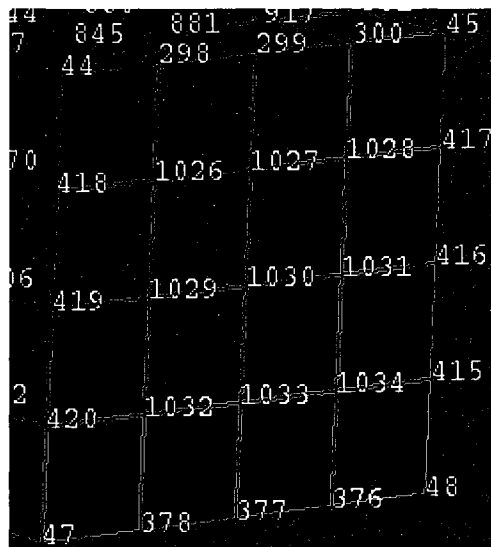


Figure 7.10 Node labels for the mid-span cross-section – the wood layer.

Figure 7.11 illustrates the relative humidity and calculated moisture content at the same five chosen node points for Beam 1 from July 3rd to November 3rd (Analysis State 2). The spatial distribution of the moisture content at the end of the second verification analysis (11:30 AM November 3rd) is shown in the Fig. 7.12. Figure 7.13 illustrates the relative humidity and calculated moisture content for one year in the five-year prediction

analysis. The results shown in figures 7.11 and 7.13 confirmed that the moisture content at inner points on the cross-section is only affected by low-frequency variation of the relative humidity. Based on this observation, for a long duration of analysis one can ignore the effects of daily variation of the relative humidity by choosing a big time step to reduce the computational time.

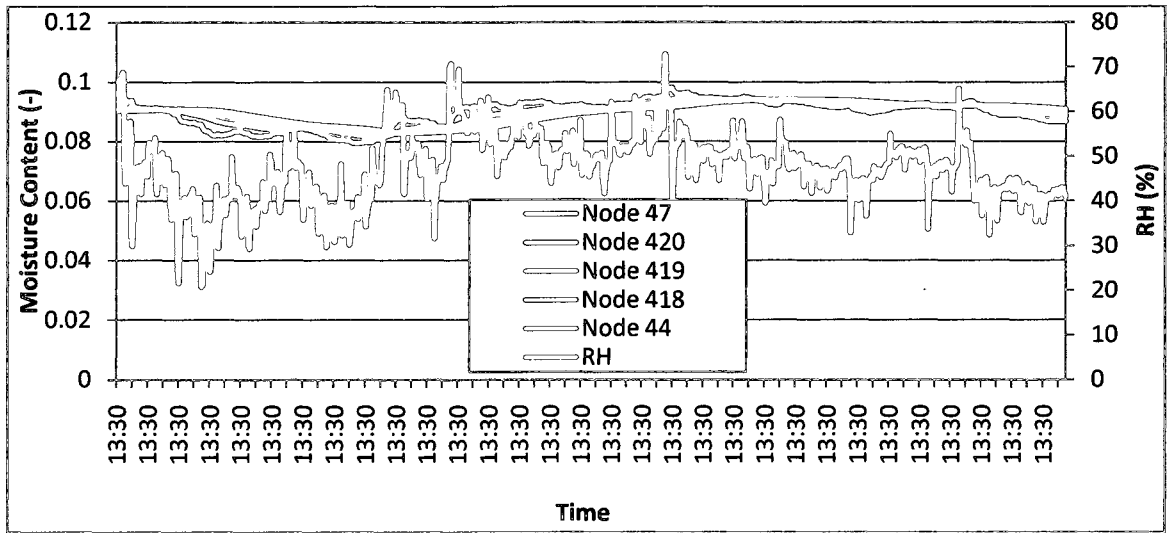


Figure 7.11 Relative humidity and calculated moisture content for Beam 1 from July 3rd to November 3rd.

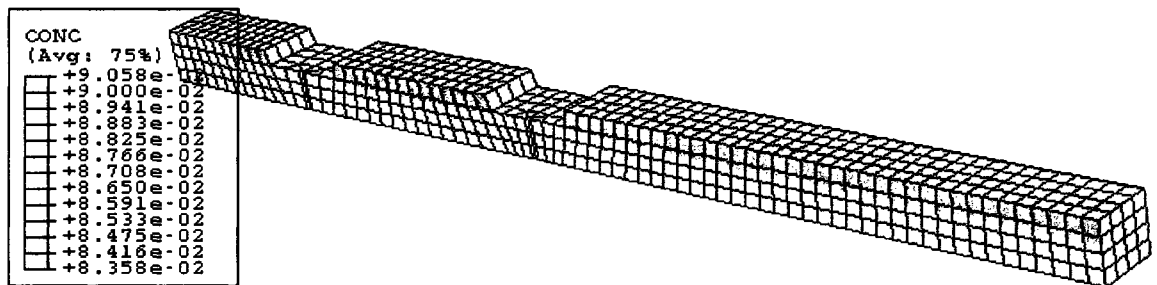


Figure 7.12 Calculated moisture content distributions in wood layer at 11:30 AM November 3rd.

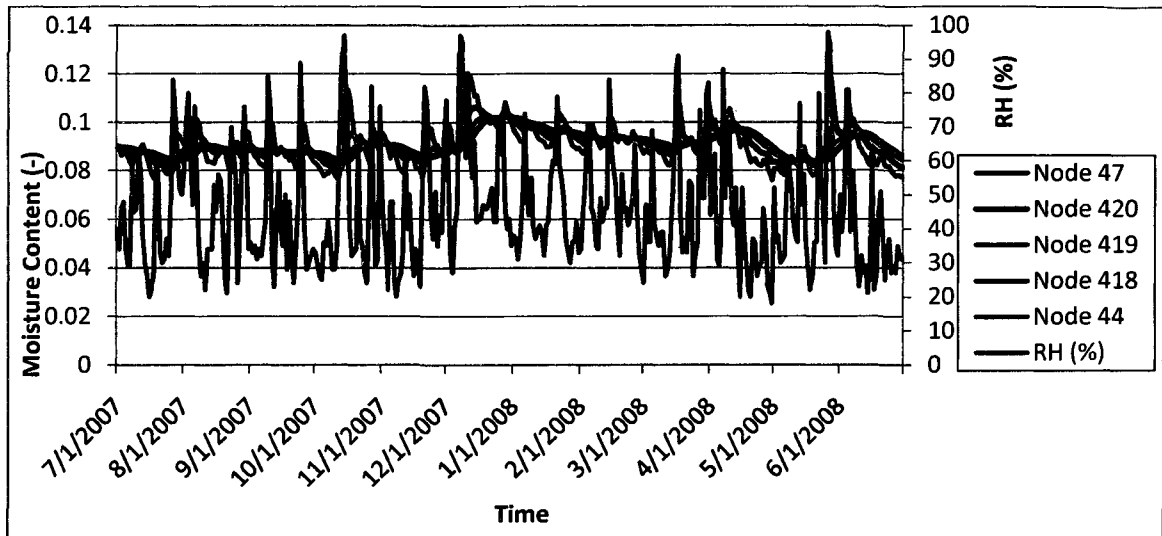


Figure 7.13 Relative humidity and predicted moisture content variations for Beam 1 in one year.

The diffusion analysis with actual relative humidity and temperature records confirmed that only low frequency variation of the relative humidity affects the variation of the moisture content at inner points. For example in the Analysis State 2, the moisture content of inner points (equal to or larger 22.26 mm from the exposure surfaces) underwent less than one wetting/drying cycle over a duration of 123 days. In five year prediction analysis, the moisture content of inner points underwent about five wetting/drying cycles each year.

Heat transfer analysis results

The results of the heat transfer analysis in the Analysis State 1 were plotted for five selected node points in both layers. The variations of the nodal temperatures and the ambient temperature for the wood are plotted in the Figure 7.14. Figure 7.15 depicts the nodal labels for the midspan cross-section of the concrete layer. The variation of temperature at nodes 86, 556, 557, 558 and 83 for the concrete layer are plotted with the ambient temperature in Figure 7.16. Figure 7.17 illustrates the overall calculated

temperature field in the entire beam at the end of the Analysis Stage 1. The nodal temperatures in the wood layer for one year in the 5 year prediction analysis are plotted with the ambient temperature in the Figure 7.18.

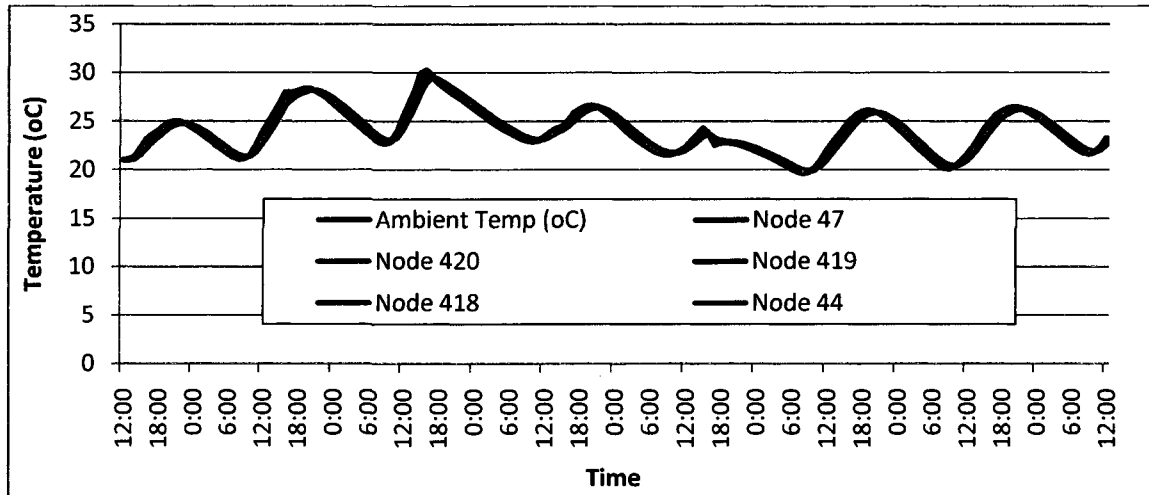


Figure 7.14 Variation of ambient temperature and calculated temperature in the first 7 days in the wood layer – the Analysis State 1.

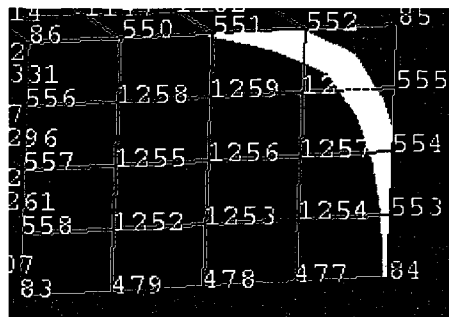


Figure 7.15 Node labels for the mid-span cross-section – the concrete layer.

Compared to the moisture diffusion process, the heat transfer process happens much faster. As seen in Figures 7.14, 7.15, and 7.18, the nodal temperatures vary closely with the variation of the ambient temperature. In analyses with one-hour or two-hour time steps, at each specific time the differences of temperature at different points are small, i.e. a maximum of about 0.8°C difference in the concrete layer and about 1.6°C difference in the wood layer. There are also phase shifts between nodal temperatures and the ambient

temperature but these differences are short (maximum less than two hours). In the 5 year prediction analysis when 24-hour time step was used, the nodal temperatures were the same as the ambient temperature.

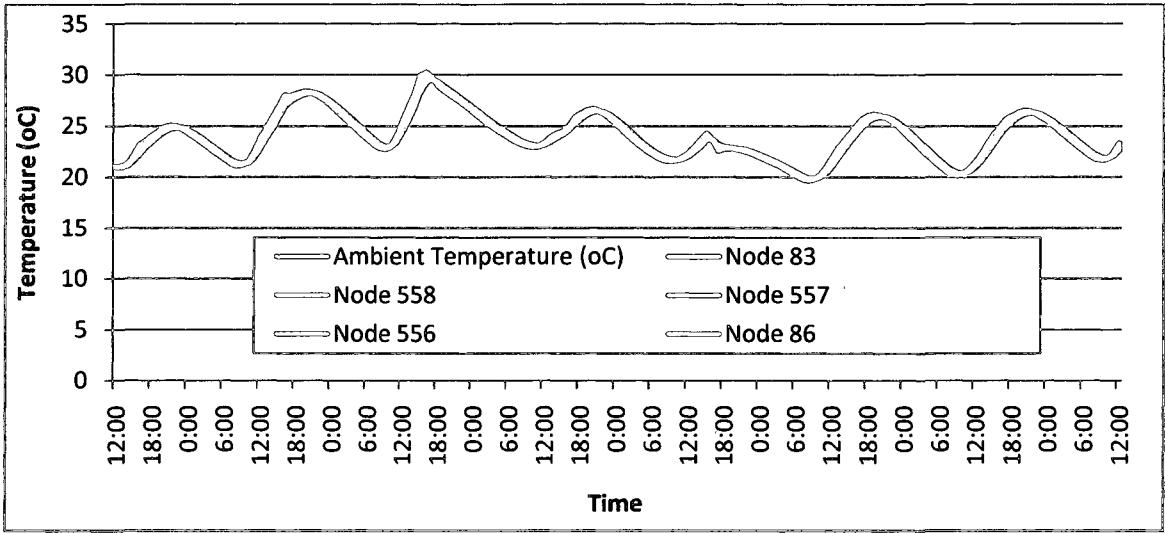


Figure 7.16 Variations of ambient temperature and calculated temperature in the first 7 days in the concrete layer – the Analysis State 1.

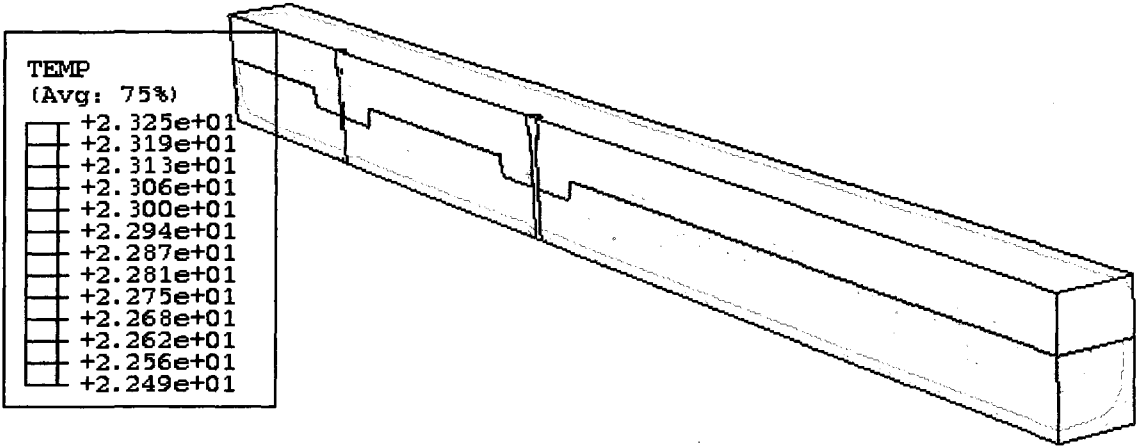


Figure 7.17 Calculated temperature distributions at the end of the Analysis State 1.

The variation of the non-uniform temperature field in each material creates a thermal stress field on that material. But the difference in the temperature is small so the thermal stress field created by a non-uniform temperature field is also small. An additional stress analysis was performed to consider the effect of the variation of the non-uniform temperature field. The results of this analysis are summarized in the Appendix C and it showed that for long-term analysis, the use of a non-uniform temperature profile from the heat transfer analysis as input information for the stress analysis is not necessary. For that reason, an assumed uniform temperature field for each layer was adopted in all subsequent analyses. This assumption helps reduce the computational time while maintaining the necessary accuracy. The adopted trend in time of such a uniform temperature was the average of nodal temperature at the midspan cross-section.

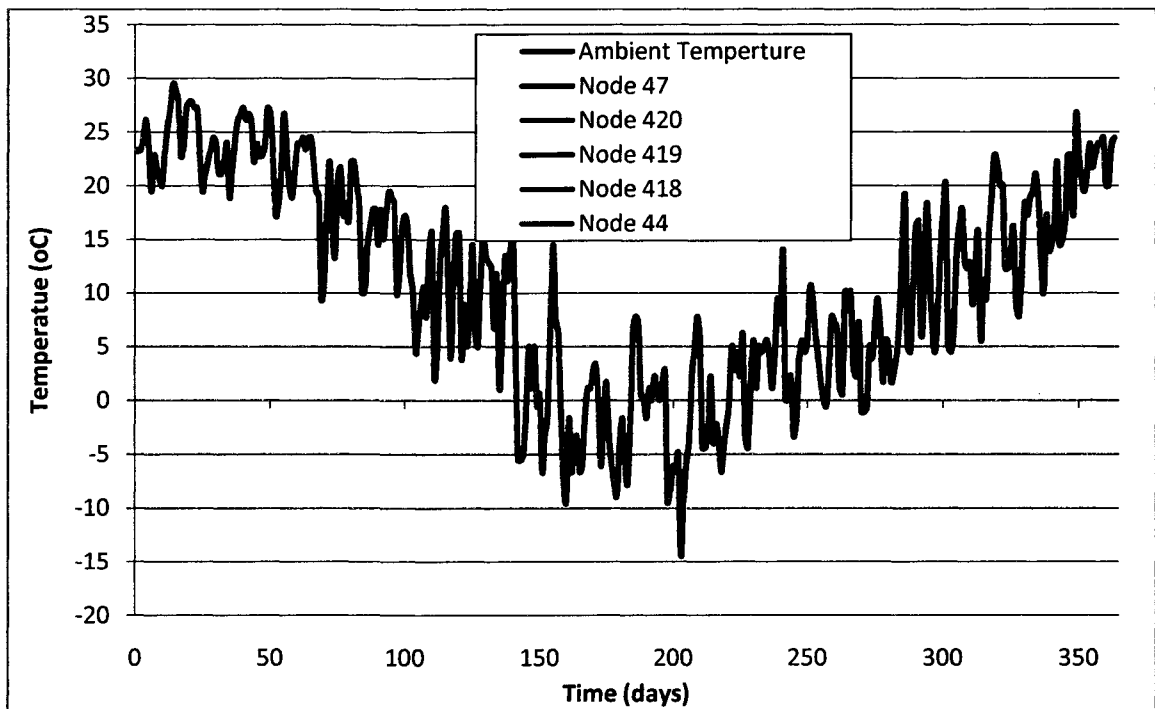


Figure 7.18 Ambient temperature and calculated nodal temperature for one year in the five-year prediction analysis.

7.2.2 Test results and model verifications

Test results

The concrete layers of the two creep specimens were cast on July 3rd 2008. Beam deflection, temperature and relative humidity have been monitored and recorded since that time. Long-term static load was applied 29 days after the concrete layers were cast. Measured beam deflections for the first 123 days (until November 3, 2008) of the test are plotted in the Figure 7.19. The measured deflections at L/4 of the Beam 1 after the day of September 26, 2008 (at 54th day) were not available because the string pots monitoring the deflection at those points were removed. Figures 7.20 and 7.21 illustrate the measured deflections of the Beam 1 plotted versus the air temperature history and the relative humidity history, respectively.

The results for the first 123 days of the creep test exhibit several important characteristics. First, the measured deflections of both specimens vary in a same pattern. Since the data were measured by separate sensors installed in two different houses, this suggests the measurements are reliable. Second, both specimens responded in the same way to the static load and the variation of the environmental conditions. Third, the time-dependent behavior of the specimens is sensitive to the variation of the ambient temperature. Fourth, the time-dependent behavior of the specimens is not sensitive to the variation of the ambient relative humidity. Any sudden change with high magnitude of the relative humidity does not yield a recognizable change in the deflection.

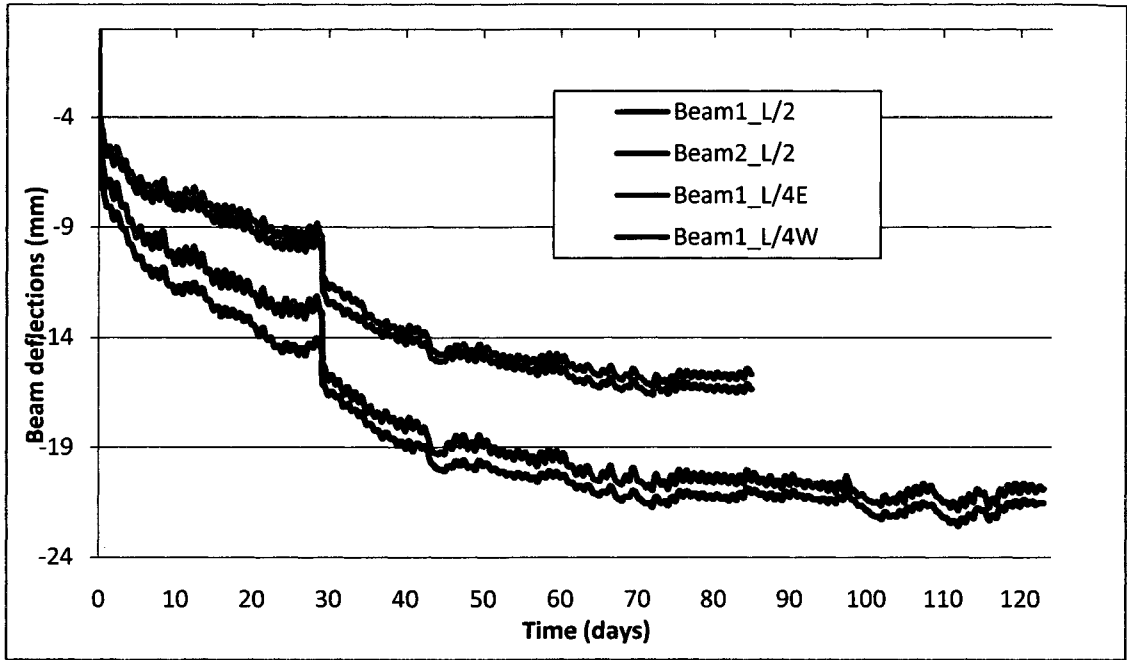


Figure 7.19 Measured beams' deflections for the first 123 days of the creep test.

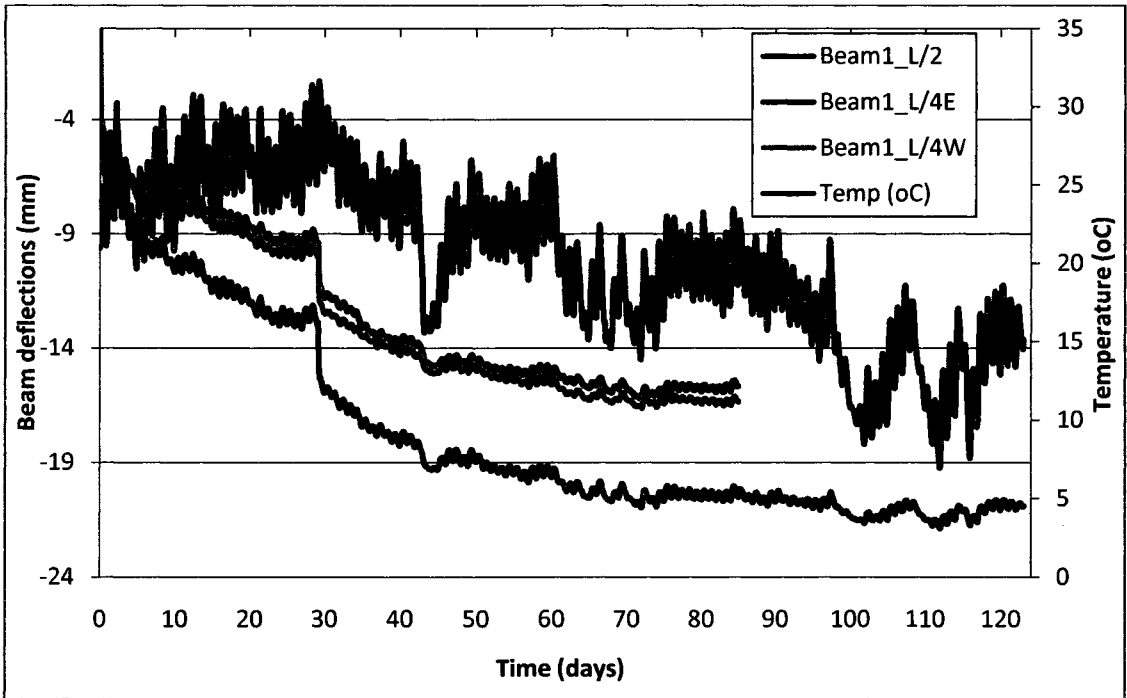


Figure 7.20 Measured deflections of the Beam 1 plotted with the air temperature.

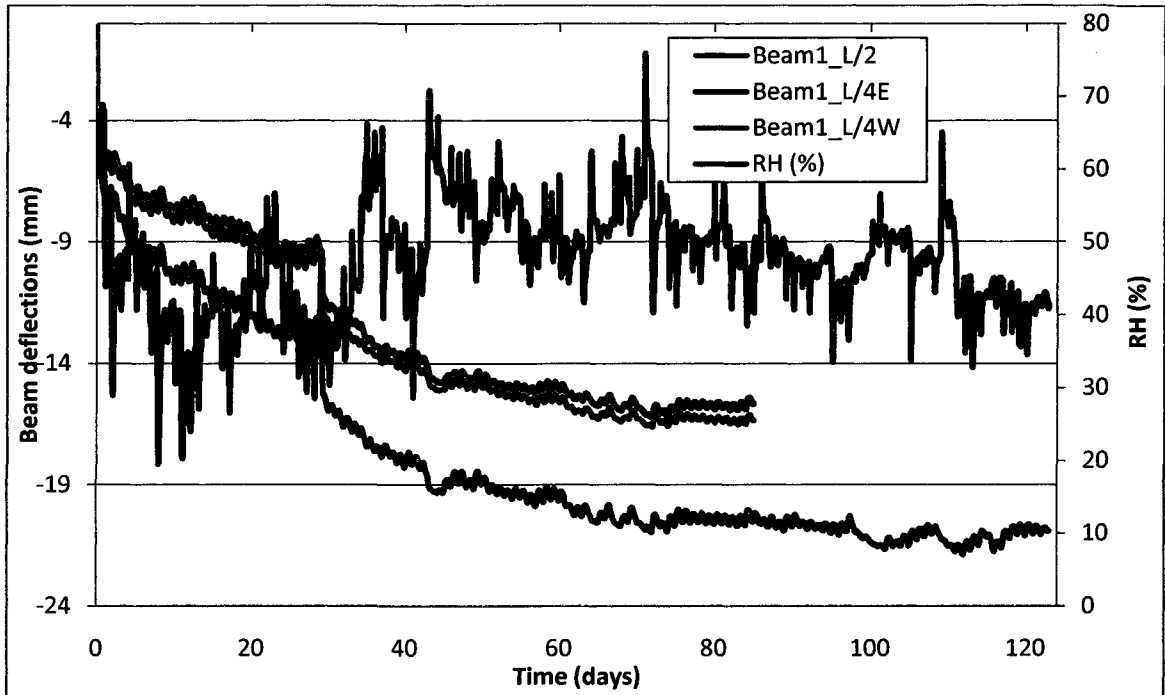


Figure 7.21 Measured deflections of the Beam 1 plotted with the relative humidity.

Stress analysis results of the model verification analyses

The two specimens were built in the identical geometry configuration, used the same mix of concrete. They were subjected to the same type and duration of load and undergone almost the identically environmental conditions. The only noticeable difference between the two specimens is in the initial modulus of elasticity of the wood layer for each of them. This difference led to a slight difference in the observed deflections as is evident in Fig. 7.19. Because of the close similarity of conditions and response, only one specimen is presented herein.

Physical and mechanical properties of wood and concrete used in the stress analysis are summarized in tables 7.1 and 7.2. For wood material, only modulus of elasticity in longitudinal direction was determined as presented in section 7.1.1, other mechanical properties were referenced based on previous works of other authors [70, 98, 109, 112].

The coefficients of moisture expansion and thermal expansion of wood material were adopted from Fragiaco [98] and Engineering toolbox website [110]. For concrete material, the modulus of elasticity was determined as mentioned in section 7.1.1; the thermal expansion coefficient was adopted from Fragiaco [98]. For steel (dowel), the coefficient of thermal expansion was 0.000011 [110].

Table 7.1 Material properties of wood material

Material properties	Meaning	Value	Unit
E_{11}	Elastic moduli	12300	N/mm^2
E_{22}		981	N/mm^2
E_{33}		981	N/mm^2
ν_{23}	Poisson's ratios	0.558	-
ν_{13}		0	-
ν_{12}		0	-
G_{23}	Shear moduli	1241	N/mm^2
G_{13}		986	N/mm^2
G_{12}		986	N/mm^2
α_{u1}	Coefficient of moisture expansion	0.003	-
$\alpha_{u2}=\alpha_{u2}$		0.006	-
α_{T1}	Coefficient of thermal expansion	0.0000049	-
$\alpha_{T2}=\alpha_{T2}$		0.0000054	-

Table 7.2 Material properties of concrete material

Material properties	Meaning	Value	Unit
E_{c28}	Elastic modulus at day 28	27400	N/mm^2
ν	Poisson's ratios	0.2	-
α_T	Coefficient of thermal expansion	0.000012	-

Results of Analysis State 1

In this analysis, the shrinkage of concrete is calculated from equation (7.3). The stress analysis is divided into three steps. The first step models the time after concrete is placed where the modulus of elasticity of the concrete is a very small arbitrary value (taken as $E_c / 1000$) so only the wood contributes to the stiffness of the beam. The load is the self weight of the concrete layer. The second step models behavior up to 6 hours after the placing of the concrete. In this step, the modulus of elasticity of the concrete layer is time-dependent and computed from equation (2.14). The shrinkage of the concrete is not considered, while the thermal expansion of concrete is included. The third step lasts from the end of the second step to 7 days after the placing of the concrete. In the third step, the modulus of elasticity of the concrete is calculated from equation (2.14), while the shrinkage of the concrete is calculated using equation (7.3).

The time increment used in each analysis step was one hour. The time increment in the measured data is 10 minutes, so to get the input series of temperature and relative humidity for diffusion analysis and heat transfer analysis as well, the measured data series were reduced in the length by averaging the data taken within each hour. The measured deflection data series were also reduced in the same way to make them comparable to the deflections from the analytical results. The measured and analyzed deflections at midspan for the first 7 days are plotted in Fig. 7.22, together with the temperature record.

The measured midspan deflection of the beam (wood layer only) due to the weight of the wet concrete layer was 5.25 mm (immediately after the fluid concrete had fully filled the formwork) while the corresponding deflection from the mathematical analysis

(ABAQUS) is 6.17 mm. This indicates that the actual beam is stiffer than the prediction from the mathematical model. The difference between the two values is explained as follows: In the beam specimen at the time of placing concrete, the formwork is attached to the wood layer. The formwork increased the stiffness of the wood layer at the time of placing concrete. The formwork is not considered in the model and it was removed at about 24 hours after placing the concrete layer. From the measured deflection series, there is no sudden change of the deflection at the time of removing the formwork. This can be explained as: at that time (after 24 hours of curing), the concrete layer gained some stiffness and contributed to the total stiffness of the composite beam; the stiffness contributed by the formwork is small compared with the total stiffness of the composite beam.

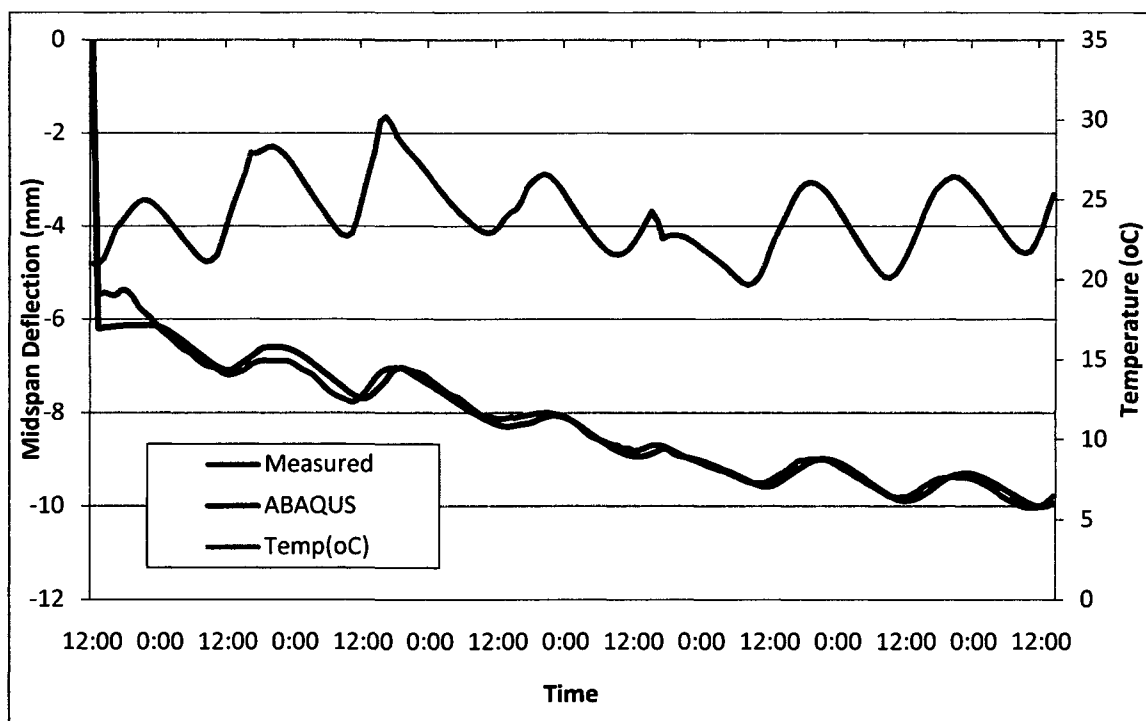


Figure 7.22 Beam deflections plotted with the temperature record for the first 7 days.

Results of Analysis State 2

The stress analysis in the Analysis State 2 includes six steps. The first three steps are the same as in the Analysis State 1. The fourth step models the behavior from the day 7 to day 29 before applying the long-term static load. The fifth step models the instantaneous response at the time of the application of long-term static load (at day 29). The sixth step models the structural response for the time of application of the applied long-term static load until day 123(November 3rd 2008) since the placing of the concrete. From the fifth step, all related physical phenomenon are considered for all materials. The time increment in each step is two hours.

The long-term applied load (See Fig. 7.3) was $P = 1263N$ (284 lbs), i.e. the weight of the concrete blocks placed at each load point. The instantaneous measured increase in deflection at midspan due to the application of concrete blocks was 0.093 inches (2.36 mm). The corresponding deflection from the developed prediction model is 0.095 inches (2.42 mm). This indicates that the finite element model predicted the outcome of the short-term deflection behavior of the specimen within 2.5%. Figs. 7.23 and 7.24 show the comparisons between measured deflection and corresponding ABAQUS results over the time period of analysis (plotted together with the temperature relative humidity records), respectively. After applying the long-term load, the predicted midspan deflection from the developed FEM model closely agrees with the measured deflection response. The proposed FEM model captures very well overall effect of all related physical phenomena that affect the long-term structural behavior of the specimen.

The results obtained from the model also suggest that the proposed model is reliable for longer duration of analysis to predict the long-term structural behavior of the wood-

concrete composite beam if the variation of the ambient environmental conditions is known.

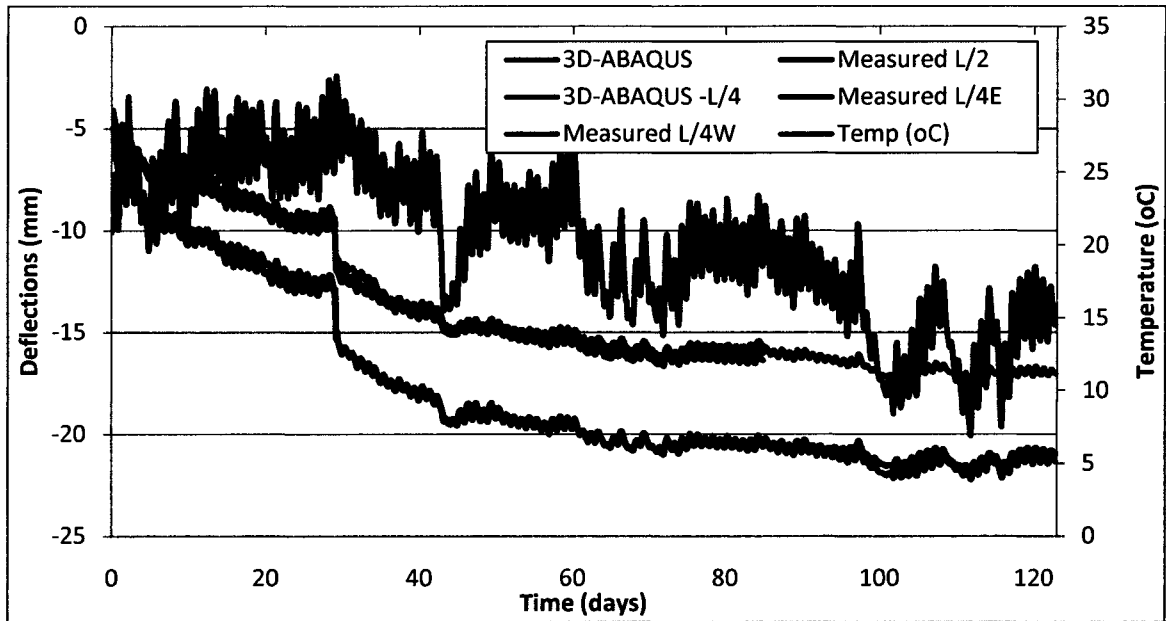


Figure 7.23 Beam deflections plotted with temperature record for the first 123 days.

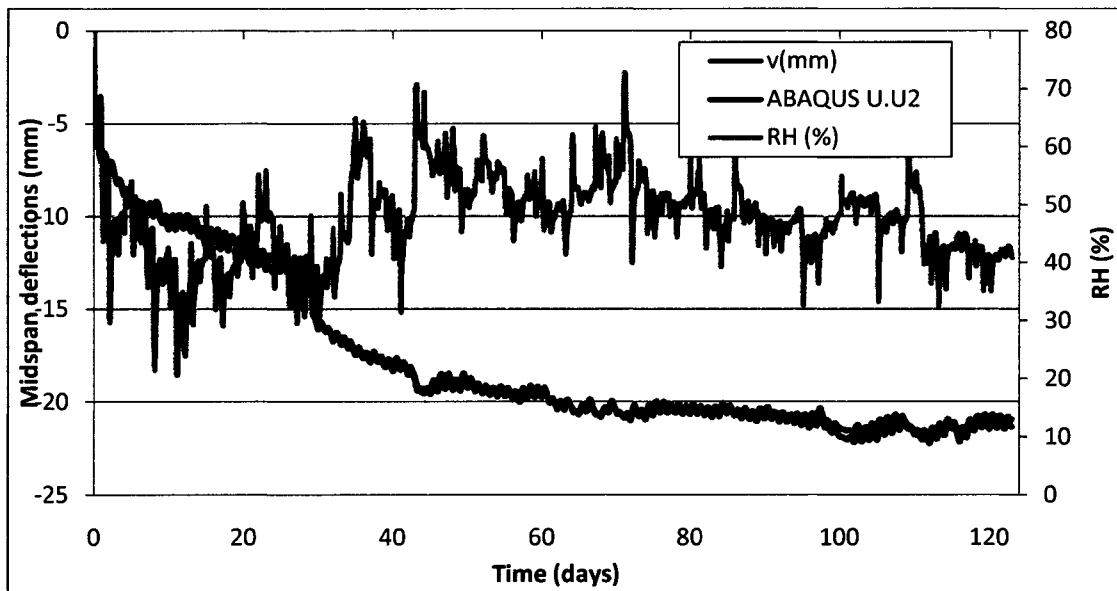


Figure 7.24 Beam deflections plotted with relative humidity record for the first 123 days.

7.2.3 Time-dependent behavior prediction based on the proposed model

An FEM prediction analysis was performed on the test specimen Beam 1 for a five-year period of time. The temperature and relative humidity records used in the analysis were replicated from a one year record (from July 1st 2007 to June 30th 2008) of data for a weather station located at Horsetooth Lake Estates, Fort Collins. The data are available at the Weather Underground website. The temperature and relative humidity are in a form of daily average values for each day, so a 24-hour time step was chosen in the prediction analysis. The loading events were applied as in the creep test: the concrete weight was applied on the wood layer at the beginning and long-term static load was applied on the composite beam at the day 29th. Figure 7.25 and 7.26 show the midspan deflection plotted with the ambient temperature and the relative humidity, respectively.

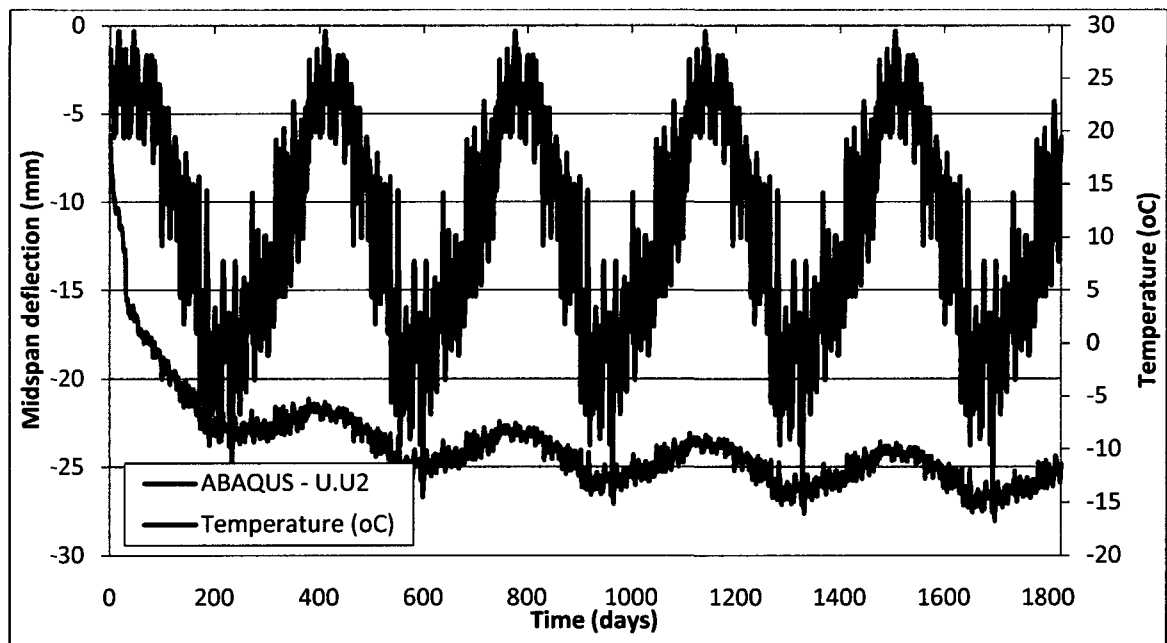


Figure 7.25 Midspan deflection plotted with the temperature record – 5-year prediction analysis.

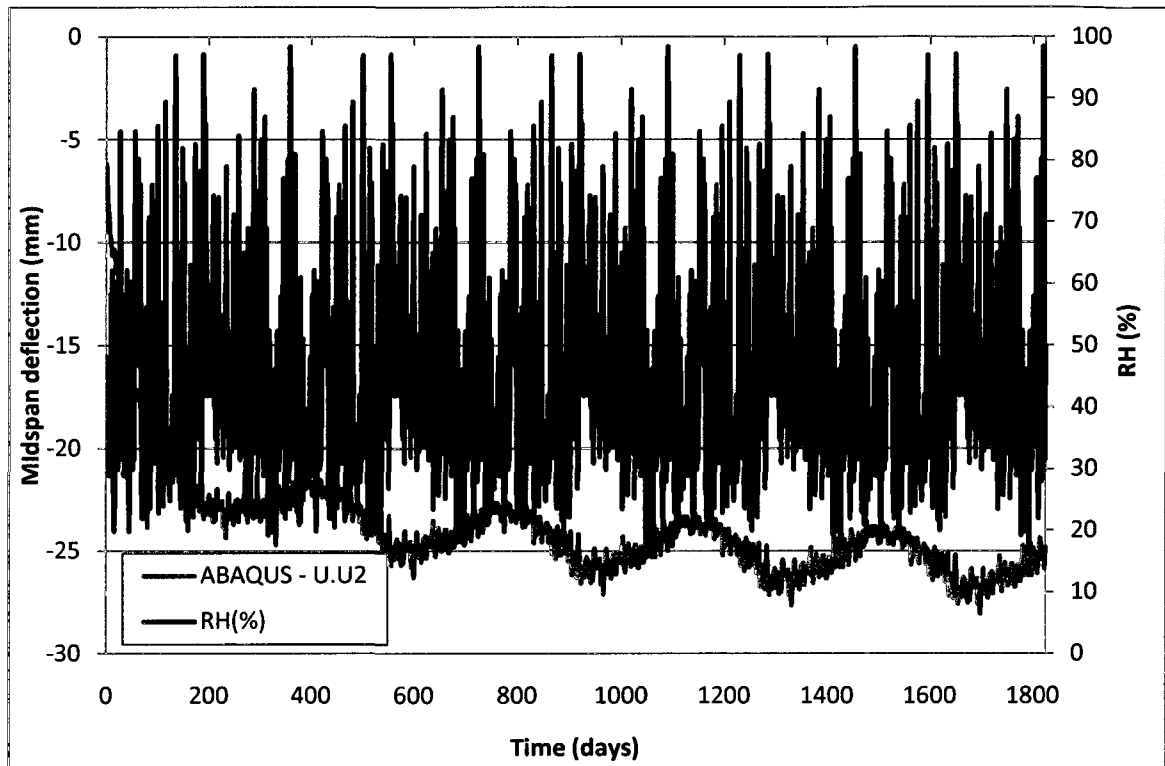


Figure 7.26 Midspan deflection plotted with the RH record – 5-year prediction analysis.

7.2.4 Comparison between proposed 3D model and 1D model

Midspan deflection comparison

The 3D constitutive model used in this research for the wood material was expanded from Toratti's model. Toratti's model was previously implemented in Fragiaco's software [4] to model the long-term behavior of the wood-concrete composite beam structures. Modeling the same problem by both the 1D and the 3D models gives another validation for assumptions used in the 3D models. To compare the results between two models, Fragiaco's software was used to model the test specimen Beam 1 for the first 123 days of the test. In 1D model, the notches are approximately modeled as spring element. The magnitude of the spring stiffness used in these analyses was 1562132 N/cm which was taken from the result of Fast's tests [2]. In the original 1D model software of

Fragiacomo, the CEB-FIP 1990 shrinkage formulation (2.15) for concrete was implemented while in the 3D models the fitted curve (7.3) and the ACI-209R shrinkage formulation (5.1) were used. To have a compatible comparison, the fitted curve (7.3) and the ACI-209R shrinkage formulation (5.1) were implemented in Fragiaco's 1D model software with the help of the software's author.

Figure 7.27 shows the comparison between the results of two models and the measured deflection. Two models capture closely the instantaneous behavior of the specimen, namely those due to: 1) the placing of concrete (wood layer only), and 2) the application of the long-term static load time (composite beam). Both models also reflect the same effect of the thermal expansion but the 3D model shows an improvement in capturing the long-term behavior of the test specimen. The 1D model with the CEB shrinkage formulation does not capture well the deflection trend of the test specimen in the first 29 day, but with the fitted curve of the experimental results for the shrinkage function and ACI formulation for concrete it captures closely the trend of the deflection during that period of time. After applying long-term load, both results from 1D model show the same deflection trend. This suggests that for long-term analysis the application of either the CEB or the ACI shrinkage formulation yields the same midspan deflection trend.

To consider the improvement from using 3D model instead of 1D model, the author uses the "norm" concept which is explained in the Appendix D. If the measured and models deflection are treated as vectors then the differential between the measured vector and the model vector is a vector. The ratio between the norm of the differential vector and the norm of the measured vector can be used to estimate the accuracy of the considered model. Using this concept with norm-2 for the midspan deflection of the first 123 days of

the test, the relative error of 1D model is 2.9% and the relative error of the 3D model is 1.4%.

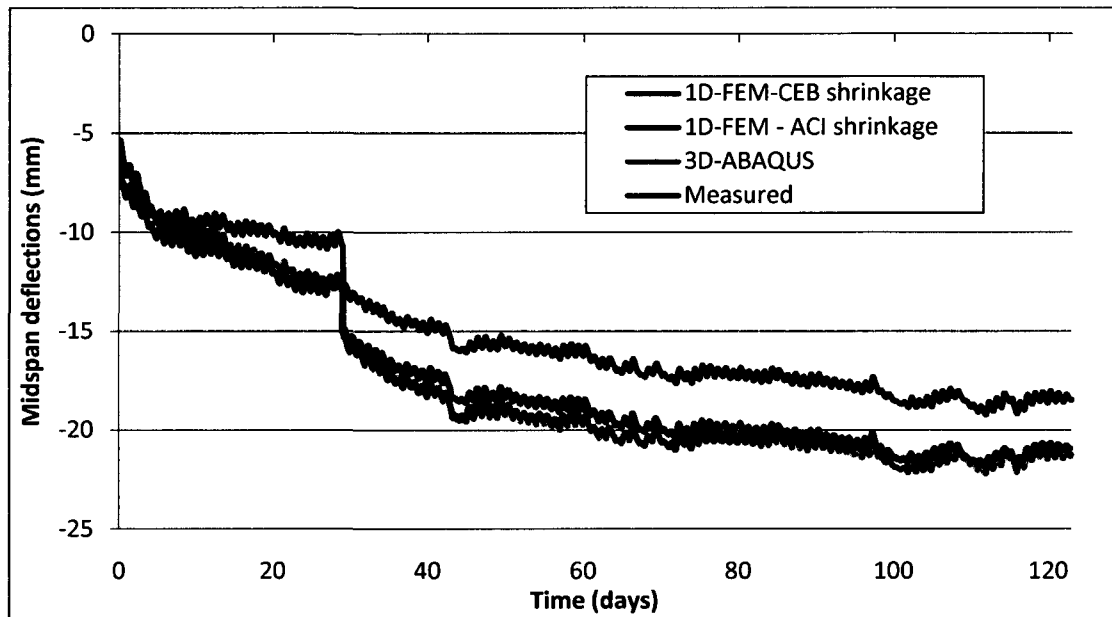


Figure 7.27 Comparison of the midspan deflections between 1D model, 3D model and test result.

The 1D model software with the fitting and ACI shrinkage formulations was then used to run the 50-year prediction analysis for the test specimen. Figure 7.28 shows the comparison of the midspan deflections resulted from the 1D model and the 3D model for the first 5 years. Overall, the 1D model predicts a higher creep rate in about the first 200 days, and beyond that point in time the 3D model predicts a higher creep rate. The midspan deflections at the 1825th day (at the end of the 5th year) were 24.93 mm for the 3D model and 24.72 mm for 1D model, i.e. the 3D model was 0.84% higher than the 1D model. The midspan deflection at the 18250th day (at the end of the 50th year) for 1D model was 25.92 mm. The 3D model was not used to run 50-year prediction analysis because of timing constrain in the research. If in the duration after 5 years both models are assumed to have the same creep rate, the results of the 1D model can be used to

extrapolate the 3D model. Doing so, the midspan deflection at the end of the 50th year for 3D model extrapolates 26.14 mm.

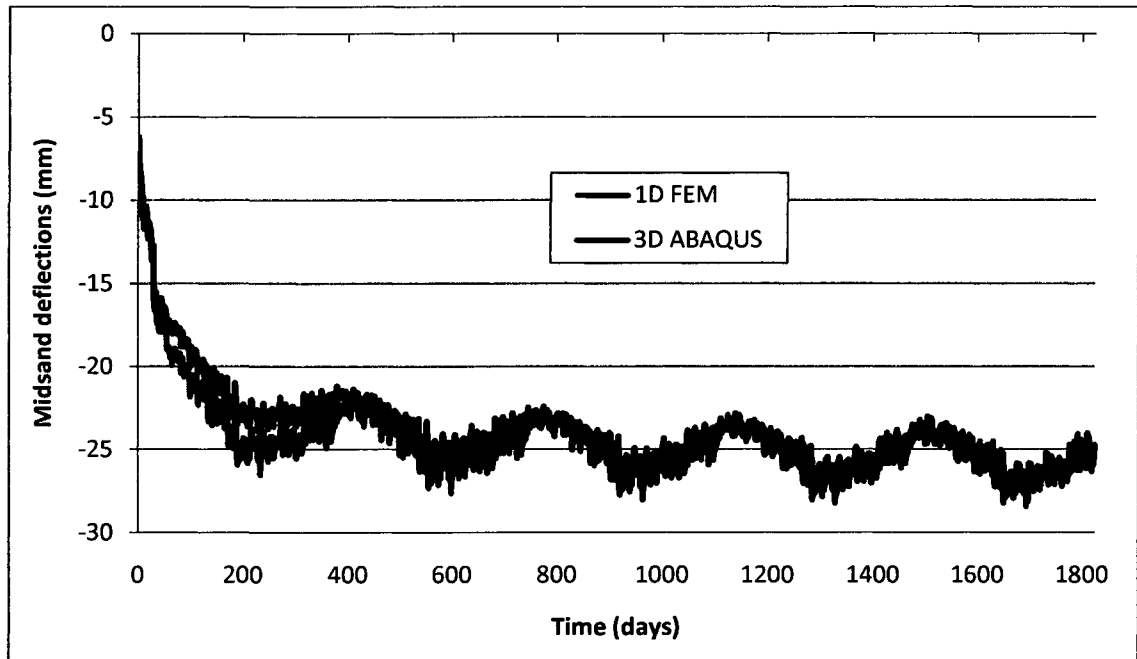


Figure 7.28 Comparison of the midspan deflections: 5-year prediction analysis.

Interlayer slip comparison.

Figure 7.29 shows the comparison interlayer slip at one end of the test specimen between 3D model and 1D model. Figure 7.30 illustrates the corresponding interlayer slip increments between two models. The results indicate that the two models capture almost the same interlayer slip due to the effects of the thermal expansion and other phenomena which affect the long-term behavior of the specimen. However, the instantaneous increase in slip due to the application of the long-term static load is quite different between the two models. The difference in elastic slip can be explained as: in 1D model the notches are approximately modeled by spring elements while in 3D model the notches works as a contact between two deformed bodies. Table 7.3 compares the measured instantaneous increase in slip with respective results of the two models. There

are four measured points at four corners of the test specimen. The average of the measured instantaneous increase in slip falls in between the respective results of the two models. But the measured slip values were not quite reliable because they are very divergent.

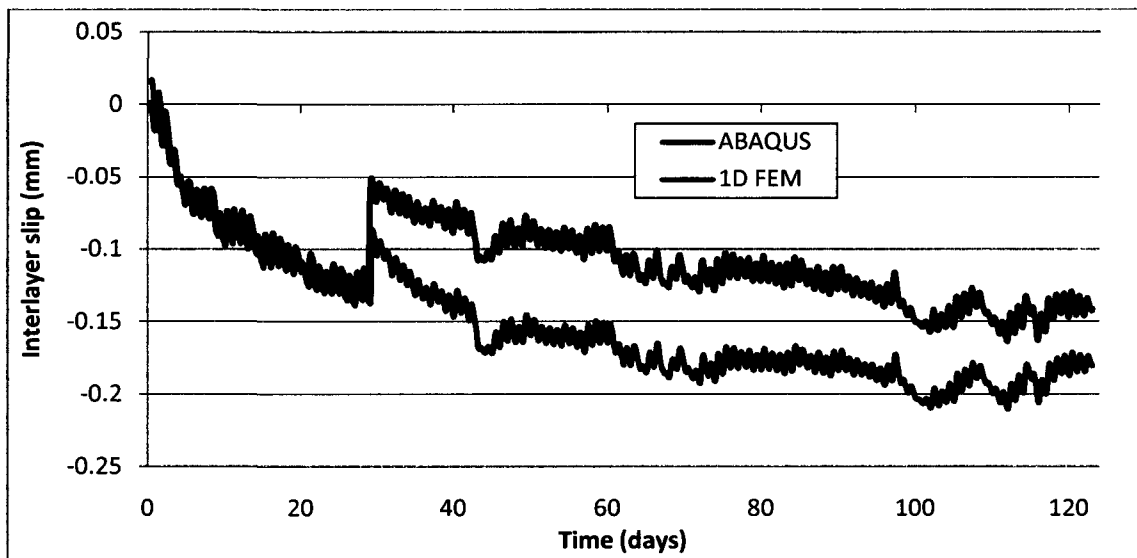


Figure 7.29 Comparison of the interlayer slips at the end of the beam for fist 123 days.

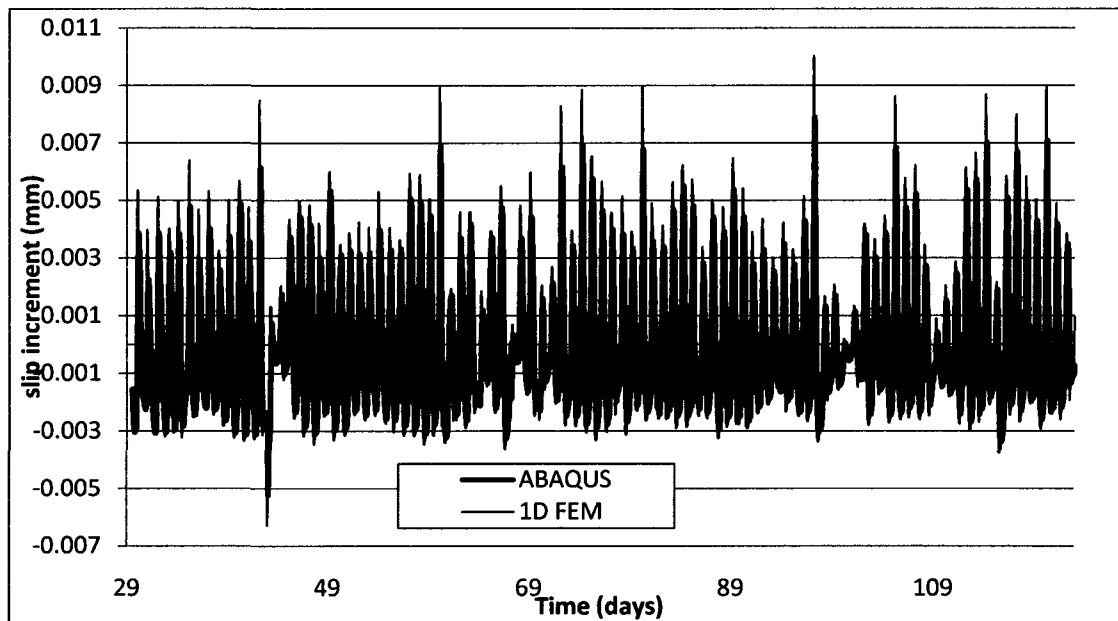


Figure 7.30 Comparison of slip increment form the day 29th to the day 123th.

Table 7.3 Instantaneous increase in slip due to the application of the long-term static load: measured and models results.

Instantaneous increase in slip due to static load (mm)						
Measured points					ABAQUS	1D FEM
NE	NW	SW	SE	Average		
0.02286	0.05842	0.11684	0.0254	0.05588	0.045195	0.061458

In general, the results of the two models on simulating the test specimen are close. Using 1D model to simulate the time-dependent behavior of a narrow wood-concrete composite beam wood would get an essential accuracy. The biggest advantage of using 1D model is computational time. Table 7.4 summarizes the computational times for stress analyses performed by 1D model and/or 3D model. The computer used in these analyses was a Windows PC with Core2Duo processor E6750, 4GB RAM and 320 GB HDD 7200 rpm.

Table 7.4 Computational time of 1D model and 3D model.

Analysis	Computational time (hour)		Explanation
	1D model	3D model	
Analysis State 1	n/a	4	No 1D model analysis
Analysis State 2	0.2	50	
5-year prediction analysis	0.24	64	
50-year prediction analysis	12	n/a	No 3D model analysis

In comparison with the 1D model, the 3D model is a time consuming solution but it can be applied to analyzed complex problems where the 1D model cannot be applied. For example with the wood-concrete beam with notched shear key, modeling the tightening interlayer gap between two layers (by applying a torque to the dowel) is impossible by using 1D model. Although ABAQUS does not allow the use to apply a bolt load at an intermediate step in long-term analysis, the tightening process can be modeled in short-term analysis. In addition, the detailed model of the notches in the 3D model permits to visualize the development of the interlayer gap and the physical interaction contact between two layers over time. In the Appendix E, the 3D render of the deformed beam end with the notch was plot at some certain times in Figs. E.1 to E.5. The opening of a gap at the slanted face of the notch before the live load application due to concrete shrinkage can be clearly noted. The gap then closes due to the load application.

Chapter 8

Discussions and Recommendations

The main goal of the study is to develop a rigorous 3D FEM model to simulate the time-dependent behavior of a specific type and geometry of wood-concrete composite beam with notched shear keys under long-term static load and environmental exposure conditions. This was accomplished by performing both theoretical and experimental tasks. A rigorous mathematical model considering was developed, and this model was incorporated all significant effects of the physical phenomena that affect to the time-dependent behavior of the wood and concrete materials. The mathematical model was then implemented in the finite element software ABAQUS by using 3D solid elements for the wood-concrete composite beam of interest. Long-term experimental creep tests were carried out initiated with the same type and geometry of the wood-concrete composite beam. Corresponding exposure measured data including ambient temperature and relative humidity for the first 129 days of the creep tests (which are still ongoing) were used as input parameters for the numerical model. The output midspan deflection was compared with the measured midspan deflection. The numerical model then was used to predict the long-term deflection of the tested beam under an assumed environmental condition for a period of 5 years. This chapter discusses observations from environmental condition data, the measured data of the creep test, and the results of the simulation done by use of the developed numerical model.

8.1 Discussions

8.1.1 Discussion of the environmental conditions

The variations of ambient relative humidity and temperature affect the time-dependent behavior of the wood material itself and the overall time-dependent behavior of the wood-concrete composite structures. The study of time-dependent behavior of the wood-concrete composite structures must consider the environmental conditions at the region where the structures are constructed. Ambient temperature and relative humidity variations are different at different geography regions so that their effects on the time-dependent behavior of a similar loaded wood-concrete composite beam would be different as well. With the same long-term static loading conditions, time-dependent behavior of the same type of wood-concrete composite structures is different at different regions.

8.1.2 Discussion of the creep test results

The long-term creep test includes two similar specimens applied the same long-term static load and exposure conditions. Midspan deflection, relative humidity and temperature have been carefully monitored by accurate and sensitive sensors. From the test results of the first 123 days of exposure, the following information was observed:

- With the same long-term static load and exposure conditions, both test specimens have essentially the same time-dependent response. This indicates that specimens work functionally and the measurements are reliable.
- The daily variation of the midspan deflection correlates directly to the daily variation of temperature. Thus, the thermal expansion phenomenon plays an important part in the daily variation and the yearly variation of the midspan deflection.

- There is no clear correlation between midspan deflection and sudden change of the relative humidity.

8.1.3 Discussion of the proposed numerical model and results of the model.

The numerical model is rigorous and incorporates all physical phenomena which affect the time-dependent behavior of the wood-concrete composite beams. Implementation and running of the model in the ABAQUS into three analyses is a complicated and time consuming process. The application of the numerical model should be applied at the research level, not in the engineering practice level. The results of the numerical model reveal some following observations.

From the diffusion analysis, diffusion process of moisture content in the wood happens slowly. The daily variation of the relative humidity affects the moisture content of a thin outer layer of the cross-section. Consequently, the rate of change of mechano-sorptive creep is not the same at different points in the member because the mechano-sorptive creep depends on the rate of change of moisture content. Thus, the size of the cross-section will affect the final mechano-sorptive creep of a wood member. The larger the cross-section of member is the lower will be mechano-sorptive creep over the exposure time for the same loading and exposure conditions.

The heat transfer is a faster time process compared to the diffusion phenomenon. The temperature of the whole volume of material varies closely with the variation of the ambient temperature. However the difference in temperatures reached at points within each material is small so the thermal stress field due to temperature differences in each layer is small. Thus, the gradient effect of thermal stress field effect is negligible. The temperature difference between the concrete layer and the wood layer is also small, but

the coefficients of thermal expansion of wood and concrete are different. Thus the thermal stress field of wood-concrete composite beams is not negligible. For long-term analysis the heat transfer analysis can be ignored, the temperature in each layer can be assumed uniform and taken as the ambient temperature.

Results of the two model verification analysis indicate that the proposed 3D model captures well the time-dependent behavior of the test specimens. The 3D model reflects closely the instantaneous behavior of the specimen at the time of applying the static load. In general, the 3D model captures very well the effects of all physical phenomena which affect the time-dependent of the wood-concrete composite beams with notched shear keys..

8.1.4 Discussion of the results of the proposed 3D model and the available 1D model

An available 1D model to predict time-dependent behavior of the wood-concrete composite beams was implemented via Fragiacomò's software. One motivation of this research was to investigate how much improvement one can obtain from using 3D model instead of using 1D model. Two analyses on the Beam1 were performed by using Fragiacomò's 1D software: 1) Analysis State 2 and 2) 50-year prediction analysis under the environmental conditions at Fort Collins. Similar to the results of 3D model for Analysis State 2, the analysis results of the 1D model capture well the effects of all physical phenomena which affect the time-dependent of the wood-concrete composite beams with notched shear keys. Although the proposed 3D model predict closer the overall time-dependent behavior of the test specimens, the improvement is insignificant in term of accuracy. But the advantage of the proposed 3D model is that it does not need to perform the short- and long-term push out tests in order to characterize the connection

properties (slip modulus and creep coefficient) and it can be applied to analyze complex 2D wood-concrete composite structures.

8.2 Conclusions

The research has studied the time-dependent behavior of the wood-concrete composite beam with notched shear keys on both theoretical and empirical aspects. A 3D finite element model implemented in the Abaqus software has been developed. The model has been validated on a long-term experimental test showing good accuracy. Some preliminary analyses have been carried out using the model, leading to some important conclusions. From the creep test results, the conclusions are:

- The obtained test results are reliable and can be used to validate any proposed model to predict the time-dependent behavior of the wood-concrete composite beam with notched shear keys.
- With a high resolution measurement in time scale with both environmental condition data and midspan deflection, the measured results show that the time-dependent response of the test specimens is sensitive to the change of temperature due to the thermal expansion phenomena. The effect of thermal exposure should be included in load combinations used in any applicable design code.
- As analyzed in the Chapter 4, the mechano-sorptive creep depends on the number of changing moisture cycle which include drying and wetting period. The results of the diffusion analysis for the first 123 days of the test showed that in this duration, most part of the wood layered underwent less than one wetting/drying cycle. Thus, for the short observation period done to date on

one size cross-section of the wood layer in test specimens, it is hard to distinguish the effect of the mechano-sorptive creep of the wood layer to the long-term behavior of the composite beam structures.

From the results performed on the numerical model, the following conclusions for the proposed mathematical and numerical models can be drawn:

- The proposed 3D model captures closely the instant and long-term behavior of the wood-concrete composite beam with notched shear keys under the static load and the variation of the environmental conditions. In comparison with using 1D model, the disadvantage of using 3D model is computational time. But this limitation can be overcome by improving the analysis procedure as well as using advanced computers. The advantages of using the 3D model include: 1) No need of shear-slip relationships for modeling the connection both in the short-and long-term analyses. In the case of long-term analysis, the creep coefficient, including the mechano-sorptive parameters of the connection detail as a whole, are needed. Such parameters can only be obtained through difficult and time consuming creep tests of push-out specimens. 2) The 3D model can be used for more complex structures in geometry and boundary conditions such 2D floor/deck which cannot be schematized as 1D beam. 3) Another possible application of the 3D model is for timber-concrete composite beams with very wide concrete flanges. The 1D model cannot be used in this case as it cannot account for the shear lag phenomenon taking place in the concrete flange. 4) The 3D model can be used where more complex phenomena such as the effect of post-tensioning of the

bolt on 2D floor/deck or the development of the interlayer gap between two layers due to the shrinkage of concrete need careful evaluation.

- The parametric study of the effect of the non-uniform temperature fields on the time-dependent behavior of the test specimen shows that the heat transfer state analysis is not necessary in long-term analysis i.e. it can be neglected. Eliminating that analysis in implementing the numerical model in the ABAQUS software, would significantly reduce the computational time.
- The diffusion analysis result shows that moisture diffusion in the wood material is a slow process. High frequency variation of the air relative humidity only affects the variation of the moisture content in a thin outer shell. This means that the mechano-sorptive creep depends on both the variation in the ambient relative humidity over time and the cross section size of the wood member.

8.3 Recommendations

The initial goals of the research were achieved. The proposed model now permits one to perform further parametric studies to answer remaining questions about time-dependent behavior of various types of the wood-concrete composite structures. The experimental and numerical analysis results also reveal several specific issues that should be addressed with the wood-concrete composite structures in the engineering practice. The following are recommendations for further studies to investigate the time-dependent behavior of the wood-concrete composite structures.

- A parametric study by using the proposed model should be performed to consider the separate effects of different physical phenomena such as

shrinkage of concrete, creep of wood and concrete, thermal expansion etc. on the long-term behavior of the test specimens.

- The mechano-sorptive creep of the wood is driven by the variation of the relative humidity. Another parametric study should be performed to consider the effect of dramatically different time histories of environmental conditions on the long-term behavior of the test specimens (local and regional effect studies).
- The influence of the thermal stresses on the load bearing capacity of the wood-concrete composite beam should be investigated. This study would be useful to determine the role of thermal load in the load combinations used in design codes.
- The proposed modeling method can be used to analyze the time-dependent behavior of other types of wood-concrete composite structures if the weather records and creep test data are available.
- The proposed model for wood material can be used to analytically study the effect of cross-section size on the mechano-sorptive creep of bending wood members.
- The composite efficiency of the wood-concrete composite structures due to instant static loads changes over the time. Theoretical and experimental studies should be performed to understand the effect on the composite efficiency over the service life time of the wood-concrete composite structures.

- The 3D FE model can be used to analyze 2D deck systems and investigate, among others, the efficiency of the anchor over the breadth of the deck and the importance of shear leg phenomenon on timber-concrete composite beams with wide concrete flanges.

References

1. Natterer, J., Hamm, J., and Favre, P. (1996). "Composite wood-concrete floors for multi-story buildings." *Proc., International Wood Engineering Conference*, New Orleans, Louisiana, U.S.A., 3431-3435.
2. Fast, R. S. (2003). "Durability studies of layered wood-concrete composite connections and beams." *MS thesis*, Dept. Civil Engineering, Colorado State Univ., Fort Collins, Colo.
3. Gutkowski, R.M., Thompson, W., Brown, K., Etournaud, P., Shigidi, A., and Natterer, J. (1999). "Laboratory testing of composite wood-concrete beam and deck specimens." *Proc., 1999 RILEM Symp. on Timber Engineering*.
4. Fragiaco, M. (2000). Long-term behavior of timber-concrete composite beams. PhD dissertation, University of Trieste, Italy (In Italian).
5. Fragiaco, M. (2005). "A finite element model for long-term analysis of timber-concrete composite beams." *Structural Engineering & Mechanics*, 20(2):173-189.
6. McCulough, C.B. (1934). "Highway viaducts in Oregon of prefabricated timber." *Wood Preserving News*, X11(11).
7. Eby, R. E. (1989) Chapter Composite T-beam bridge deck on timber, pages 149-153, *Classic Wood Structures*, American Society of Civil Engineers.
8. Godycky, T., Pawlica, J. and Kleszczewki, J. (1984). "Verdundecke aus Holzrippen und Betonplatte." *Der Bauingenieur*, 59:477-483.
9. Zajicek, P. (1985). "Verstärkung der alten Deckenkonstruktion." *Österreichische Ingenieur – und Architekten-Zeitschrift*, 130(7/8):237-242.
10. Zajicek, P. (1989). "Bemessungsvorschlag für Holz-Beton-Verbunddecken." *Österreichische Ingenieur – und Architekten-Zeitschrift*, 134(9):456-462.
11. Murthy, C.K. (1984). "Timber concrete for low cost housing." *Housing Science*, 8(2):209-215

12. Rilem CT111 CST (1992). "Behavior of timber-concrete composite load-bearing structures." *Proceeding of ACMAR-Ravenna International Symposium*, Dept. of Civil Engineering, University of Florence, Italia.
13. Nauta, F. (1984). "New Zealand Forrest Service Timber Bridges." *Pro. of 1984 Pacific Timber Engineering Conference*, Auckland, New Zealand.
14. K ng, R. (1987). *Verbunddecke holz-leichtbeton (Composite floor timber-Lightweight concrete)*, TU Graz, Austria.
15. Ceccotti, A., and Covan, C. (1990). "Behaviour of timber and concrete composite load-bearing structures." *Proc., The 1990 IUFRO S5.02 Timber Engineering*, Saint John, New Brunswick, Canada, Vol. 2.
16. Bathon, L.A., and Graf, M. (2000). "A continuous wood-concrete-composite system." *Proc., World Conf. of Timber Engineering*, Whistler, British Columbia, Canada, 8.2.2.
17. Clouston, P., Bathron, L.A., and Schreyer, A. (2005). "Shear and bending performance of a novel wood-concrete composite system." *Journal of Structural Engineering*, 131(9), 1404-1412.
18. Ahmadi, B. H., and Saka, M. P. (1993). "Behavior of composite timber-concrete floors." *J. Struct. Eng.*, **119**(11), 3111–3130.
19. *Timber construction manual*. (1980). 3rd Ed., American Institute of Timber Construction, Denver, Colo.
20. "Building code requirements for reinforced concrete." (1989). *ACI 318-89*, American Concrete Institute (ACI), Detroit, Mich.
21. Spirig, H. (1985). "Architektonische Gestaltungsm glichkeiten dank Doppelkopfschraube". *STZ*, Nr.10.
22. Sonda, B. (2001). "Experimental Verification of New Connector for Timber-Concrete-Composite Structures". *IABSE Report*, ISSU 85, pages 519-524.

23. Mungwa, M.S., Jullien, J.-F., Foudjet, A., and Hentges, G. (1999). "Experimental study of a composite wood-concrete beam with the INSA-Hilti new flexible shear connector." *Construction and Building Materials*, 13(7), 371-382.
24. Said, E.B., Jullien, J.-F., and Siemers, M. (2002). "Non-linear analyses of local composite timber-concrete behaviour." *Proc., 7th World Conf. on Timber Engineering, WCTE 2002*, Shah Alam, Malaysia, 1, 183–191.
25. Yttrup, PJ, Nolan, G, 'Performance of Timber Beam Bridges in Tasmania, Australia', *International Wood Engineering Conference*, New Orleans, USA, 75-80 (1996).
26. Van der Linden, M. L. R. (1999) "Timber–concrete composite floor systems." *Doctoral Thesis*. Technical University of Delft.: I–XVII: 1–364.
27. Werner, H. (1992). "Holz-Beton-Verbunddecke mit einer neuartigen Fugenausbildung." *Bauen mit Holz* Nr.4.
28. Natterer, J. (1990) "Verbundkonstruktionen im Holzbau – Entwicklung und Tendenzen". 14. *Dreiländer-Holztagung*, Interlaken, Switzerland.
29. Brown, K.T. (1998). "Testing of a shear key/anchor in layered wood-concrete beams." *MS thesis*, Colorado State Univ., Fort Collins, Colo.
30. Koike, E. (1998). "Analysis of composite wood–concrete layered beams." *MS thesis*, Dept. Civil Engineering, Colorado State Univ., Fort Collins, Colo.
31. Etournaud, P.J. F. (1998). "Load tests of composite wood–concrete deckings under point loads." *MS thesis*, Dept. Civil Engineering, Colorado State Univ., Fort Collins, Colo.
32. Gutkowski, R.M., Balogh, J., Brown, K., Etournaud, P., Koike, E., Natterer, J. (2000). "Laboratory testing of composite wood–concrete beam and floor specimens." *Proc., World Conf. on Timber Engineering–2000*, Dept. of Civil Engineering, Dept. of Wood Science, School of Architecture, Univ. of British Columbia, Vancouver, Canada.

33. Gutkowski, R.M., Balogh, J., and SaRiberio, R.A. (2001). "Modeling and testing of composite wood–concrete deep beam specimens." *Proc., Structural Faults + Repair–01, 10th Int. Conf. and Exhibition*, London.
34. Gutkowski, R.M., Brown, K., Shigidi, A., and Natterer, J. (2004). "Investigation of notched composite wood-concrete connections." *Journal of Structural Engineering*, 130(10), 1553-1561.
35. Gutkowski, R.M., Brown, K., Shigidi, A., and Natterer, J. (2008) "Laboratory tests of composite wood–concrete beams". *Construction and Building MATERIALS*, Volume 22, Issue 6, June 2008, Pages 1059-1066.
36. Thompson, W. (1997). "Slip tests of wood-concrete composite specimen." Plan B master report, Dept. Civil Engineering, Colorado State Univ., Fort Collins, Colorado State University.
37. Negrão JH, Oliveira FM, Oliveira CL (2006). "Investigation on timber–concrete glued composites." *In: 9th world conference on timber engineering WCTE 2006*, Portland, Oregon, USA, 6–10, CD
38. Brunner, M. and Gerber, C., (2002). "Long-term tests on a glued timber-concrete composite", *Proceeding of the 7th WCTE, paper 10-4-2 (in CD)*, Kuala-Lumpur, Malaysia.
39. Dias, A.M.P.G. (2005). "Mechanical behavior of timber-concrete joints", *Doctoral thesis*, ISBN: 90-901-9214-X.
40. Clark, L. G. (1954). "Deflections of laminated beams." *Transactions, ASCE*, Vol. 119, Paper No.2694, 1954, pp.721-736.
41. Newmark, N.M., Siess, C.P., and Viest, I.M. (1951). "Tests and analysis of composite beams with incomplete interaction." *Proc., Society for Experimental Stress Analysis*, 9(1), 75–92.
42. Möhler, K. (1956). "Über das Tragverhalten von Biegeträgern und Druckstäben mit zusammengesetztem Querschnitt und nachgiebigen Verbundmitteln." *Habilitation*, Technische Universität Karlsruhe, Germany.

43. Eurocode 5 part 1 (2003) "Eurocode 5 – Design of timber structures – Part 1 – General rules and rules for buildings". CEN.
44. Ceccotti, A. (1995). "Timber-concrete composite structures." *Timber Engineering, Step 2*, First Edition, Centrum Hout, The Netherlands, E13/1-E13/12.
45. Natterer J., M. Hoefl, (1992). "Holz-Beton-Verbundkonstruktionen, Entwicklung eines neuen Verbindungssystems." *Forschungsbericht CERS Nr. 1638, IBOIS*, Ecole Polytechnique Federale de Lausanne, M.rz.
46. Zakaria, ML, and Ghazali, MZ (1989) "Finite Element Analysis of Timber Concrete Composite T-Beams". *2^o PTEC* Vol. 2, pp. 171 – 175.
47. Goodman, J. R.; Popov, E. P. (1968). "Layered Beam Systems with Interlayer Slip." *J. Struct. Div., ASCE* **94** 2535-2547.
48. Goodman, J. R. (1969),. "Layered Wood Systems with Interlayer Slip,". *Wood Science*, Vol.01, No.3, pp. 148-158.
49. Ko, M. F.(1973). "Layered beam systems with interlayer slip." *Struct. Res. Rep.* No. 8, Dep. of Civ. Eng.,Colorado State Univ.
50. Thompson, E. G., Goodman, J. R, and Vanderbilt, M. D. (1975). "Finite element analysis of layered wood systems." *J. of the Struct. Div., ASCE*, 101 (ST12):2659-2672.
51. Thompson, E. G., Goodman, J. R, and Vanderbilt, M. D. (1977). "FEAFLO: a program for the analysis of layered wood systems." *Comput. And Struct.* VII 237-248.
52. Vanderbilt, M. D., Goodman, J. R. and Criswell, M. E. (1974). "Service and overload behavior of wood joist floor systems." *J. of the Struct. Div., ASCE*, 100(ST1).
53. Tremblay, G.A., Goodman, J.R., Thompson, E.G., Griswell, M.E., and Bodig, J. (1974). "Nonlinear analysis of layered T-beams with interlayer slip." *Structural Research Rep. No. 12*, Civil Engineering Dept., Colorado State Univ., Fort Collins, Colo.

54. Wheat, D. L. (1980). "Nonlinear analysis of wood joist floors." *Ph.D. dissertation*, Colorado State University, Fort Collins, CO, 1980.
55. Chen, M.T., Gutkowski, R.M., and Pellicane, P.J. (1992). "Tests and analysis of mixed concrete-wood beams." *Structural Research Rep. No. 69*, Civil Engineering Dept., Colorado State Univ., Fort Collins, Colo.
56. Wieligmann
57. , M. (2004). "Strain-Stress-Behavior of Dowel Connections for Partially Composite Wood-Concrete Floors and Decks." *Diploma Thesis*, Technical University of Dresden.
58. Inter-CAD Kft. (2001). AxisVM - Finite Element Program, *User's Manual*, version 6.0 edition.
59. Leicester, R. H. (1971). "A rheological model for mechano-sorptive deflections of beam". *Wood Science and Technology* Vol.5 p.211-220.
60. Ranta Maunus, A. (1975). "The viscoelasticity of wood at varying moisture content." *Wood Science and Technology*, 9, 189-205.
61. Mårtensson, A. (1992). "Mechanical behavior of wood exposed to humidity variations." *Report TVBK-1006*, Lund Institute of Technology, Lund, Sweden.
62. Toratti, T. (1992). "Creep of timber beams in a variable environment." *Rep. No. 31*, Helsinki Univ. of Technology, Helsinki, Finland.
63. Hanhijärvi, A. (1995). "Deformation kinetics based rheological model for the time-dependent and moisture induced deformation of wood." *Wood Science and Technology*, 29, 191-199.
64. Hanhijärvi, A., and Hunt, D. (1998). "Experimental indication of interaction between viscoelastic and mechano-sorptive creep." *Wood Sci. Technol.*, 32, 57-70.
65. Eberhardsteiner, J., Hofstetter, G., Meschke, G., Helnwein, P. M., (2003). "Coupled material modelling and multifield structural analyses in civil engineering." *Engineering Computations*, Vol. 20, pp. 524 – 558.

66. Bou Saïd, E. (2003). "A contribution to the modeling of the long-term effects for wood and the concrete under variable climatic conditions and application to the wood-concrete composite structures." *Ph.D. Thesis*, INSA of Lyon (In French).
67. Chassagne, P., Bou Saïd, E., Jullien, F. J., and Galimard, P. (2005) "Three Dimensional Creep Model for Wood under Variable Humidity-Numerical Analyses at Different Material Scales." *Mechanics of Time-Dependent Materials*, Volume 9, Number 4, pp. 1-24.
68. Capretti, S. (1992). "Time dependent analysis of timber and concrete composite (TCC) structures." *Proc., RILEM Int. Symp. On Behaviour of Timber and Concrete Composite Load-Bearing Structures*, Ravenna, Italy.
69. Kuhlmann, U., and Schänzlin, J. (2001). "Composite of vertically laminated timber decks and concrete." *Proc., IABSE Conference "Innovative wooden structures and bridges"*, Lahti, Finland, 507-512.
70. Fragiaco, M., and Ceccotti, A. (2006). "Long-term behavior of timber-concrete composite beams. I: Finite element modeling and validation." *Journal of Structural Engineering, ASCE*, 132(1), 13-22.
71. Fragiaco, M. (2006). "Long-term behavior of timber-concrete composite beams. II: Numerical analysis and simplified evaluation." *Journal of Structural Engineering, ASCE*. 132(1), 23-33.
72. American Concrete Institute (ACI), ACI Committee 209, Subcommittee II. (1992). "Prediction of Creep, Shrinkage and Temperature Effects in Concrete Structures." *Report ACI 209R-92*, Detroit, March, pp. 1- 12.
73. CEB-FIP (1990) Comité Euro-International du Béton. "CEB-FIP Model Code 1990." *First Draft*, Lausanne, Mar., pp. 2-3, 2-28 to 2-40 (Information Bulletin No. 195).
74. RILEM Model B3 (1995). "Creep and shrinkage model for analysis and design of concrete structures - model B3." draft RILEM Recommendation, prepared by Bazant, Z.P. and Baweja, S., *Materials and Structures*, Vol. 28, pp. 357-365, 415-430, 488-495, with Errata in Vol. 29 (1996) pp. 126.

75. H.S. Müller, C.H. Küttner and V. Kvitsel, Creep and shrinkage models of normal and high-performance concrete—concept for a unified code-type approach. In: *Creep and Shrinkage of Concrete, Special Issue of French Revue Of Genie CivilHermes* vol. 3–4 (1999), pp. 113–132.
76. Gardner, N. J., and Lockman, M. J. (2001a). “Design provisions for drying shrinkage and creep and normal-strength concrete.” *ACI Mater. J.*, **98**(2), 159–167.
77. Gardner, N. J., and Lockman, M. J. (2001b). “Discussion of ‘Design provisions for drying shrinkage and creep of normal-strength concrete.’” *ACI Mater. J.*, **99**(1), 111.
78. ABAQUS (2005). Abaqus reference manuals. Providence, RI.
79. Findley, W. N., Lai, J. S., and Onaran, K. (1976). Creep and relaxation of nonlinear viscoelastic materials. *Book*, North-Holland Publishing Company.
80. Thelandersson S. (1987). Node on Linear Viscoelasticity, *Report TVSM-3009*, Department of Structural Engineering, Lund Institute of Technology, Lund, Sweeden.
81. Bažant, Z. P. and Wu, S. T. (1974). Rate-Type creep law of ageing concrete based on Maxwell chain, *Materials and Structures* 7(37), pp. 45-59.
82. Schniewind, A. P. (1967). Creep rupture life of Douglas-fir under cyclic environmental conditions. *Wood Science and Technology*, vol. 1, pp. 278-288.
83. Le Govic, C. (1994). Chapter 5, Sensitivity of creep to different constant environments. In: *Morlier, P. (Ed.) Creep in timber structures. Report of RILEM Technical Committee 112-TSC*. London: E&FN Spon., pp 43-60. ISBN 0-419-18830-4.
84. Morlier, P. and Palka, P. (1994). Chapter 2, Basic knowledge. In: *Morlier, P. (Ed.) Creep in timber structures. Report of RILEM Technical Committee 112-TSC*. London: E&FN Spon., pp 9-42. ISBN 0-419-18830-4.
85. Hunt, G. G. and Shelton, C. F. (1988). Longitudinal moisture-shrinkage coefficient of softwood at the mechano-sorptive creep limit. *Wood Science and Technology*, vol. 22, pp. 199-210.

86. Hearmon, R. F. S. and Palton, J. M. (1964). Moisture content changes and creep of wood. *Forest Products Journal*, vol. 14, no. 8, pp. 357-359.
87. Gril, J. (1988). Une modelisation du comportement hygro-rheologique du bois a partir de sa microstructure. *Doctoral dissertation* (In French). University of Paris France.
88. Toratti, T. (1988). The creep properties of kerto-laminated-veneer-lumber. Espoo: Helsinki University of Technology, Laboratory of Structural Engineering and Building Physics.
89. Mohager, S. (1987). Studies of creep in wood. *TRITA-BYMA 1987:1* (In Swedish). Department of Building Materials, The Royal Institute of Technology, Stockholm.
90. Van Per Put, T. A. C. M. (1989). Deformation and damage processes in wood. *Doctoral dissertation*. Delft University Press, Delft, Netherland.
91. Boyd, J. D. (1982). An anatomical explanation for visco-elastic and mechano-sorptive creep in wood and effects of loading rate on strength. In: *Baas, P. (Ed.): New perspectives in Wood Anatomy*. Hague: Nijhoff/Junk, pp. 171-222.
92. Makudai, J. and Yata, S. (1986). Modeling and simulation of viscoelastic behavior of wood under moisture change. *Wood Science and Technology*, vol. 20, pp. 335-348.
93. Makudai, J. and Yata, S. (1987). Further modeling and simulation of viscoelastic behavior of wood under moisture change. *Wood Science and Technology*, vol. 21, pp. 49-63.
94. Makudai, J. and Yata, S. (1987). Verification of Mukudai's mechano-sorptive model. *Wood Science and Technology*, vol. 22, pp. 43-58.
95. Hoffmeyer, P. and Davidson, R. W. (1989). Mechano-sorptive creep mechanism of wood in compression and bending. *Wood Science and Technology*, vol. 23, pp. 215-227.
96. Svensson, S. and Toratti, T. (2002). Mechanical response of wood perpendicular to grain when subjected to changes of humidity. *Wood Science and Technology*, vol. 36, pp. 145-156.

97. Davies, M. and Fragiacomio, M. (2008). Long-term Behavior of Laminated Veneer Lumber Members Prestressed with Unbonded Tendons. *Proceeding of WCTE 2008*.
98. Mirianon, F., Fortino, S. and Toratti, T. (2008). A method to model wood by using ABAQUS finite element software. *Technical Report*. VTT Technical Research Centre of Finland.
99. Rajeev Goel, Ram Kumar, and D. K. Paul (2007). Comparative study of various creep and shrinkage prediction model for concrete. *Journal of Material in Civil Engineering*, vol. 19, no. 3, March 2007.
100. Lacidogna, G. and Napoli, P (1993). Analytical modeling of relaxation in concrete in accordance with the CEB MC 90 creep formulation, *Proceedings of the 5th International RILEM Symposium, Creep and Shrinkage of Concrete*. Barcellona, Spain, pp. 665-671.
101. Lacidogna, G. (1994). Modellazione matematica del comportamento viscoelastico del calcestruzzo, *Tesi di dottorato*, Politecnico di Torino, Italia.
102. Bazant, Z. P. and Wu, S. T. (1974). Rate-Type Creep Law of Aging Concrete Based on Maxwell Chain. *Material and Structures (RILEM)*.
103. Macorini L, Fragiacomio M, Amadio C, Izzuddin BA. (2006). Long-term analysis of steel-concrete composite beams: FE modeling for effective width evaluation. *Engineering Structures* **28**(8): 1110-1121
104. Zienkiewicz, O. C. and Taylor, R. L. (2000). Finite Element Method: Volume 2- Solid Mechanics. Butterworth Heinemann, London, 2000, 480 pp ISBN 0750650559.
105. Bathe, K. J. (1995). Finite Element Procedures. Prentice-Hall, Englewood Cliffs, 1995, 1037 pp. ISBN 0-13-301458-4.
106. Fung, Y.C. and Tong, P. (2000) *Classical and Computational Solid Mechanics*, World Publishing Co, USA.
107. Liping Cai (2005). Determination of diffusion coefficients for sub-alpine fir, *Wood Sci Technol* 39 pp. 153–162.

108. Avramidis, S. (1989). Evaluation of “three-variable” models for the prediction of equilibrium moisture content in wood. *Wood Science and Technology*, vol. 23, pp. 251-258.
109. Forest Products Laboratory (1999). Wood Handbook Wood as an engineering material. *General Technical Report*, FPL-GTR-113. Madison, WI: U.S. Department of Agriculture Forest Service, Forest Products Laboratory.
110. Engineering Toolbox Website, <http://www.engineeringtoolbox.com> (accessed March 20 2008).
111. LeBorgne, M. R., Gutkowski, R.M. Provisional Accepted, “Effects of Various Admixtures and Shear Keys in Wood-Concrete Composite Beams.” *Construction and Building MATERIALS*, Elsevier Ltd., Edinburgh, Scotland.
112. ACI Committee 318 (2002a). "Building code requirements for structural concrete." *ACI 318-02* and "Commentary" *ACI. 318R-02*, American Concrete Institute, Detroit.
113. LeBorgne, M. R. (2007). Analysis of Wood-Concrete Beams Incorporating Recycled Utility Poles. *M.S Thesis*. Colorado State University.
114. Bodig, J. Jayne, BA. (1982). “Mechanics of Wood and Wood Composites”. *Book* New York: Van Nostrand; 1982.

Appendix A

Characteristics of the variation of the environmental conditions at Fort Collins

Temperature and relative humidity are random complex functions. Their variabilities relate to the amount of energy provided by the sun and meteorological phenomena in the atmosphere. By investigating the temperature and relative humidity records at Fort Collins and some other locations, the author observed the following:

- On a daily basis, the weather conditions are divided into two groups: normal weather condition days and severe weather condition days. Figures from A.1 to A.3 show the variations in the temperature and relative humidity in three different days at a weather station in Fort Collins: one cold day in winter, one moderate temperature day in spring, and one hot day in summer. Weather condition in the winter and spring days (shown in the Fig. A.1 and the Fig. A.2) can be classified as normal weather condition days while the weather condition in the summer day (shown in the Fig. A.3) can be classified as a severe weather condition day. On the normal weather condition days, the variations of temperature and relative humidity look like sine/cosine functions in opposite directions and the period of sine/cosine function is 24 hours. The relative humidity decreases when the temperature increases and vice versa. On the severe weather condition days (heavy storm, hurricane or passing of hot or cold fronts), there is no defined pattern in the variation of temperature and relative humidity.
- Fig. A.4 and Fig. A.5 show the variations in the temperature and relative humidity over one particular year at a weather station in Fort Collins. Fig. A.6 shows the

daily average of temperature and relative humidity record over a particular four year period at the same weather station. The variation of the temperature has a clear pattern while there is no apparent pattern in the variation of the relative humidity. On a yearly basis, the overall pattern of temperature variation looks like sine/cosine function with a period of 1 year.

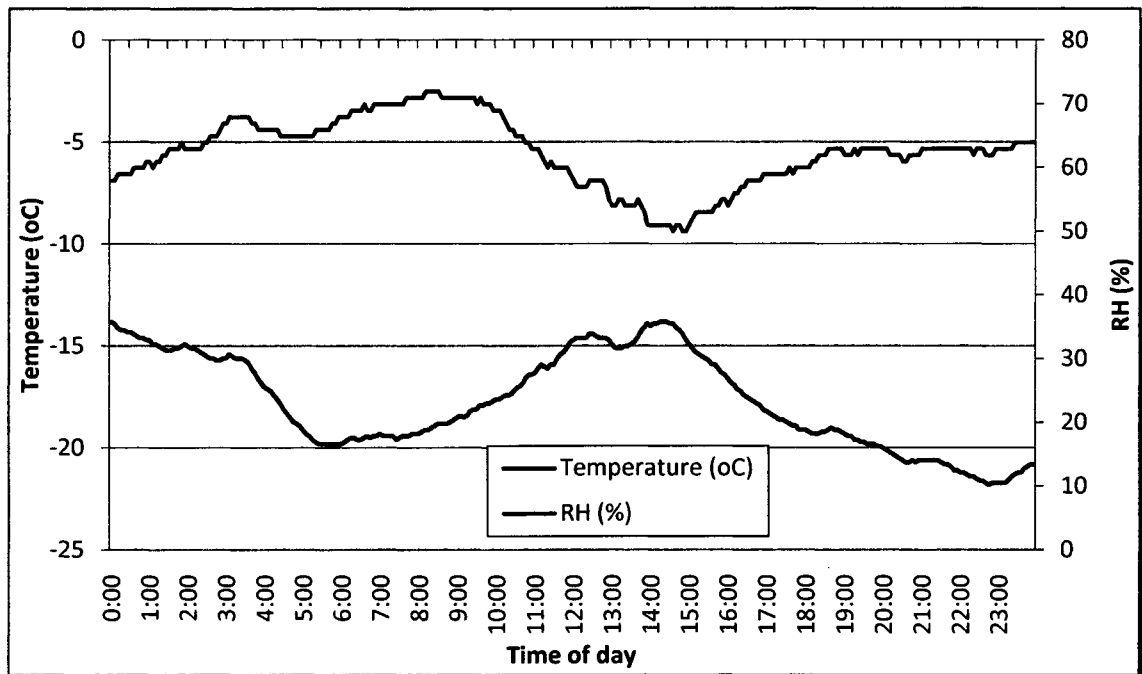


Figure A.1 Typical temperature and RH variations in one cold day (Jan 3rd 2004).

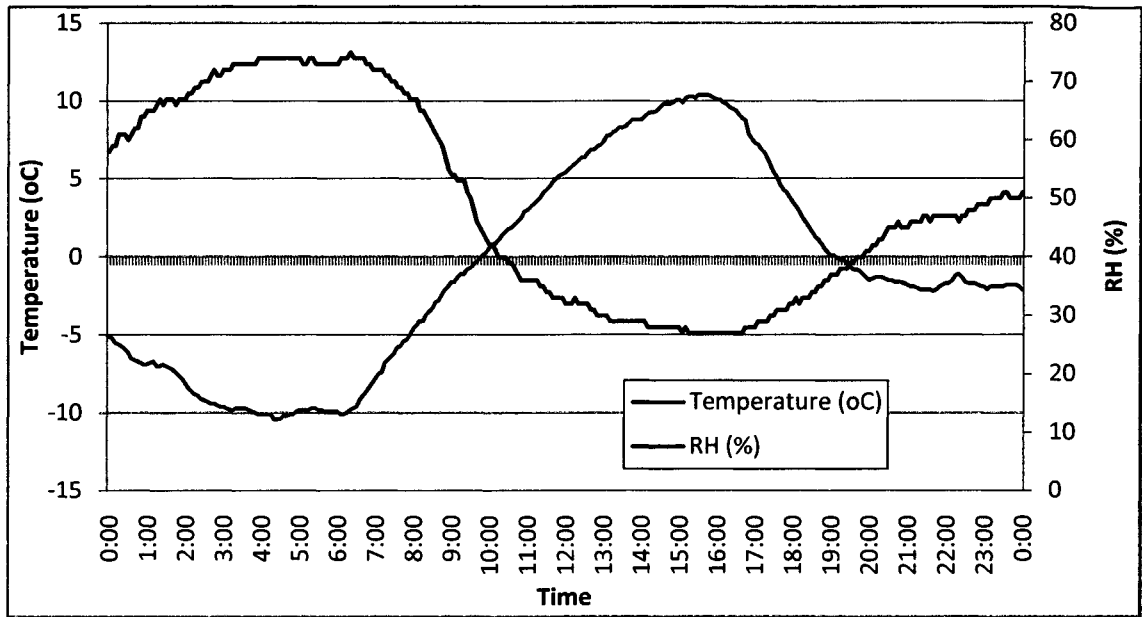


Figure A.2 Typical temperature and RH variations in one spring day (Mar 1st 2004).

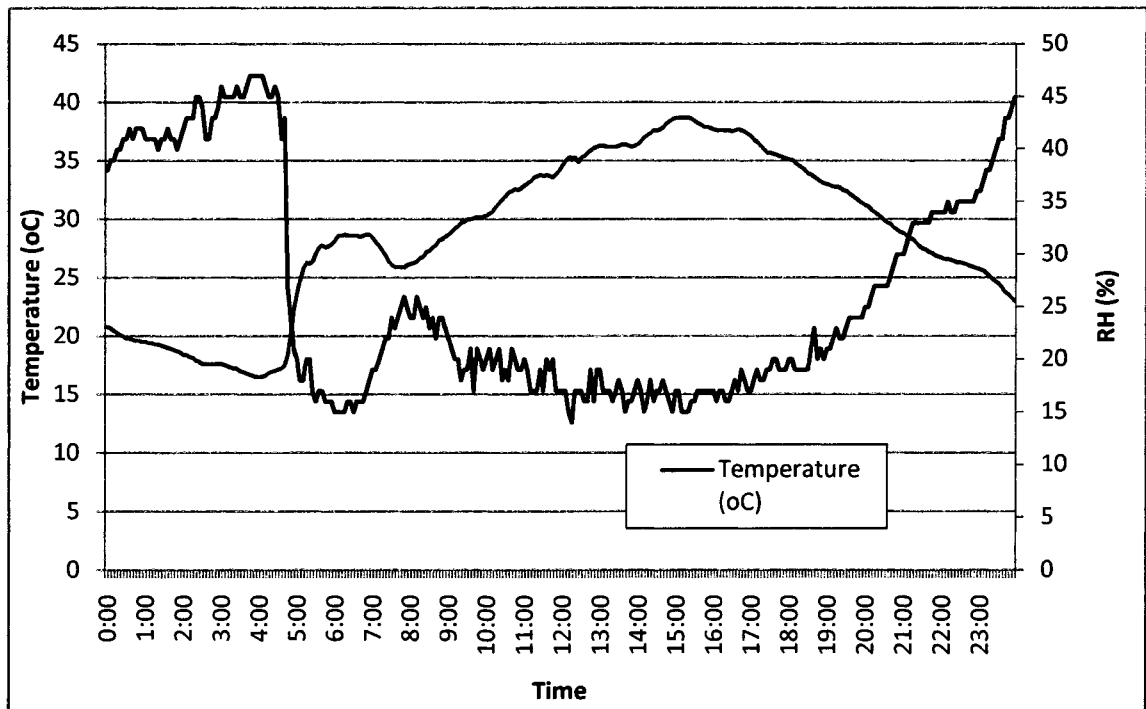


Figure A.3 Typical temperature and RH variations in one hot day (July 10th 2004).

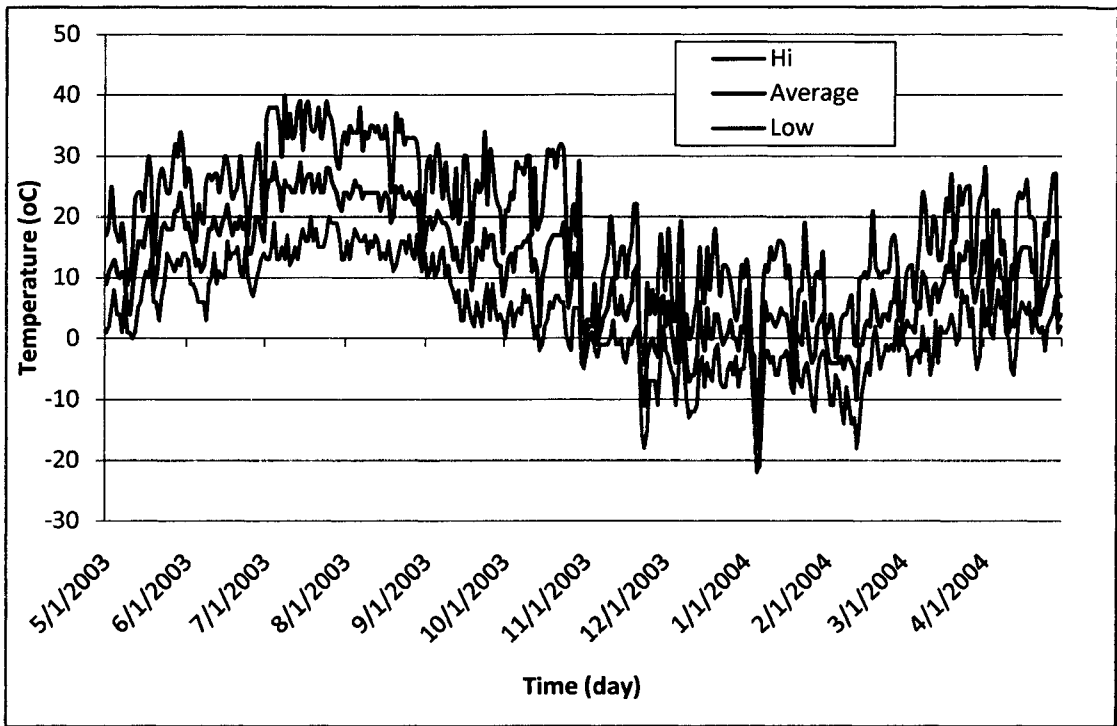


Figure A.4 Daily temperature series in one year (May 1st 2003 to April 30th 2004).

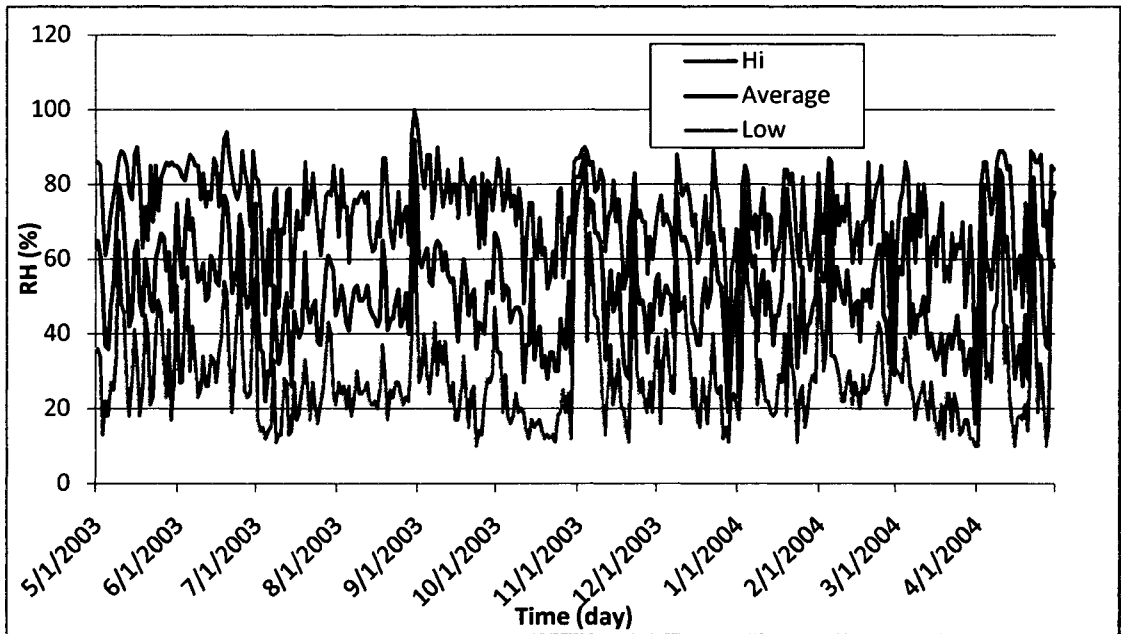


Figure A.5 Daily RH series in one year (May 1st 2003 to April 30th 2004).

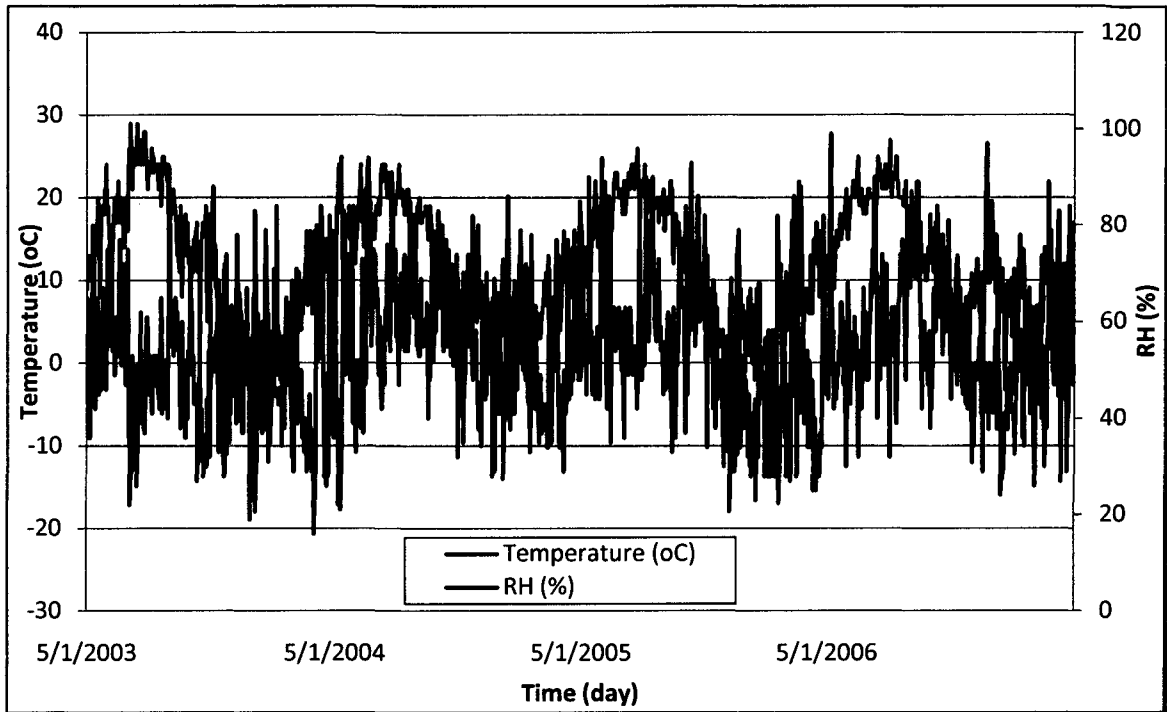


Figure A.6 Variations of daily average of temperature and RH (May 2002 – May 2007).

Examining the RH and temperature records shown in figures from the Figure A.1 to A.6, it is evident that they have the following characteristics:

- The daily variation of the relative humidity has a pattern of a sine/cosine function while the yearly variation has no clear pattern. The daily average of the relative humidity varies in a range of 30%-70% while daily variation ranges from 20-80%.
- Both daily variation of the temperature and yearly variation of the daily average of the temperature have a pattern of a sine/cosine function. The average magnitude of daily variation is about 16°C and the magnitude of yearly variation of daily average is about 30°C. The different temperature between record high and record low at a weather station in Fort Collins from May 2003 to May 2007 is 66°C.

Appendix B

Analysis on mesh sizes

To consider the effect of the mesh size on the convergence ability and the accuracy of the developed model, a 7 day simulation (Analysis State 1) was performed using three different mesh sizes. The different mesh sizes are shown in the Figure B.1. The global seeds for three different meshes were 50.4 mm (2 inches – Mesh size 1), 25.4 mm (1 inch – Mesh size 2), and 12.7 mm (0.5 inches – Mesh size 3).

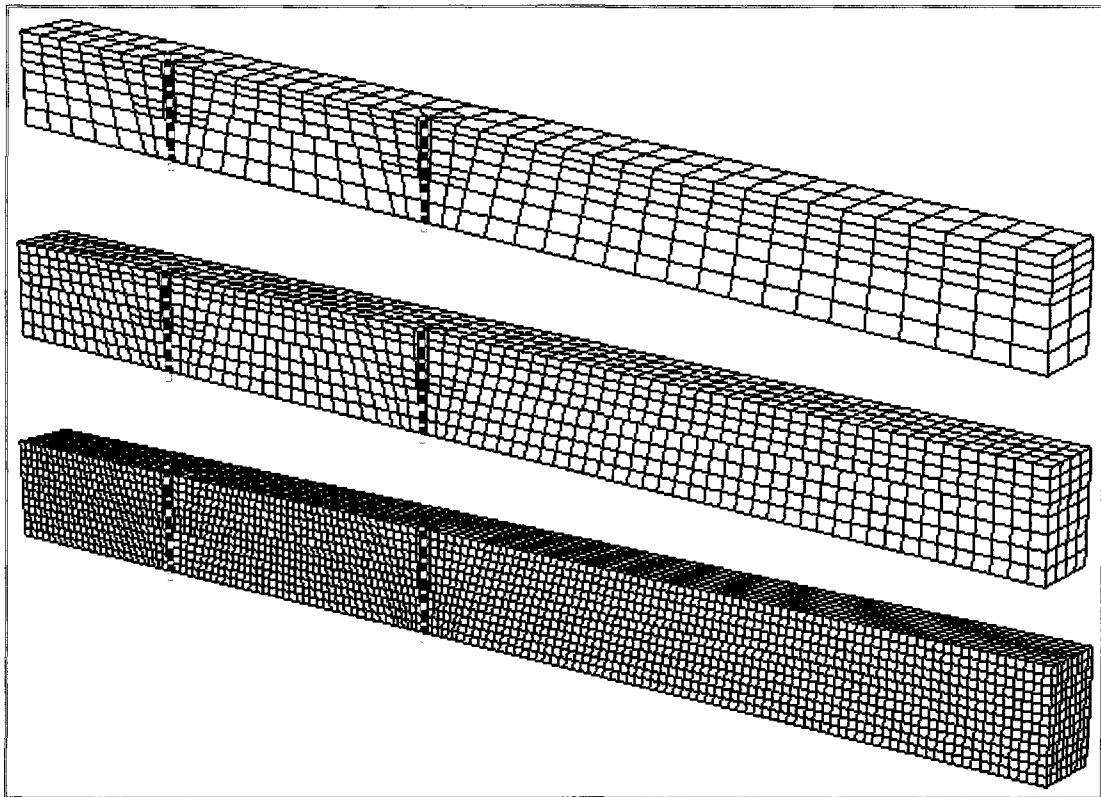


Figure B.1 Different mesh sizes.

Table B.1 summarizes the number of elements which were automatically generated by the ABAQUS for each assigned mesh size.

Table B.1 Numbers of element for different mesh sizes.

	Mesh seed (mm)	Numbers of element			
		Concrete	Wood	Each dowel	Total
Mesh Size 1	50.8	392	226	22	662
Mesh Size 2	25.4	1288	1124	46	2504
Mesh Size 3	12.7	6256	7636	80	14052

Figure B.2 compares the midspan deflections resulting from the different mesh sizes and plotted with the measured deflection. There was no convergence problem with three applied mesh sizes in all three analyses (diffusion, heat transfer and stress analysis) when the normal convergence standard in the ABAQUS was used. The different deflections rendered by different mesh sizes are small. For stress/displacement analysis, structure is stiffer with more refined mesh.

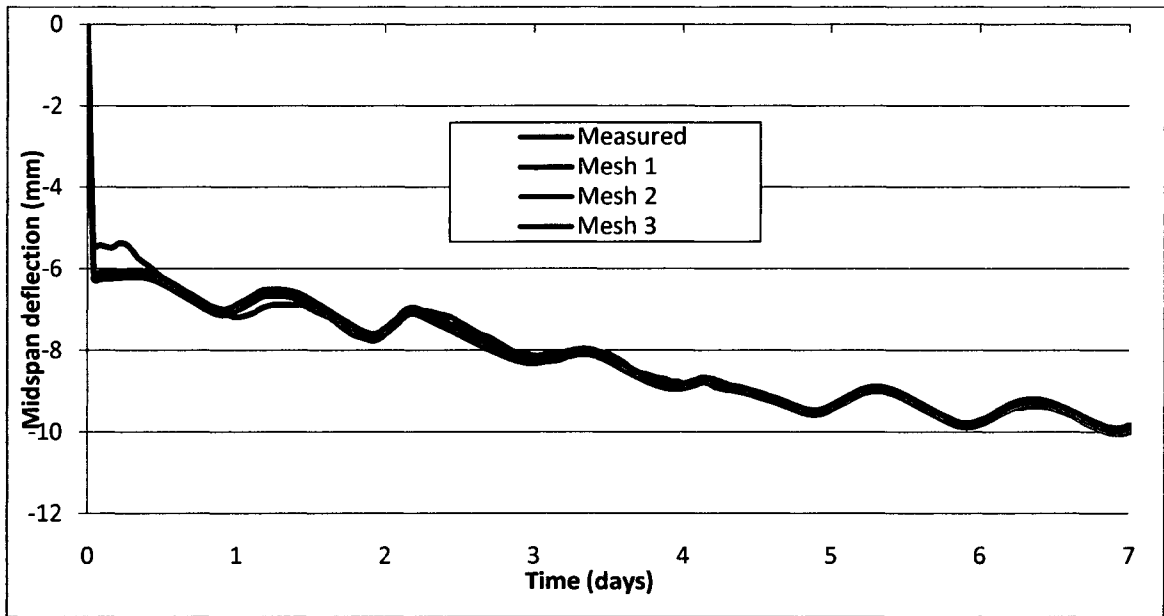


Figure B.2 The midspan deflections rendered by different mesh sizes and the measured deflection.

Appendix C

Effects of uniform vs. non-uniform temperature field in stress/displacement analysis results

The heat transfer analysis yields the temperature field profiles in the wood layer, concrete layer and dowels to be used in the stress/displacement analysis. The temperature field in each layer or component is non-uniform at any specific moment in time. The use of the exact non-uniform temperature field profiles in the stress analysis permits modeling closely the thermal expansion effect to the time-dependent behavior of the composite beams. But using the exact non-uniform temperature field profiles increases enormously the computational time for the stress analysis phase. The results of the heat transfer analysis show that the spatial differences of temperature are small. Thus, the thermal expansion effect due to the variation of the non-uniform temperature fields is small and can be neglected. This means that the thermal expansion effect doesn't affect the time-dependent behavior at the material level. But the thermal expansion phenomenon still affects the time-dependent behavior of the composite structure at the structural level because the coefficient of thermal expansion of concrete is about two times greater than that of wood.

To reduce the computational time, the temperature fields can be assumed to be uniform. One additional analysis for the Analysis State 1 was performed to consider the different stress analysis results rendered by different assumptions on temperature fields. Figure C.1 shows the midspan deflections when different input temperature fields were used. One analysis used the exact non-uniform temperature field from the heat analysis. Two other analyses used assumed uniform temperature fields: one using medium temperatures

(temperature at node 419 for the wood layer and node 557 for the concrete layer), the other using the average temperatures of all nodes at the midspan cross-section for each layer. The results of the stress/displacement analysis show that the effects of the non-uniform temperature fields on the time-dependent behavior of the wood-concrete structure are small. The variation in the midspan deflection due to the variation of the ambient temperature is mostly caused by the difference between the coefficients of thermal expansion of the wood and concrete materials.

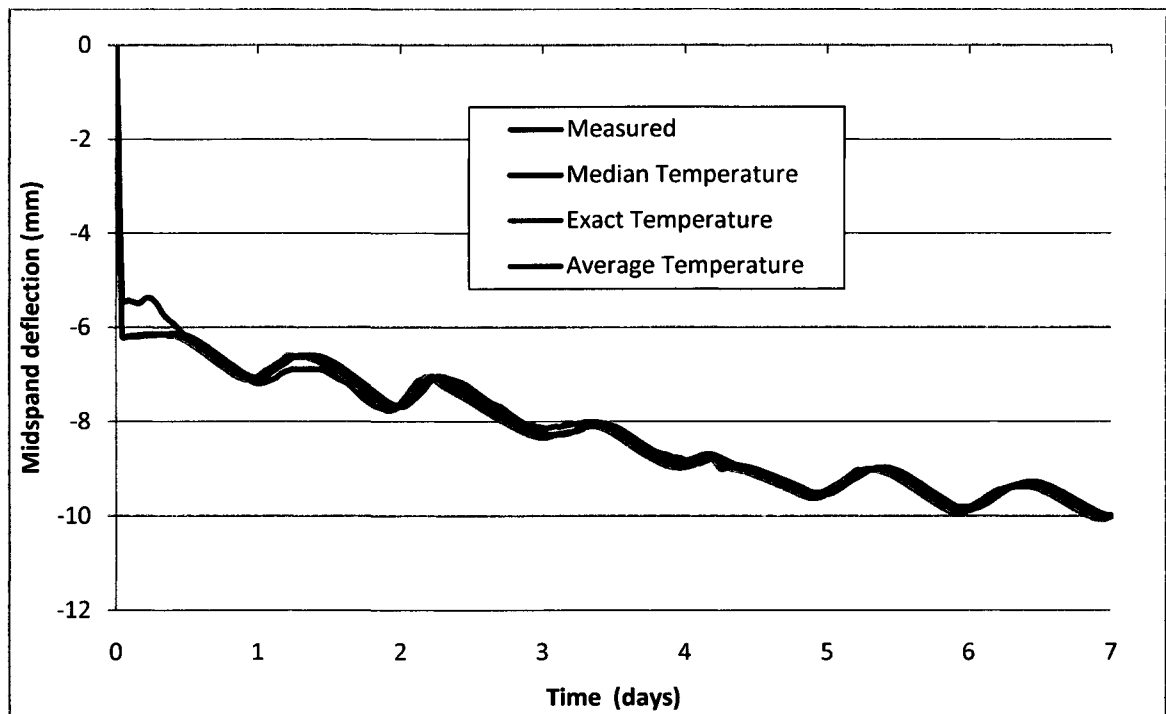


Figure C.1 Midspan deflections due to different temperature fields.

The heat transfer analysis results in Chapter 7 show that there are phase shifts between the ambient temperature and the nodal temperature. The magnitude of a phase shift depends on the distance between the node and the exposure surface but the maximum is smaller than two hours for both the wood and concrete materials. These phase shifts result in a phase shift between the ambient temperature and the midspan deflection. For

an analyses with a short time step (less than two hours), using either the median temperature or the average temperature from the heat analysis helps to capture closely the peaks of the midspan deflection variation. But for an analysis with a longer time step, the temperature differences are smaller and the phase shifts don't appear in the heat transfer analysis results, thus the ambient temperature can be used as the uniform temperature for all materials.

Appendix D

Vector norm and error estimation

Definition

If $x_i (1 \leq i \leq n)$ is an n -space vector then one can define a class of vector norm called p -norms as:

$$\|x\|_p = (|x_1|^p + \dots + |x_n|^p)^{\frac{1}{p}} \quad p \geq 1, x \in \mathbb{R}^n \quad (\text{D.1})$$

The most widely used are the 1-norm, 2-norm, and ∞ -norm:

$$\begin{aligned} \|x\|_1 &= |x_1| + \dots + |x_n| \\ \|x\|_2 &= \sqrt{|x_1|^2 + \dots + |x_n|^2} = \sqrt{x^T x} \\ \|x\|_\infty &= \max |x_i| \quad 1 \leq i \leq n \end{aligned}$$

The 2-norm is also called the Euclidean vector norm and most widely used in the error estimation.

Absolute and relative error

Suppose $\hat{x} \in \mathbb{R}^n$ is an approximation to $x \in \mathbb{R}^n$. For a give vector norm $\|\cdot\|$ we define that

$$\varepsilon_{abs} = \|\hat{x} - x\| \quad (\text{D.2})$$

is the absolute error in \hat{x} . If $\|x\| \neq 0$ then

$$\varepsilon = \frac{\|\hat{x} - x\|}{\|x\|} \quad (\text{D.3})$$

is the relative error in \hat{x} .

Appendix E

3D render of the beam end with notch

The 3D render of the test beam end with notch at certain time, result of Analysis State 2, were plotted in figures from E.1 to E.3 in the following pages.

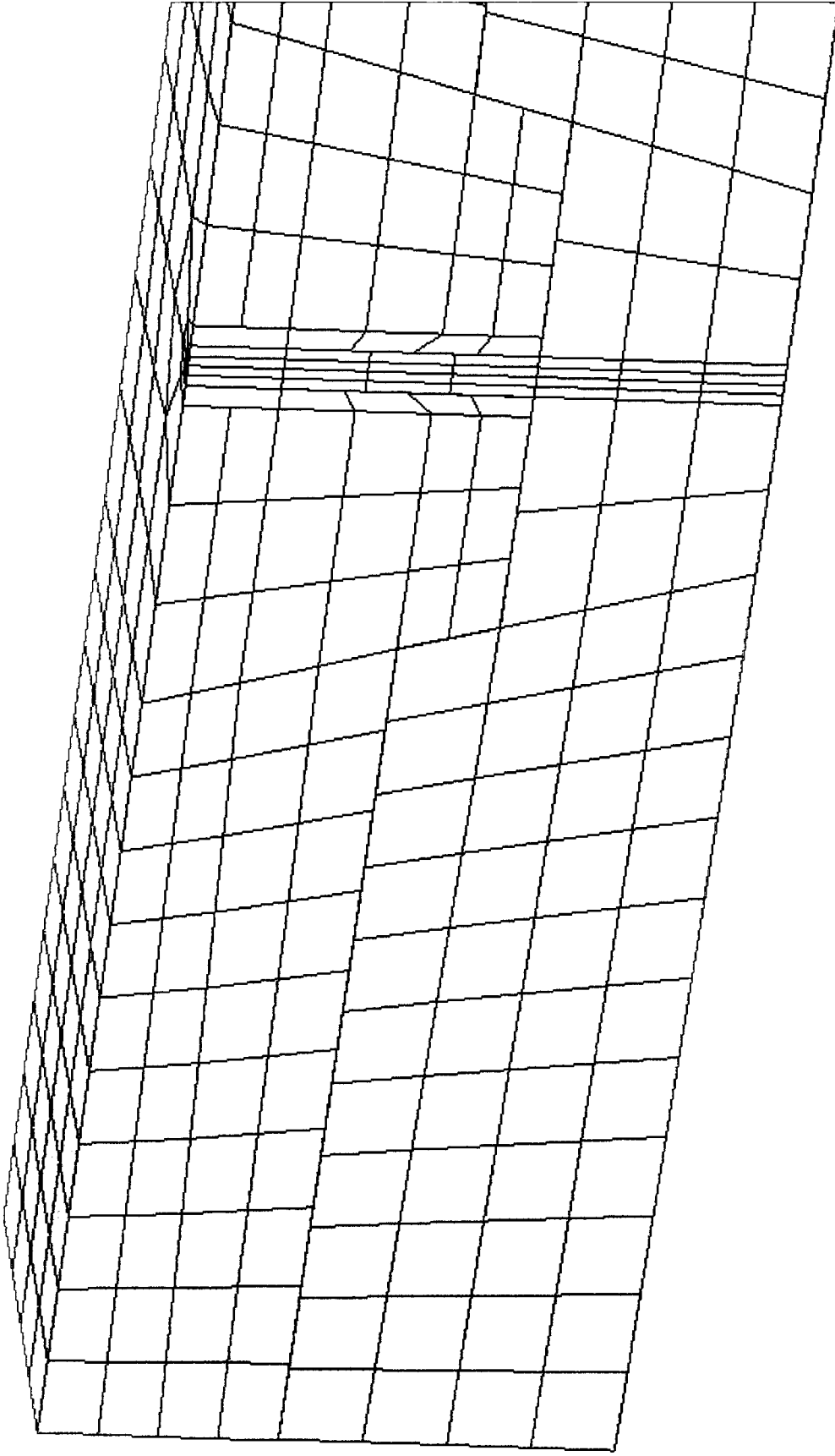


Figure E.1 3D render of beam end with notch at the time of placing concrete.

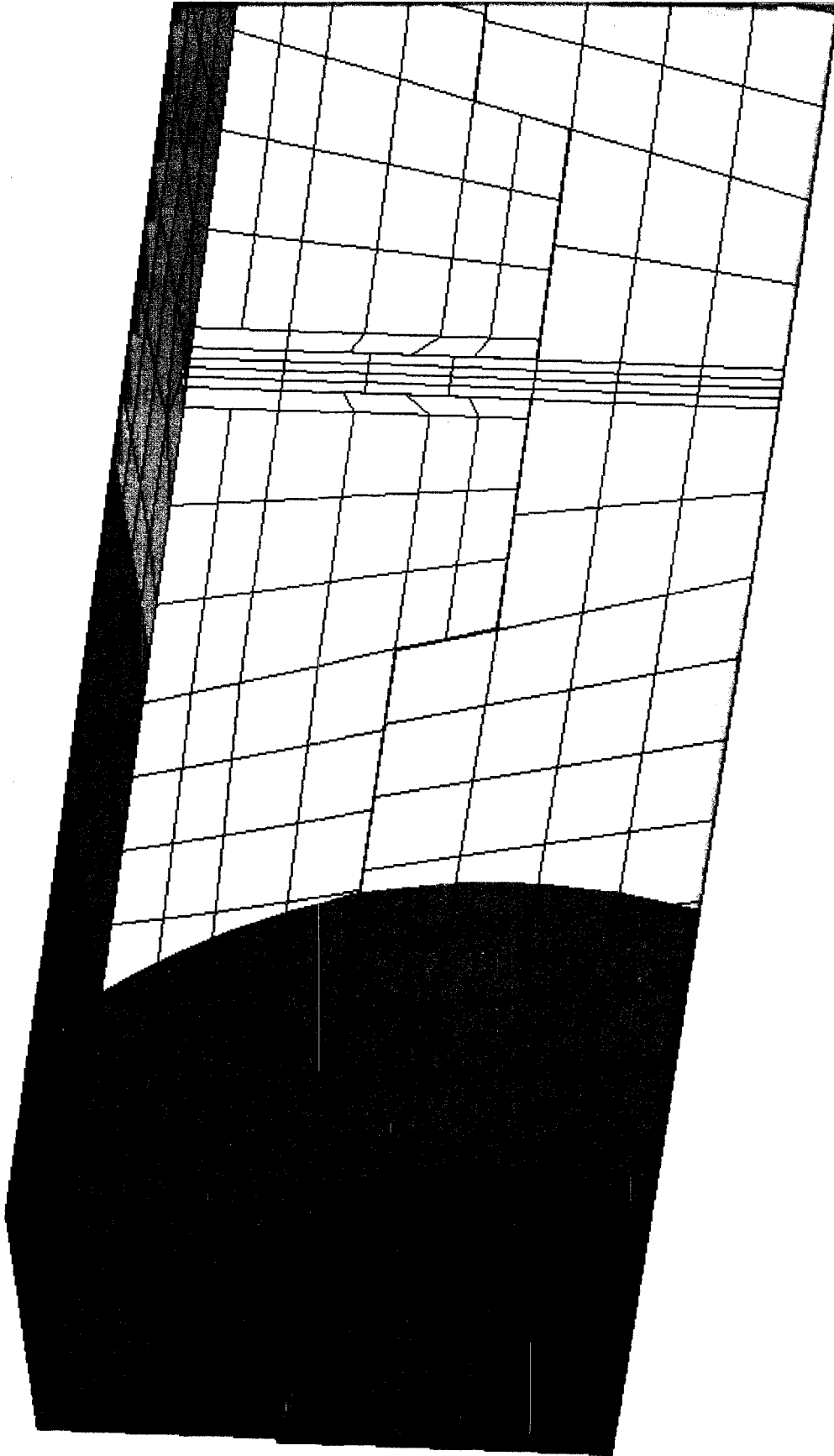


Figure E.2 3D render of beam end with notch at day 7.

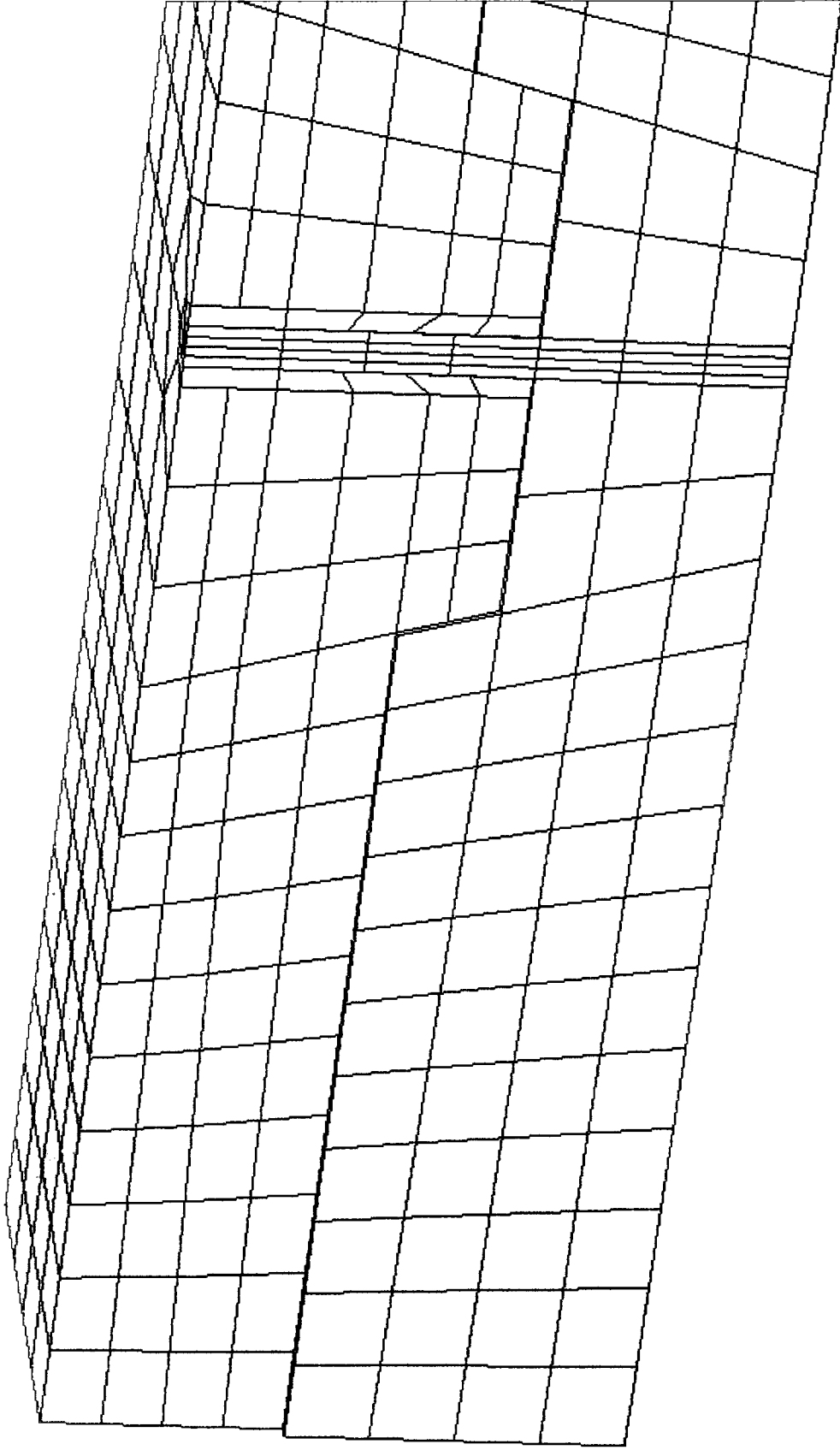


Figure E.3 3D render of beam end with notch at day 29 before applying long-term static load.

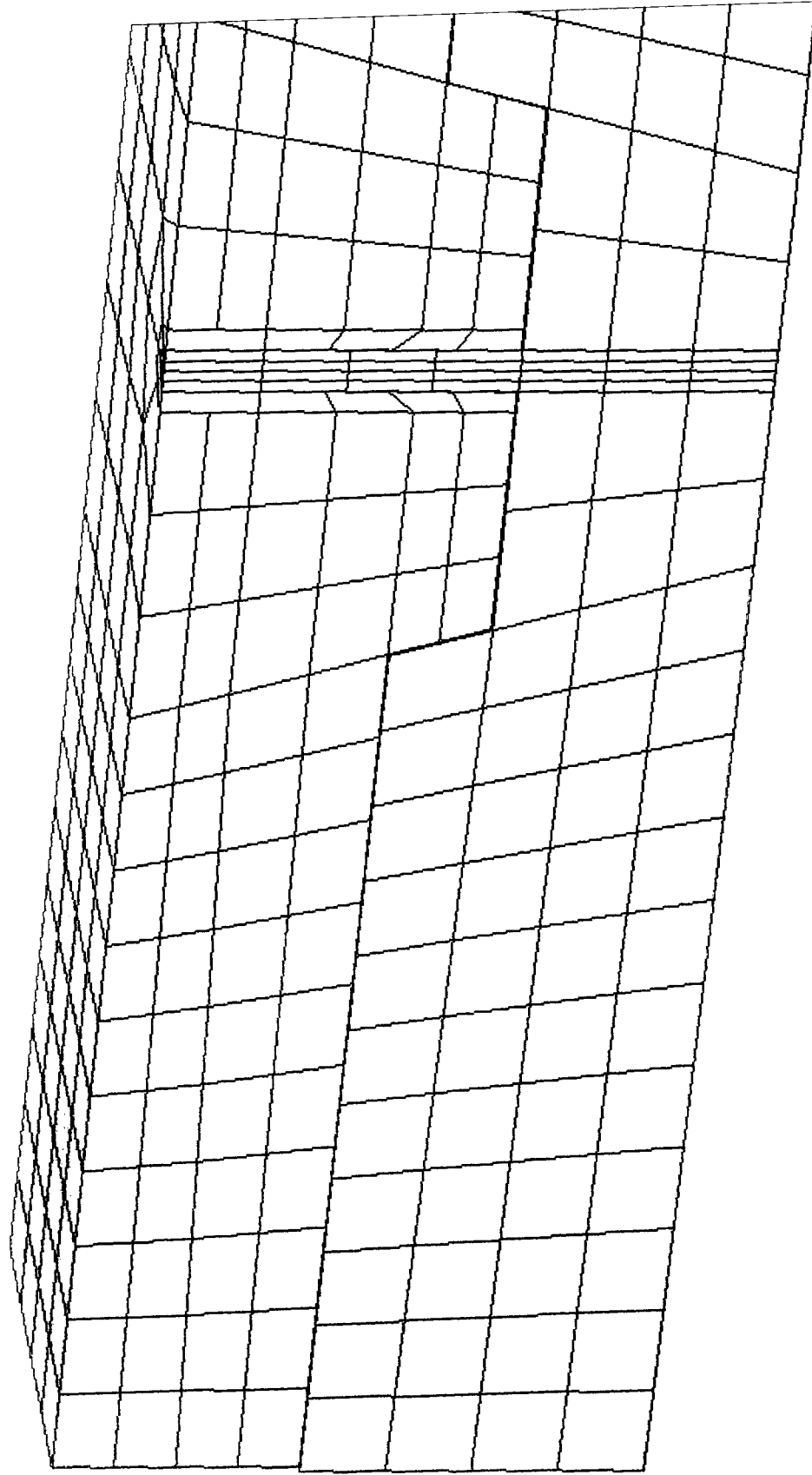


Figure E.4 3D render of beam end with notch at day 29 after applying long-term static load.

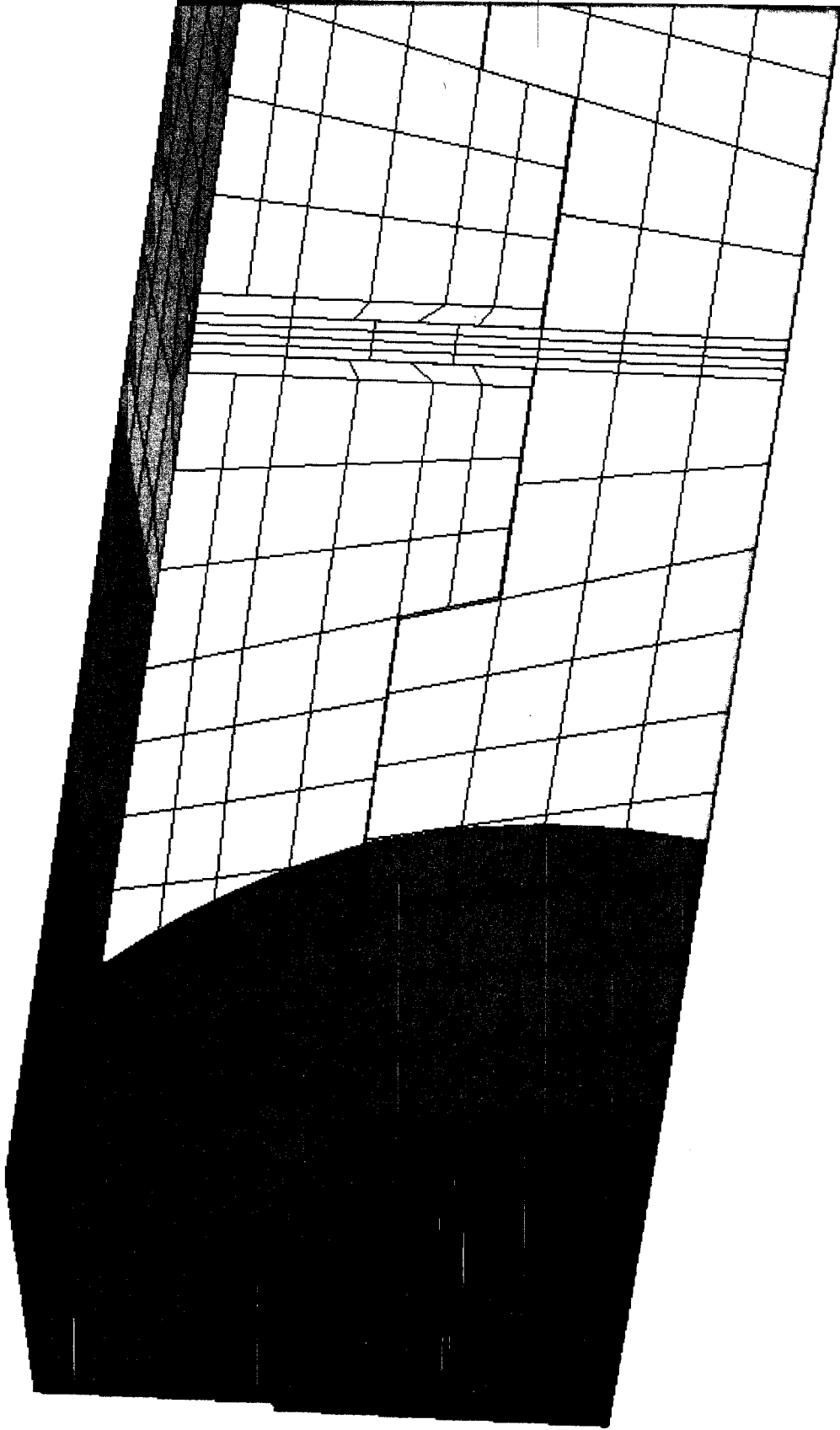


Figure E.5 3D render of beam end with notch at day 123.